Louisiana State University
LSU Digital Commons

LSU Master's Theses | Graduate School

2004

A simplified thermohydrodynamic stability analysis of the plain cylindrical hydrodynamic journal bearings

Sumit Singhal
Louisiana State University and Agricultural and Mechanical College, ssingh2@lsu.edu

Follow this and additional works at: https://digitalcommons.lsu.edu/gradschool_theses

 Part of the Mechanical Engineering Commons

Recommended Citation
Singhal, Sumit, "A simplified thermohydrodynamic stability analysis of the plain cylindrical hydrodynamic journal bearings" (2004). *LSU Master's Theses*. 1518.
https://digitalcommons.lsu.edu/gradschool_theses/1518

This Thesis is brought to you for free and open access by the Graduate School at LSU Digital Commons. It has been accepted for inclusion in LSU Master's Theses by an authorized graduate school editor of LSU Digital Commons. For more information, please contact gradetd@lsu.edu.

A SIMPLIFIED THERMOHYDRODYNAMIC STABILITY ANALYSIS OF THE PLAIN CYLINDRICAL HYDRODYNAMIC JOURNAL BEARINGS

A Thesis

Submitted to the Graduate Faculty of the
Louisiana State University and
Agricultural and Mechanical College
in partial fulfillment of the
requirements for the degree of
Master of Science in Mechanical Engineering

in

The Department of Mechanical Engineering

By
Sumit Singhal
Bhilai Institute of Technology, Bhilai, India 2000
August 2004

Acknowledgments

I wish to thank my major professor, Dr. Michael Khonsari for providing me with constant guidance and inspiration throughout the entire period of my thesis work. During the initial phase, he helped me to understand the basic concepts and theories that were the building blocks for this research. Later on, his sound suggestions helped me shape ideas into reality. This research work was a great learning experience for me, and it's being a great privilege to work with him.

I am very thankful to Dr. Yitshak Ram who was a great help especially during the early phase of this research work. His insight about the Vibrations and Rotordynamics made it easier for me to understand the concepts.

I am sincerely thankful to Dr. Su-Seng Pang for his support and spending his valuable time in evaluating my thesis work. My special thanks go to Dr Jang for all the fruitful discussions we had that were instrumental for the successful completion of this thesis.

I also thank all my friends in the tribology group (CeRoM), for their moral and technical support, without which I would not have succeeded in finishing my thesis.

This work was partially sponsored by Louisiana Board of Regents and Gulf South Compression-Rotating Machinery Symposium (GSCC).

Table of Contents

List of Tables

List of Figures

Nomenclature

C	Radial clearance
$\bar{C}_{ij}$	Dimensionless damping coefficients where first and second subscript refer to the component of force and the direction of the displacement, respectively
c_v	Specific heat of oil
D	Journal diameter
e	Eccentricity
F_e, F_ϕ	Fluid film forces in radial and tangential direction.
$\bar{F}_\varepsilon, \bar{F}_\phi$	Dimensionless fluid film forces in radial and tangential direction.
$F_{Bi(=x,y,z)}$	Body forces
$h, \bar{h}$	Film thickness, $\bar{h} = h/C$
$\bar{K}_{ij}$	Dimensionless stiffness coefficients where first and second subscript refer to the component of force and the direction of the displacement, respectively
k_o	Thermal conductivity of oil
k_b	Thermal conductivity of bush
L	Length of bearing
$M, \bar{M}$	Mass of rotor, critical mass ($\bar{M} = MC\omega^2/W$)
$P,\ \bar{P}$	Pressure, dimensionless pressure
R	Radius of journal
q_x, q_y	Volumetric flow rate in circumferential, axial (leakage) direction respectively.

S	Sommerfeld Number
$\theta, \bar{z}$	Dimensionless coordinate system
$T, \bar{T}$	Oil film temperature, dimensionless temperature
T_i	Inlet temperature of oil
$t, \bar{t}$	Time, dimensionless time
u,v,w	Partial fluid velocity in X,Y,Z direction.
U_a, U_b	Sliding velocity of upper plate, bottom plate respectively
w_a, w_b	Squeeze velocity of upper plate, bottom plate respectively
W, $\bar{W}$	Steady state load,($\bar{W} = W C^2 / \mu_i \omega R^3 L$)
$\bar{x}, \bar{y}, \bar{z}$	Dimensionless Cartesian co-ordinate system
β_1	Temperature-viscosity coefficient
$\varepsilon, \varepsilon_0$	Eccentricity ratio, ε_0 = steady state eccentricity ratio
ϕ, ϕ_0	Attitude angle, ϕ_0 = steady state attitude angle
κ_1	Temperature rise parameter
ξ	Offset of center of mass from geometric center.
ρ	Density of oil
θ_{cav}	Cavitation angle
μ, μ_i	Viscosity of oil, inlet viscosity
ω	Angular velocity of journal
$\bar{\omega}_r$	Dimensionless threshold speed

Abstract

A journal bearing is used to support radial loads under high speed operating conditions. In a journal bearing, pressure or hydrodynamic lift is generated in the thin lubricant oil film that separates the shaft and the bushing, thus preventing metal-to-metal contact. Some journal-bearing configurations are susceptible to large-amplitude, lateral vibrations due to a “self-excited instability” known as oil whirl. In order to investigate the effects of lubricant viscosity on oil whirl, a simplified Thermohydrodynamic analysis (THD) analysis of a plain cylindrical journal bearing system has been developed. The “classical” form of the Reynolds equation coupled with simplified, first-order energy equations are solved in an approximate fashion by assuming a parabolic pressure distribution in axial direction. THD design charts for the rapid evaluation of dynamic coefficients and the threshold speed are developed to investigate the effects of temperature on oil whirl instability. A non-linear transient stability analysis is also presented. This investigation reveals that the inlet viscosity has a pronounced influence on the bearing dynamic coefficients of the lubricating oil film. This investigation also reveals that it is possible to stabilize a journal bearing either by heating the oil or by cooling the oil depending upon the operating region.

1. Introduction

Hydrodynamic type journal bearings are considered to be a vital component of all rotating machinery. A journal bearing consists of a stationary cylindrical body (sleeve) separated from a rotating shaft by a layer of lubricant. A journal bearing is used to support radial loads under high speed operating conditions. In a journal bearing, pressure or hydrodynamic lift is generated in the thin lubricant oil film that separates the shaft and the bushing, thus preventing metal-to-metal contact.

Some journal-bearing configurations are susceptible to large-amplitude, lateral vibrations due to a “self-excited instability” known as oil whirl. Oil whirl is independent of rotor unbalance or misalignment. A self-excited instability is caused by the forces generated in the lubricating oil film due to hydrodynamic action. During oil whirl the rotor orbits in its bearings at a frequency approximately half the rotor angular speed. If not controlled, this non-synchronous, self-excited orbiting motion will grow without bound and may lead to catastrophic bearing failure.

It has been observed that at the onset of oil whirl, rotor behavior is unlike critical speed resonance where the amplitude of motion builds up as the rotor reaches its critical speed and then decreases as it passes critical speed. At the inception of non-synchronous whirl the amplitude of rotor motion continually builds up at the frequency of approximately half of that of the rotor speed and never dies down. Thus for a rotor dynamic system designer non-synchronous oil-whirl is a more serious issue than critical speed resonance.

Since the discovery of this phenomenon by Newkirk [1] in 1925, many experimental and theoretical investigations have been conducted to understand and predict the onset of this non-synchronous whirling. From various published experimental work and in-house experimental work at LSU, it has been concluded that lubricant viscosity plays a major

role in oil whirl instability. Under normal operating conditions, the lubricant undergoes a significant change in temperature along the circumferential direction, which causes a change in viscosity and other bearing performance parameters such as minimum film thickness and the load carrying capacity. Although the effect of viscosity on bearing parameters such as load carrying capacity, leakage flow rate, power loss and frictional force is predictable, the effect of viscosity on oil whirl instability of the plain cylindrical 360^0 hydrodynamic bearings has not been yet fully understood [2]. In fact, some contradictory experimental results have been reported concerning the effects of viscosity on the shaft instability. Pinkus [3] reported that the lower lubricant temperature tended to have stabilizing effects on the rotor-bearing system, while Newkirk and Lewis [4] from their experiments found that higher lubricant inlet temperatures promoted stability.

The purpose of the present work is to establish the effect of viscosity on the oil whirl stability of a bearing. For this purpose a simplified Thermohydrodynamic analysis (THD) analysis of a plain cylindrical journal bearing system has been developed. The “classical” form of the Reynolds equation coupled with simplified, first-order energy equations are solved in an approximate fashion by assuming a parabolic pressure distribution in axial direction [5]. THD design charts for the rapid evaluation of dynamic coefficients and the threshold speed are developed to investigate the effects of temperature on oil whirl instability. A non-linear transient stability analysis is also presented.

2. Literature Review

Newkirk and Taylor [1] in 1925, based on their experimental findings, reported a new kind of self-excited rotordynamic instability in hydrodynamic type journal bearings. They observed that during this instability the rotor orbits in its bearing at a frequency approximately half of the rotor speed. They reported that at the onset of this self-excited instability, the rotor behavior is unlike critical speed resonance where the amplitude of motion builds up as the rotor reaches its critical speed and then decreases as it passes the critical speed. At the inception of this non-synchronous whirling, the amplitude of the rotor motion continuously builds up at the frequency of approximately half of that of the rotor speed and never dies down. They concluded that these types of lateral vibrations of rotor are due to the action of lubricating oil film and referred to this self-excited rotordynamic instability as oil whirl. They found that oil whirl can be prevented by shutting off the oil supply to the bearings. From their experiments they also concluded that these sub-synchronous vibrations may be prevented by misaligning the bearings slightly, by the use of friction damped bearings or by avoiding the lightly loaded shafts.

Hagg [6] provided some theoretical insights into the phenomenon of oil whirl. He stated that during the stable motion or steady state condition of rotor in a bearing, the hydrodynamic fluid forces developed by the oil film are equal to the external load. But during the whirling motion of the shaft, the hydrodynamic fluid forces overcome the external load and act as an “energy source” accelerating the shaft in circular orbit.

Pinkus [3] in 1957 conducted an extensive experimental investigation on oil whirl. During his work he investigated the effects of loading, speed, viscosity, amount of oil, unbalance, flexibility and external excitation on oil whirl. His work led to very important conclusions such as the fact that the whirl is independent of balancing. Pinkus also

reported that a lower lubricant temperature tended to have stabilizing effects on the rotor bearing system which is opposite to findings reported by Newkirk and Lewis [4] stating that a higher lubricant inlet temperature promoted stability.

Holmes [7] in 1960 showed that it is possible to predict the oil whirl threshold speed by considering oil film as an elastic and a viscous system. He developed a stability chart for the prediction of onset of oil whirl by expressing the dynamic oil film forces acting on the shaft journal in terms of the linearized velocity dependent (damping) and displacement dependent (stiffness) terms. He tabulated the stability chart by using a linear perturbation stability analysis. It should be mentioned that the idea of representing the dynamic response characteristics of a journal bearing by means of stiffness and damping coefficients originates from Stodola and Hummel in 1926. Their aim was to improve the calculation of critical speed of a rotor by including the flexibility of bearing oil film.

Holmes [8] in 1970 performed a non-linear transient analysis of rotor-bearing system using the short bearing theory. He concluded that linearity might be assumed for peak-peak vibration values of about one-third of the radial clearance at an eccentricity ratio of 0.7. Kirk and Gunter [9] in 1970 also performed a similar kind of non-linear transient analysis. They considered the case of a horizontal, a vertical and an unbalanced journal in their analysis. They reached to the important conclusion that as opposed to the linear perturbation theory, the journal motion is bounded and the motion forms “limit cycle” at the whirl threshold speed. They also calculated the dynamic fluid forces transmitted to the bearing surface due to whirl and unbalance. Akers et al. [10], in their transient non-linear analysis of a journal bearing system, concluded that the stability of the bearing is unaffected by the initial disturbance given to the shaft. Khonsari and Chang [11] performed non-linear transient analysis of the journal bearing system and concluded that

stability of the system is a strong function of the initial conditions. They showed that there exists a stability boundary within the bearing clearance circle outside of which any initial condition $\left(\varepsilon_0, \phi_0, \dot{\varepsilon}(0) = 0, \dot{\phi}(0) = 0\right)$ will make the bearing unstable although according to the linearized stability analysis, the bearing should be stable. They also gave the procedure to determine the stability boundary in terms of the initial conditions for the shaft release.

In the last half of the twentieth century many researchers and engineers focused their attention on the study of thermal effects in bearings. Khonsari [2] gave an extensive survey of the various experimental and theoretical papers pertaining to the thermal effects in hydrodynamic bearings. Dowson et al. [12] based on their experimental findings reported that the cyclic variation in shaft surface temperature is small and the rotating shaft can therefore be considered as an isothermal body. Dowson's test results also showed that the shaft temperature is very close to the mean temperature of the bush surface. Dowson's research also revealed that the axial temperature gradient within bush is negligible.

Tonnesen and Hansen [13] from their experimental investigations reported that viscosity was found to have a significant effect on the operating temperatures of the bearing. They also concluded that the oil flow has a pronounced effect on the steady state operating conditions. More recently Ma and Taylor [14] conducted an experimental investigation on the thermal effects on the plain and elliptical journal bearings. Their experimental investigation shows that the temperature variation is significant along the circumferential direction but not in axial direction. They also reported that the temperatures on the center plane are slightly higher than towards the edges of the bearing. Further more, they

concluded that the thermal behavior of the journal bearings is significantly affected by the rotational speed, the maximum bush temperature and the power loss.

As the importance of thermal effects was recognized together with the availability of sound and repeatable experimental data researchers were motivated to predict the pressure and temperature fields accurately in the bearing. As a result Thermohydrodynamic models had been developed. Thermohydrodynamic analysis (THD) of a bearing refers to realistic solutions of Reynolds equation in which viscosity field is predicted based on the computation of temperature field obtained from the energy equation. Predictions of the bearing performance parameters based on THD analysis requires simultaneous solution of the Reynolds equation (pressure field) coupled with the energy equations (temperature field) through Vogel's viscosity equation (viscosity field).

Knight and Barrett [15] performed a simplified THD analysis of a multilobe journal bearing where they considered shaft and bushing to be insulated and assumed that all the heat generated in the bearing by viscous shear is convected out bearing by oil. Bearing maximum temperature and pressure predictions from their analysis were in agreement with the experimental findings of Tonnesen and Hansen [13]. Although the THD models for the predictions of bearing performance parameters had been available long back, the use of the theory was limited among practicing designers due to lack of generalized design charts. Khonsari et al. [16] performed an extensive set of THD simulations. They presented the results in the form of generalized THD design charts which enables one to predict the maximum temperature and effective bearing temperatures. They characterized the steady state thermal behavior of the hydrodynamic journal bearings with two unique dimensionless temperature rise parameters κ_1 and κ_2. The parameter κ_1 which incorporates all of oil properties and shaft linear velocity was associated with the viscous

dissipation term in energy equation. Very recently Jang and Khonsari [17] gave a set curve fits equations and a very simple design procedure which enables one to rapidly predict the maximum bearing temperature, the shaft temperature and other bearing design performance parameters.

The effect of viscosity on bearing parameters such as load carrying capacity, leakage flow rate, power loss and frictional force is predictable. However, the effect of viscosity on oil whirl instability of the plain cylindrical 360^0 hydrodynamic bearings has not been yet fully understood [2]. In fact, some contradictory experimental results have been reported concerning the effects of viscosity on the shaft instability. As discussed earlier in the section, Pinkus [3] reported that a lower lubricant temperature tended to have stabilizing effects on the rotor-bearing system, while Newkirk and Lewis [4] from their experiments found that higher lubricant inlet temperatures promoted stability.

Maki and Ezzat [18] conducted a detailed experimental investigation, to examine the effects of lubricant inlet temperature on the oil whirl instability. They reported that whenever the lubricant inlet temperature was higher than that of mean bearing surface temperature, a self–excited whirl occurred. But when the bearing temperature was higher than that of the lubricant, whirl did not occur even at rotor speed was much higher than the whirl threshold predicted by the isothermal hydrodynamic theory of lubrication. Although the experimental results were repeatable and predictable, no quantitative explanation was given in that paper for this phenomenon. From the result of these experiments it was very clear that the inlet temperature of lubricant plays a significant role in the dynamics of high-speed bearings.

3. Mathematical Model and Theory

3.1 Equations of Motion

Generally, the theoretical investigation of oil whirl instability starts from the equations of motion of a journal inside the bearing. The reactive fluid forces generated by the oil film are obtained by solving the Reynolds equation. Accordingly, in this section first the equations of motion for the rotating journal are presented followed by the derivation of Reynolds lubrication equation.

The following assumptions are made in deriving the equations of motion:

1) The rotor consists of a single disk on an elastic shaft mounted on two identical bearing supports.
2) The mass of the shaft is small compared with the mass of the disk $2m$.
3) The disk is fixed on the shaft between the two supports.
4) There is no misalignment.

Let the shaft rotate at a constant angular velocity ω. The stiffness of the shaft is k. In view of the above assumptions, the motion of the disk may be considered simply as a plane motion. Let x and y be the co-ordinates of the disk geometric center O' (Figure 3.1). The eccentricity of the center of gravity of the disk T is denoted by ξ.

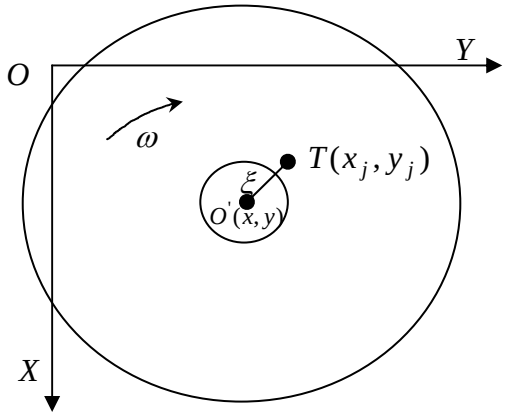

Figure 3.1: Journal Bearing Co-ordinate System [19]

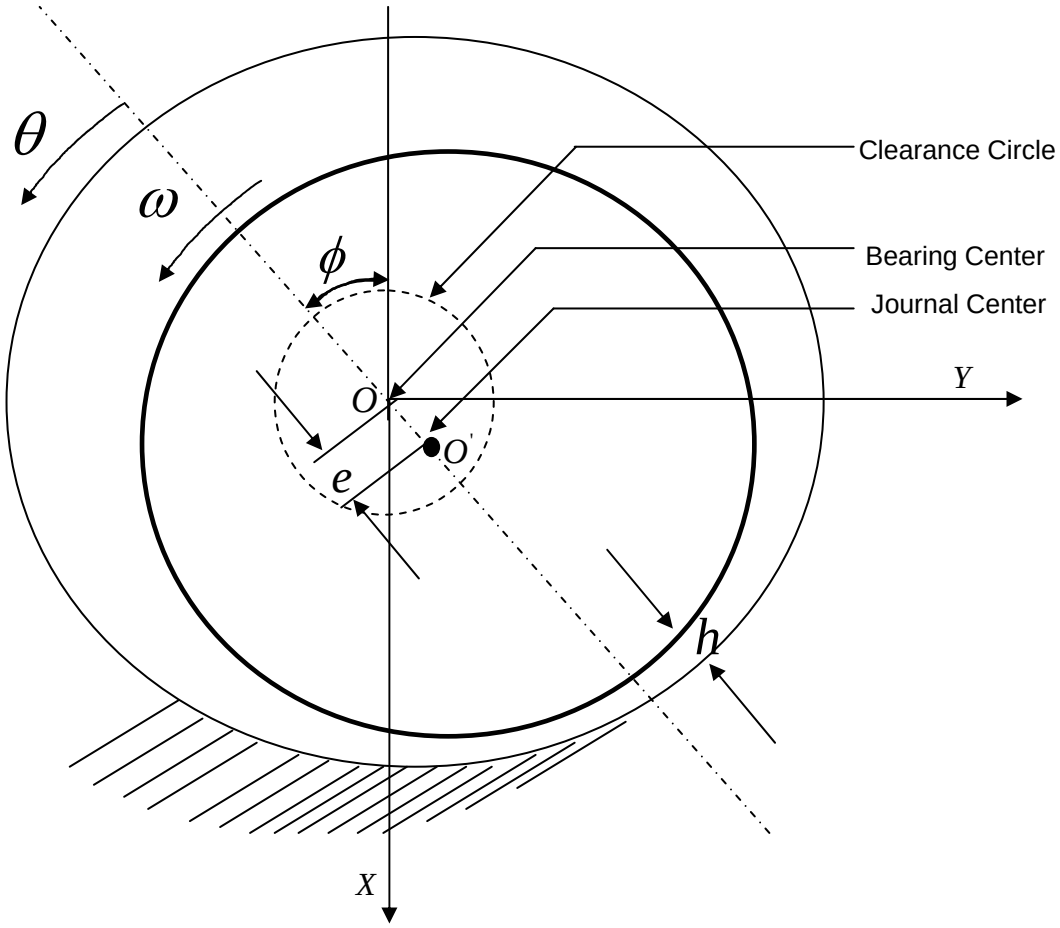

Figure 3.2: Journal Bearing Nomenclature

Where

e = Eccentricity

ϕ = Attitude Angle

h = Oil film thickness

O =Journal center

O' =Bearing Center

ω = Journal velocity

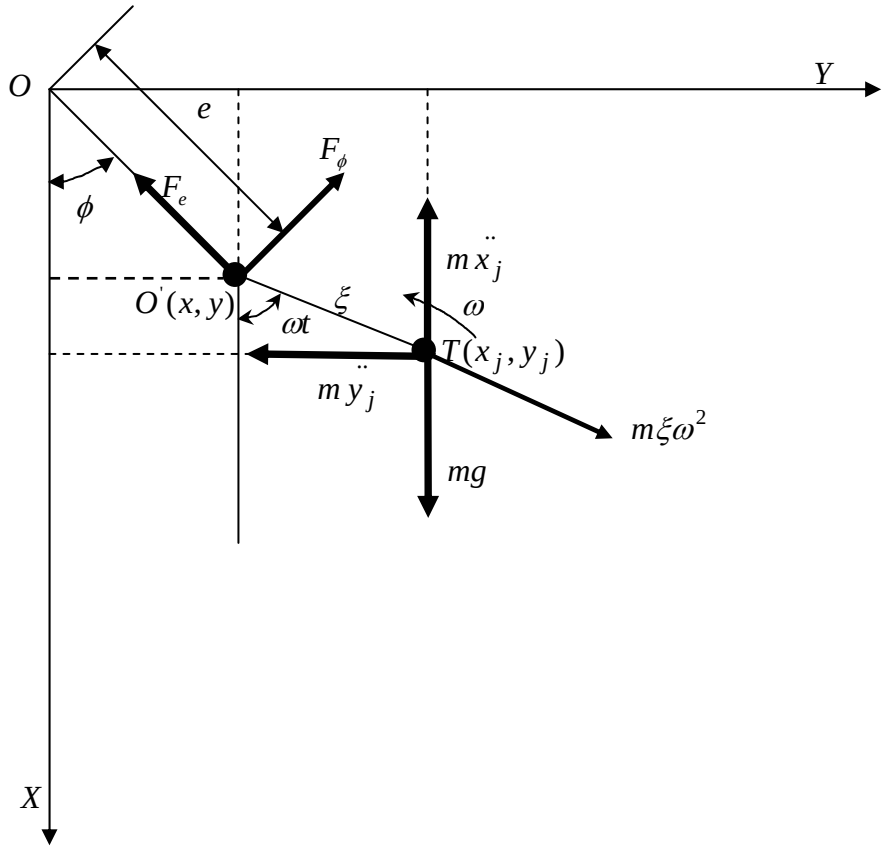

Figure 3.3: Stability of Equilibrium Position of Journal with Unbalance [19]

Where

T = Journal center of mass

$O'T = \xi$

$x, y =$ Journal geometric center

x_j, y_j = Journal center of gravity

F_e = Fluid-film forces in radial direction

F_ϕ = Fluid-film forces in tangential direction

- **Equations of Motion for an Unbalanced Rotor**

From the Figures 3.2 and 3.3 one can express the co-ordinates of the center of gravity of the journal in terms of x, y, ξ, ω :

$$x_j = x + \xi \cos \omega t \tag{3.1}$$

$$y_j = y + \xi \sin \omega t \tag{3.2}$$

$$\dot{x}_j = \dot{x} - \xi \omega \sin \omega t \tag{3.3}$$

$$\dot{y}_j = \dot{y} + \xi \omega \cos \omega t \tag{3.4}$$

$$\ddot{x}_j = \ddot{x} - \xi \omega^2 \cos \omega t \tag{3.5}$$

$$\ddot{y}_j = \ddot{y} - \xi \omega^2 \sin \omega t \tag{3.6}$$

Balancing the components of forces at the equilibrium position in X & Y co-ordinates yields the following equations:

In X- Direction

$$m\ddot{x}_j + F_e \cos \phi + F_\phi \sin \phi = mg \tag{3.7}$$

In Y- Direction

$$m\ddot{y}_j + F_e \sin \phi - F_\phi \cos \phi = 0 \tag{3.8}$$

Substituting equations (3.5) and (3.6) in equations (3.7) and (3.8), respectively

$$m(\ddot{x} - \xi \omega^2 \cos \omega t) + F_e \cos \phi + F_\phi \sin \phi = mg \tag{3.9}$$

$$m(\ddot{y} - \xi \omega^2 \sin \omega t) + F_e \sin \phi - F_\phi \cos \phi = 0 \tag{3.10}$$

Dividing equations (3.9) and (3.10) by m and rearranging the terms gives:

$$\ddot{x} + \frac{1}{m}(F_e \cos\phi + F_\phi \sin\phi) = mg + \xi\omega^2 \cos\omega t \tag{3.11}$$

$$\ddot{y} + \frac{1}{m}(F_e \sin\phi - F_\phi \cos\phi) = \xi\omega^2 \sin\omega t \tag{3.12}$$

Expressing the co-ordinates x & y in terms of the polar co-ordinates e & ϕ

$$x = e\cos\phi \tag{3.13}$$

$$y = e\sin\phi \tag{3.14}$$

$$\dot{x} = \dot{e}\cos\phi - e\dot{\phi}\sin\phi \tag{3.15}$$

$$\dot{y} = \dot{e}\sin\phi + e\dot{\phi}\cos\phi \tag{3.16}$$

$$\ddot{x} = \ddot{e}\cos\phi - 2\dot{e}\dot{\phi}\sin\phi - \dot{\phi}^2 e\cos\phi - \ddot{\phi}e\sin\phi \tag{3.17}$$

$$\ddot{y} = \ddot{e}\sin\phi + 2\dot{e}\dot{\phi}\cos\phi - \dot{\phi}^2 e\sin\phi + \ddot{\phi}e\cos\phi \tag{3.18}$$

From equations (3.13)-(3.18) we arrive at the following relationships:

$$x\cos\phi + y\sin\phi = e \tag{3.19}$$

$$-x\sin\phi + y\cos\phi = 0 \tag{3.20}$$

$$\ddot{x}\cos\phi + \ddot{y}\sin\phi = \ddot{e} - \dot{\phi}^2 e \tag{3.21}$$

$$-\ddot{x}\sin\phi + \ddot{y}\cos\phi = \ddot{\phi}e + 2\dot{e}\dot{\phi} \tag{3.22}$$

Multiply the equation (3.11) by $\cos\phi$ and equation (3.12) by $\sin\phi$ and add them together, and then multiply equation (3.11) by $-\sin\phi$ and equation (3.12) by $\cos\phi$ and add them again, following equations of motion in polar co-ordinates are obtained:

$$\ddot{e} - \dot{\phi}^2 e + \frac{1}{m} F_e = \xi\omega^2(\cos\omega t\cos\phi + \sin\omega t\sin\phi) + g\cos\phi \tag{3.23}$$

$$\ddot{\phi}e + 2\dot{e}\dot{\phi} - \frac{1}{m} F_\phi = \xi\omega^2(-\cos\omega t\sin\phi + \sin\omega t\cos\phi) - g\sin\phi \tag{3.24}$$

Equations (3.23) and (3.24) can be written in the form

$$\ddot{e} - \dot{\phi}^2 e + \frac{1}{m} F_e = \xi\omega^2\cos(\omega t - \phi) + g\cos\phi \tag{3.25}$$

$$\ddot{\phi}e + 2\dot{e}\dot{\phi} - \frac{1}{m} F_\phi = \xi\omega^2\sin(\omega t - \phi) - g\sin\phi \tag{3.26}$$

- **Idealized Balanced Bearing**

Let us consider the case where shaft and rotor are perfectly balanced i.e. there geometric center and center of gravity coincide i.e. $\xi = 0$. Equations (3.25) and (3.26) reduces to much simpler form

$$\ddot{e} - \dot{\phi}^2 e + \frac{1}{m} F_e - g\cos\phi = 0 \tag{3.27}$$

$$\ddot{\phi}e + 2\dot{e}\dot{\phi} - \frac{1}{m} F_\phi + g\sin\phi = 0 \tag{3.28}$$

To solve the equations (3.27) and (3.28), one must determine the components of the fluid-film forces in the radial (F_e) and tangential (F_ϕ) directions. This requires solving the Reynolds equation as presented in following section.

3.2 Derivation of the Classical Reynolds Lubrication Equation for Thin Film Flows

The fluid-film forces F_ϕ and F_e in equations (3.27) and (3.28) , respectively are obtained by solving the basic lubrication equation for the pressure distribution the so called Reynolds equation. The governing equations for viscous flow are as follows:

- **Conservation of Mass (Continuity equation)**

Conservation of mass simply states that the net rate of mass flow into and out of differential control volume must be zero.

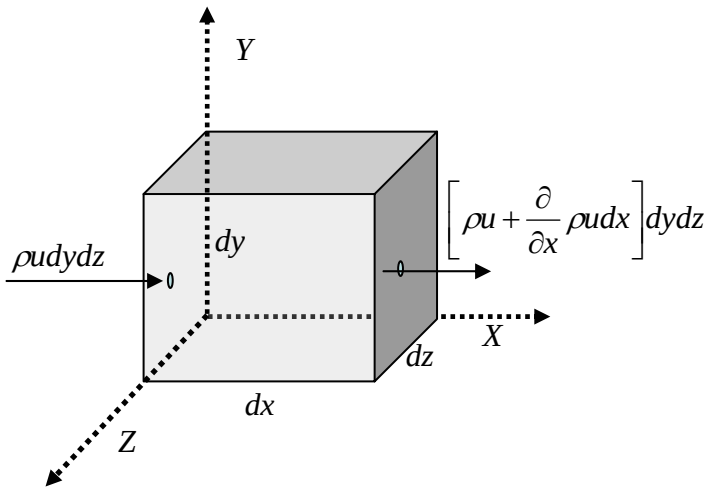

Figure 3.4: Differential Fluid Element

Referring to Figure 3.4, the continuity equation in Cartesian co-ordinates $V = V(x, y, z)$ reads:

$$\frac{\partial \rho}{\partial t} + \frac{\partial (\rho u)}{\partial x} + \frac{\partial (\rho v)}{\partial y} + \frac{\partial (\rho w)}{\partial z} = 0 \qquad (3.29)$$

Where *u, v, w* are the components of the velocity in the *X, Y, Z* directions, respectively.

If the flow is incompressible then there is no change in density and $\partial\rho/\partial t$ =0 regardless of whether the flow is steady or unsteady. Then the equation (3.29) in vector form is:

$$\nabla.V = 0 \tag{3.30}$$

- **Conservation of Momentum (Navier-Strokes Equations)**

The Navier-Strokes equation is derived by a force balance and by applying the Newton's second law of motion $\sum F = ma$ to a fluid element. Navier-Strokes equation is given by [20]:

$$\underbrace{\rho\frac{DV}{Dt}}_{\text{inertia Forces}} = \underbrace{F_B}_{\text{body Forces}} - \underbrace{\nabla p}_{\text{pressure Forces}} + \underbrace{\nabla.\tau_{ij}}_{\text{viscous Forces}} \tag{3.31}$$

where

P = pressure

τ = Shear Stress

The differential operator $D/Dt \equiv$ total derivative, material derivative, or particle derivative is defined as follows [20]:

$$\frac{D}{Dt} \equiv \underbrace{\frac{\partial}{\partial t}}_{\text{local derivative}} + \underbrace{u\frac{\partial}{\partial x} + v\frac{\partial}{\partial y} + w\frac{\partial}{\partial z}}_{\text{convective derivatives}} \tag{3.32}$$

In Cartesian co-ordinates the conservation of momentum reduces to the following equation [20]:

X-Momentum:

$$\rho\left(\frac{\partial u}{\partial t} + u\frac{\partial u}{\partial x} + v\frac{\partial u}{\partial y} + w\frac{\partial u}{\partial z}\right) = \left(\frac{\partial}{\partial x}\tau_{xx} + \frac{\partial}{\partial y}\tau_{yx} + \frac{\partial}{\partial z}\tau_{zx}\right) - \frac{\partial p}{\partial x} + F_{Bx} \tag{3.33}$$

Y-Momentum:

$$\rho\left(\frac{\partial v}{\partial t}+u\frac{\partial v}{\partial x}+v\frac{\partial v}{\partial y}+w\frac{\partial v}{\partial z}\right)=\left(\frac{\partial}{\partial x}\tau_{xy}+\frac{\partial}{\partial y}\tau_{yy}+\frac{\partial}{\partial z}\tau_{zy}\right)-\frac{\partial p}{\partial y}+F_{By} \tag{3.34}$$

Z-Momentum:

$$\rho\left(\frac{\partial w}{\partial t}+u\frac{\partial w}{\partial x}+v\frac{\partial w}{\partial y}+w\frac{\partial w}{\partial z}\right)=\left(\frac{\partial}{\partial x}\tau_{xz}+\frac{\partial}{\partial y}\tau_{yz}+\frac{\partial}{\partial z}\tau_{zz}\right)-\frac{\partial p}{\partial z}+F_{Bz} \tag{3.35}$$

where F_{Bx}, F_{By}, F_{Bz} are the body forces acting on the fluid element in X,Y,Z direction , respectively.

For Newtonian fluids the normal stress and shear stress components are given by the equations (3.36) and (3.37) [20]:

$$\tau_{xx}=2\mu\frac{\partial u}{\partial x} \qquad \tau_{yy}=2\mu\frac{\partial v}{\partial y} \qquad \tau_{zz}=2\mu\frac{\partial w}{\partial z} \tag{3.36}$$

$$\tau_{xy}=\mu\left(\frac{\partial u}{\partial y}+\frac{\partial v}{\partial x}\right)=\tau_{yx}\ ; \qquad \tau_{xz}=\mu\left(\frac{\partial u}{\partial z}+\frac{\partial w}{\partial x}\right)=\tau_{zx}$$

$$\tau_{yz}=\mu\left(\frac{\partial w}{\partial y}+\frac{\partial v}{\partial z}\right)=\tau_{zy} \tag{3.37}$$

Substituting equations (3.36) and (3.37) in equations (3.33), (3.34) and (3.35)

X-Momentum:

$$\rho\left(\frac{\partial u}{\partial t}+u\frac{\partial u}{\partial x}+v\frac{\partial u}{\partial y}+w\frac{\partial u}{\partial z}\right)=\mu\left(\frac{\partial^2 u}{\partial x^2}+\frac{\partial^2 u}{\partial y^2}+\frac{\partial^2 u}{\partial z^2}\right)-\frac{\partial p}{\partial x}+F_{Bx} \tag{3.38}$$

Y-Momentum:

$$\rho\left(\frac{\partial v}{\partial t}+u\frac{\partial v}{\partial x}+v\frac{\partial v}{\partial y}+w\frac{\partial v}{\partial z}\right)=\mu\left(\frac{\partial^2 v}{\partial x^2}+\frac{\partial^2 v}{\partial y^2}+\frac{\partial^2 v}{\partial z^2}\right)-\frac{\partial p}{\partial y}+F_{By} \tag{3.39}$$

Z-Momentum:

$$\rho\left(\frac{\partial w}{\partial t}+u\frac{\partial w}{\partial x}+v\frac{\partial w}{\partial y}+w\frac{\partial w}{\partial z}\right)=\mu\left(\frac{\partial^2 w}{\partial x^2}+\frac{\partial^2 w}{\partial y^2}+\frac{\partial^2 w}{\partial z^2}\right)-\frac{\partial p}{\partial z}+F_{Bz} \tag{3.40}$$

- **Nondimesionalization of Flow Equations**

To see the effect of various terms in a governing differential, one has to perform a nondimensionalization analysis. Equations (3.38) can be written in non-dimensional form as [20]:

$$\left(\frac{\partial \bar{u}}{\partial \bar{t}}+\bar{u}\frac{\partial \bar{u}}{\partial \bar{x}}+\bar{v}\frac{\partial \bar{u}}{\partial \bar{y}}+\bar{w}\frac{\partial \bar{u}}{\partial \bar{z}}\right)=\frac{1}{\mathrm{Re}}\left(\frac{\partial^2 \bar{u}}{\partial \bar{x}^2}+\frac{\partial^2 \bar{u}}{\partial \bar{y}^2}+\frac{\partial^2 \bar{u}}{\partial \bar{z}^2}\right)+\frac{\partial \bar{p}}{\partial \bar{x}} \tag{3.41}$$

where

$$\bar{v}=\frac{v}{U}\ ;\ \ \bar{w}=\frac{w}{U};\ \bar{u}=\frac{u}{U};\ \bar{x}=\frac{x}{L};\ \bar{y}=\frac{y}{L};\ \ \bar{z}=\frac{z}{L};\ \bar{t}=\frac{U}{L}t$$

$$\bar{p}=\frac{p}{p_{ref}};\ \ p_{ref}=\rho U^2$$

U and *L* are the reference velocity and length. In equation (3.41), Re is the Reynolds number. Physically, Reynolds number represents the ratio of inertia forces to viscous forces. When Re is large then the viscous forces are insignificant in comparison to the inertia forces. When Re is small then the inertia forces becomes insignificant in comparison to the viscous forces. Most of the lubrication problems are characterized by low Reynolds number condition where the flow is laminar and the viscous forces dominate over the inertia terms. Equations (3.29) – (3.41) cover the background required to understand and derive Reynolds Lubrication Equation (RLE).

Subjected to the thin-film lubrication approximation, the pressure in a lubricant film is governed by Reynolds equation. Assuming laminar, incompressible, inertialess, Newtonian fluid; the Reynolds equation in Catesian-cordinate system for a slider bearing obtained from momentum equations is given by [20]:

$$\underbrace{\frac{\partial}{\partial x}\left(\frac{\rho h^3}{12\mu}\frac{\partial P}{\partial x}\right)+\frac{\partial}{\partial y}\left(\frac{\rho h^3}{12\mu}\frac{\partial P}{\partial y}\right)}_{Poiseuille\ terms}=\frac{1}{2}\underbrace{\frac{\partial}{\partial x}\left[\rho(U_a+U_b)h\right]}_{Couette\ term}-\underbrace{\rho U_b\frac{\partial h}{\partial x}}_{\substack{geometric\\ Squeeze}}$$

$$\underbrace{\rho(w_b-w_a)}_{normal\ Squeeze}+\underbrace{h\frac{\partial \rho}{\partial t}}_{Local\ Expansion} \qquad (3.42)$$

where U_a and U_b are linear velocities of the top and bottom plate, respectively as shown in Figure 3.5. w_a and w_b are the normal squeeze component of top and bottom plates, respectively in the *z* direction and $h = h(x, y)$ is the arbitrary lubricant film thickness as shown in Figure 3.5.

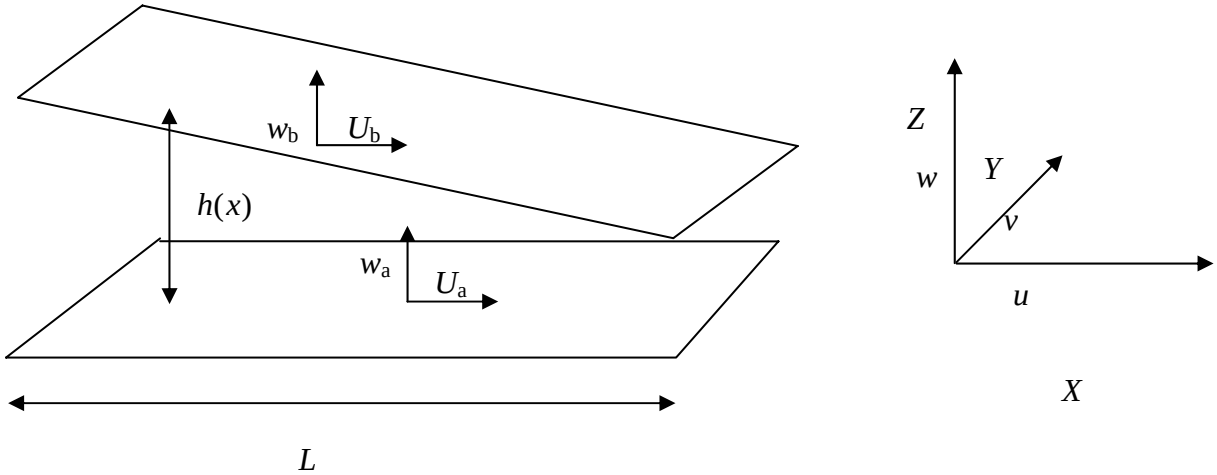

Figure 3.5: Slider Bearing Configuration [20]

Equation (3.42) is known as classic Reynolds lubrication equation. To further gain insight in to the mechanism of pressure development in thin oil film we expand the Couette terms on RHS of the equation (3.42) [20].

$$\underbrace{\frac{1}{2}\frac{\partial}{\partial x}\left[\rho(U_a+U_b)h\right]}_{Couette\ term}=\underbrace{\frac{1}{2}\rho h\frac{\partial}{\partial x}(U_a+U_b)}_{Physical\ Stretch}+\frac{1}{2}\rho(U_a+U_b)\underbrace{\frac{\partial h}{\partial x}}_{\substack{Physical\\ Wedge}}$$

$$\frac{1}{2}\rho(U_a+U_b)\underbrace{\frac{\partial \rho}{\partial x}}_{\substack{Density\\ Wedge}} \qquad (3.43)$$

For the analysis of a hydrodynamic journal bearing we can neglect the stretch terms, density wedge and the local expansion terms. A simplified Reynolds equation is given by [20]:

$$\underbrace{\frac{\partial}{\partial x}\left(\frac{\rho h^3}{12\mu}\frac{\partial P}{\partial x}\right)+\frac{\partial}{\partial y}\left(\frac{\rho h^3}{12\mu}\frac{\partial P}{\partial y}\right)}_{Poiseuille\ terms}=\frac{1}{2}\rho(U_a+U_b)\underbrace{\frac{\partial h}{\partial x}}_{\substack{Physical\\ Wedge}}+\underbrace{\rho(w_b-w_a)}_{normal\ Squeeze} \qquad (3.44)$$

In a self acting oil bearings pressure or lift is generated by the oil film due to the presence of physical wedge and due to normal squeeze action. Pressure development due to normal squeeze is based on the fact that it takes finite amount of time to squeeze out the lubricant between two approaching surfaces.

3.3 Reduction of Reynolds Lubrication Equation (RLE) to Short Bearing Approximation

Equation (3.64) is a Partial differential equation (PDE) but with few approximations can be reduced to linear ordinary differential equation (ODE) for which closed form analytical solution exists. But first equation (3.44) has to non-dimensionalised. Let us

consider the simple case of a slider bearing with stationary bottom plate and top plate moving with velocity *U*. RLE for incompressible fluid equation (3.44) is [20]:

$$\frac{\partial}{\partial x}\left(\frac{h^3}{12\mu}\frac{\partial P}{\partial x}\right)+\frac{\partial}{\partial y}\left(\frac{h^3}{12\mu}\frac{\partial P}{\partial y}\right)=\frac{1}{2}U\frac{\partial h}{\partial x}+\frac{\partial h}{\partial t}$$

(3.45)

Let

$$\bar{x}=\frac{x}{L};\ \bar{y}=\frac{x}{B};\ \ \bar{h}=\frac{h}{h_2};\ \ \bar{t}=\frac{t}{t_{ref}};\ \bar{P}=\frac{P}{P_{ref}} \tag{3.46}$$

Substituting the equation (3.46) in equation (3.45) [20]:

$$\frac{P_{ref}h_2^2}{12\mu L^2}\frac{\partial}{\partial \bar{x}}\left(\bar{h}^3\frac{\partial \bar{P}}{\partial \bar{x}}\right)+\frac{P_{ref}h_2^2}{12\mu B^2}\frac{\partial}{\partial \bar{y}}\left(\bar{h}^3\frac{\partial \bar{P}}{\partial \bar{y}}\right)=\frac{U}{2L}\frac{\partial \bar{h}}{\partial \bar{x}}+\frac{1}{t_{ref}}\frac{\partial \bar{h}}{\partial \bar{t}} \tag{3.47}$$

Let $P_{ref}=\mu LU/h_2^2$ and $t_{ref}=L/U$ equation (3.47) simplifies to

$$\frac{\partial}{\partial \bar{x}}\left(\bar{h}^3\frac{\partial \bar{P}}{\partial \bar{x}}\right)+\left(\frac{L}{B}\right)^2\frac{\partial}{\partial \bar{y}}\left(\bar{h}^3\frac{\partial \bar{P}}{\partial \bar{y}}\right)=6\frac{\partial \bar{h}}{\partial \bar{x}}+12\frac{\partial \bar{h}}{\partial \bar{t}} \tag{3.48}$$

Infinitely Short Bearing (ISA) approximation. $B<<L\ \Rightarrow\ (L/B)^2>>1$ then the first term on LHS in equation (3.48) can be neglected in comparison to the second term on LHS. Physically this means that the flow in the direction of motion is negligible in comparison to the leakage term. Also neglecting the squeeze term i.e. for steady state case equation (3.48) reduces to

$$\left(\frac{L}{B}\right)^2\frac{d}{d\bar{y}}\left(\bar{h}^3\frac{d\bar{P}}{d\bar{y}}\right)=6\frac{d\bar{h}}{d\bar{x}} \tag{3.49}$$

Equation (3.49) is a linear ODE which has close form analytical solution. To relate equation (3.49) for plain cylindrical journal bearing configuration the film thickness profile can be approximated by (Figure 3.2):

$$h \approx C + e\cos\theta$$

where

C = radial clearance

For journal bearing the ISA pressure equation is given by [20]:

$$\frac{d}{dy}\left(\frac{h^3}{\mu}\frac{dP}{dy}\right) = 6U\frac{dh}{dx} \tag{3.50}$$

Integrating the equation (3.50) twice we get

$$P = \frac{3\mu U}{h^3}\frac{dh}{dx}y^2 + Ay + B \tag{3.51}$$

Applying the boundary conditions $P = 0$ at $y = \pm L/2$ to equation (3.51) [20]:

$$P = \frac{3\mu U}{h^3}\left(y^2 - \frac{L^2}{4}\right)\frac{dh}{dx} \tag{3.52}$$

Since the clearance C is very small in comparison to the journal radius R then curvature effects can be neglected and the oil film can be regarded as a film between two parallel plates. Considering $x = R\theta$ and $dh/d\theta = -C\varepsilon\sin\theta/R$ then the pressure distribution in equation (3.52) is reduced to [20]:

$$P = -\frac{3\mu U}{C^2 R}\left(y^2 - \frac{L^2}{4}\right)\frac{\varepsilon\sin\theta}{(1+\varepsilon\sin\theta)^3} \tag{3.53}$$

To non-dimensionalize the above equation let $\bar{h} = h/C,\ \bar{y} = y/L,\ \bar{P} = (C^2 R/\mu U L^2)P$ [20]:

$$\bar{P} = 3\left(-\bar{y}^2 + \frac{1}{4}\right)\frac{\varepsilon \sin\theta}{(1+\varepsilon\sin\theta)^3} \tag{3.54}$$

Once the pressure profile is obtained by solving the simplified Reynolds equation. Then the other bearing performance parameters such as load carrying capacity, oil flow rate, and leakage rate can be calculated.

Load Carrying Capacity

Referring to Figure 3.6 the components of pressure in radial and tangential directions given by [20]:

$$F_{\varepsilon} = \int_{-L/2}^{L/2}\int_{0}^{2\pi} P\cos\theta d\theta \tag{3.55}$$

$$F_{\phi} = \int_{-L/2}^{L/2}\int_{0}^{2\pi} P\sin\theta d\theta \tag{3.56}$$

Figure 3.7 shows the non-dimensional fluid-film forces in radial and tangential directions obtained by solving equations (3.55) and (3.56), respectively.

The various design parameters for Short bearing assuming half Sommerfeld condition are [20]:

$$\bar{F}_{\varepsilon} = \frac{-\varepsilon^2}{\left(1-\varepsilon^2\right)^2} \;;\; \bar{F}_{\phi} = \frac{\pi}{4}\frac{-\varepsilon}{\left(1-\varepsilon^2\right)^{3/2}} \tag{3.57}$$

$$\bar{W} = \sqrt{\bar{F}_{\varepsilon}^2 + \bar{F}_{\phi}^2} = \frac{\pi}{4}\frac{\varepsilon}{\left(1-\varepsilon^2\right)^2}\sqrt{\left(\frac{16}{\pi^2}-1\right)\varepsilon^2+1} \tag{3.58}$$

$$\phi = \frac{\bar{F}_{\phi}}{\bar{F}_{\varepsilon}} = \tan^{-1}\left(\frac{\pi}{4}\frac{\sqrt{1-\varepsilon^2}}{\varepsilon}\right) \tag{3.59}$$

$$S = \frac{\left(1-\varepsilon^2\right)^2}{\pi\varepsilon\left[\pi^2(1-\varepsilon^2)+16\varepsilon^2\right]^5}\left(\frac{D}{L}\right)^2 \tag{3.60}$$

Figure 3.7 shows the non-dimensional fluid-film forces in radial and tangential directions obtained by solving equation (3.57).

This entire section was dealt with stationary film with no transient effects. In later sections this thesis deals with transient effects where $dh/dt \neq 0$.

3.4 Theoretical Prediction of Oil Whirl Instability Based on Linearized Theory

As discussed earlier, the source of oil whirl instability is the hydrodynamic forces generated in the lubricant film. These forces as shown in Figure 3.7 are the strong functions of the journal eccentricity ε and the attitude angle ϕ. If the squeeze film terms in the simplified RLE are also considered, then these forces will also be the function of velocity components $d\varepsilon/dt$ and $d\phi/dt$ as shown in equation (3.61) and (3.62). Squeeze film terms makes the simplified RLE transient. Usually any unbalance in the rotor or any other dynamic forces are incorporated in RLE through squeeze film terms. The fluid-film forces for the short bearing are given by [21]:

$$\bar{F}_\varepsilon = -\mu RL\left(\frac{L}{C}\right)^2\left[\frac{(\omega-2\dot{\phi})\varepsilon^2}{\left(1-\varepsilon^2\right)^2}+\frac{\pi(1+2\varepsilon^2)\dot{\varepsilon}}{2\left(1-\varepsilon^2\right)^{2.5}}\right] \tag{3.61}$$

$$\bar{F}_\phi = \mu RL\left(\frac{L}{C}\right)^2\left[\frac{(\omega-2\dot{\phi})\pi\varepsilon}{4\left(1-\varepsilon^2\right)^{1.5}}+\frac{2\varepsilon\dot{\varepsilon}}{\left(1-\varepsilon^2\right)^2}\right] \tag{3.62}$$

In this section the bearing dynamic coefficients as shown in Figure 3.9 and the threshold speed of oil whirl instability are obtained by a linear perturbation analysis. The oil-film

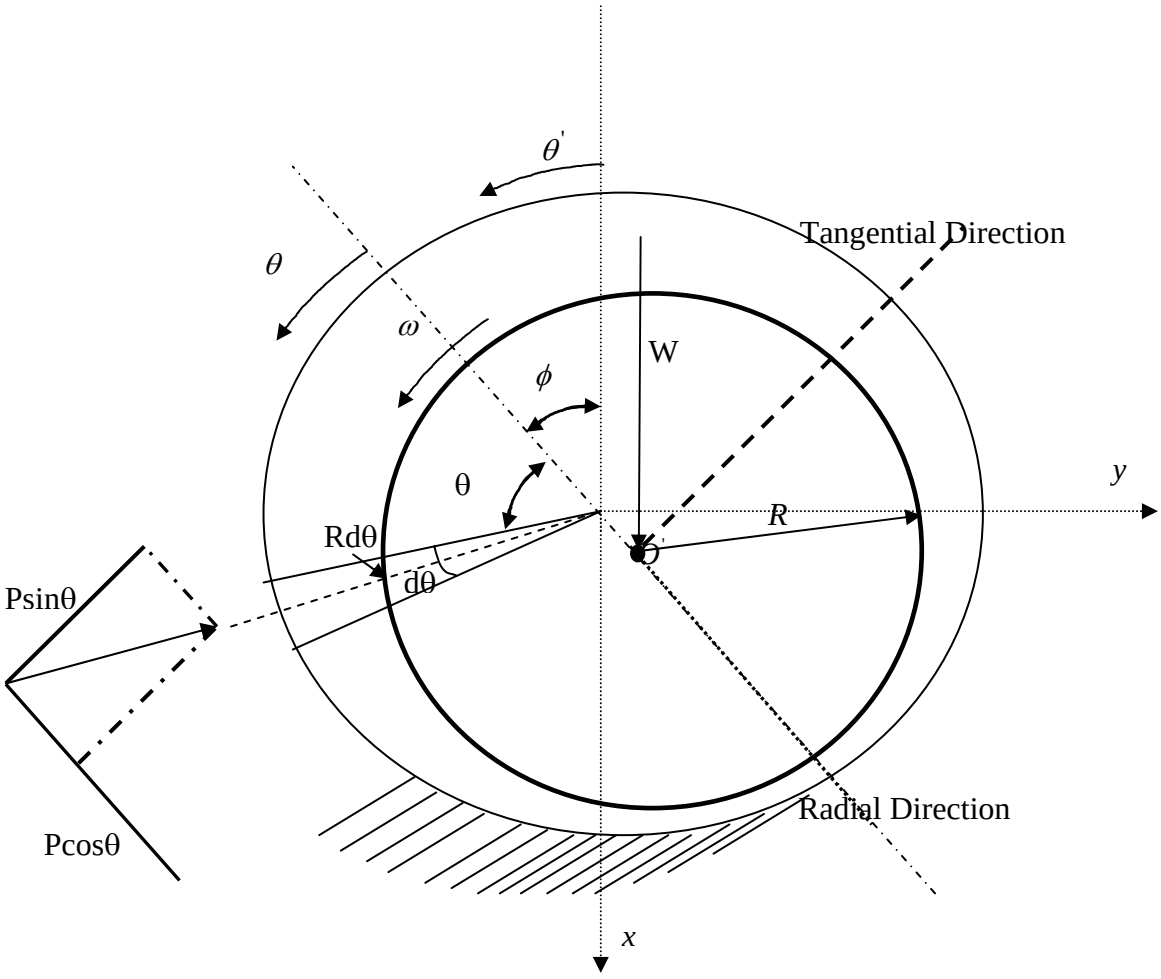

Figure 3.6: Radial and Tangential Force Components

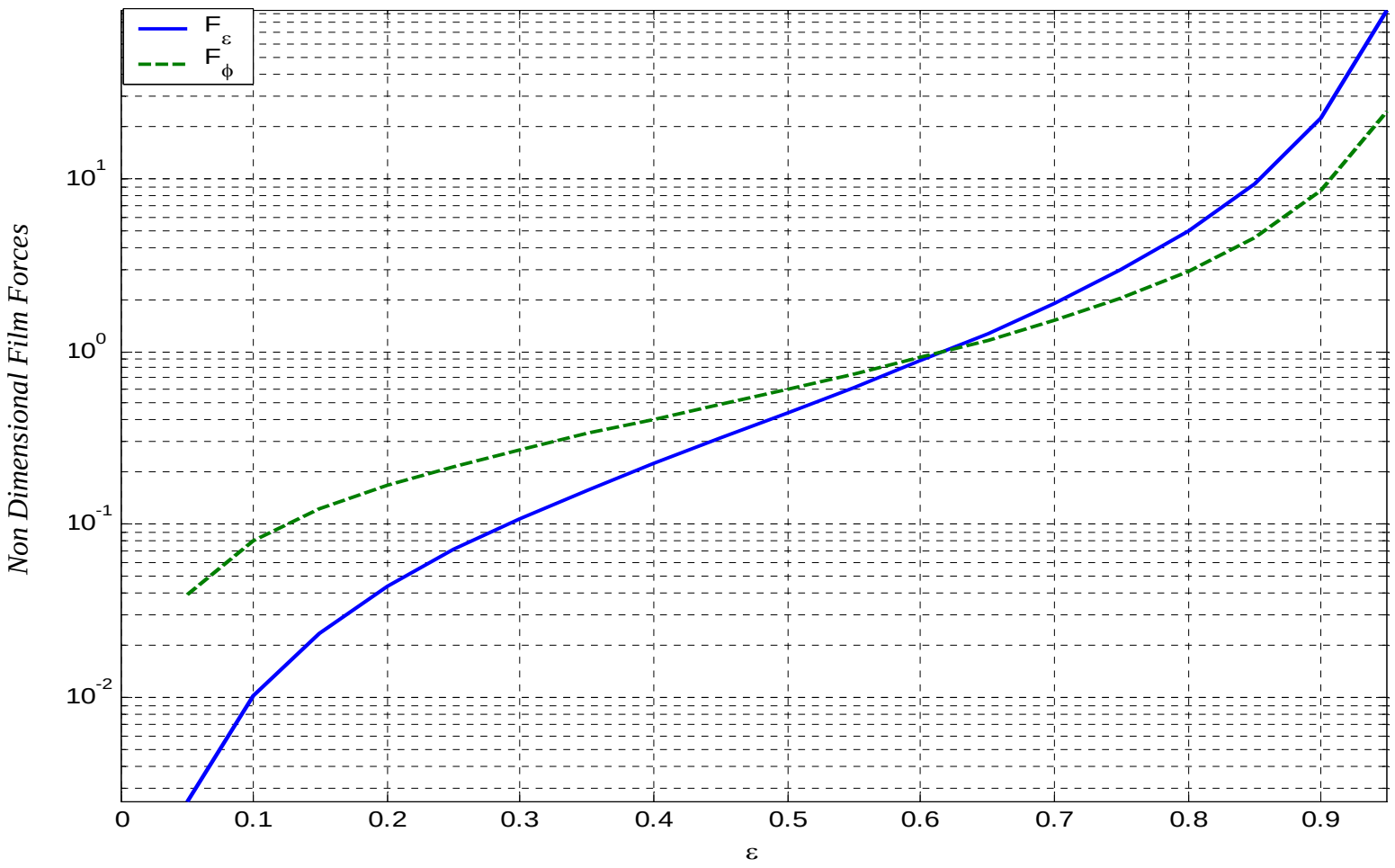

Figure 3.7: Oil Film Forces in Radial and Tangential Direction vs. Eccentricity ratio

forces obtained from equations (3.61) and (3.62) are non-linear (but continuous) functions of the journal motion in the bearing. Thus, fluid-film forces may be expanded in a Taylor series about the static equilibrium position. For sufficiently small motions, the corresponding changes in the journal fluid-film force components about equilibrium can thus be linearized for displacement and velocity perturbations. By neglecting the higher order inertia forces (a function of acceleration $\ddot{\varepsilon}$ and $\ddot{\phi}$), using the Taylor series expansion, a small perturbation of the displacement and the velocity about steady state position (ε_0, ϕ_0) in the radial and tangential direction fluid-film forces can be expressed as:

$$\bar{F}_{\varepsilon} = \bar{F}_{\varepsilon_0} + \frac{\partial \bar{F}_{\varepsilon}}{\partial \varepsilon}\Delta\varepsilon + \frac{\partial \bar{F}_{\varepsilon}}{\varepsilon_0 \partial \phi}\varepsilon_0 \Delta\phi + \frac{\partial \bar{F}_{\varepsilon}}{\partial \dot{\varepsilon}}\Delta\dot{\varepsilon} + \frac{\partial \bar{F}_{\varepsilon}}{\varepsilon_0 \partial \dot{\phi}}\varepsilon_0 \Delta\dot{\phi} \tag{3.63}$$

$$\bar{F}_{\phi} = \bar{F}_{\phi_0} + \frac{\partial \bar{F}_{\phi}}{\partial \varepsilon}\Delta\varepsilon + \frac{\partial \bar{F}_{\phi}}{\varepsilon_0 \partial \phi}\varepsilon_0 \Delta\phi + \frac{\partial \bar{F}_{\phi}}{\partial \dot{\varepsilon}}\Delta\dot{\varepsilon} + \frac{\partial \bar{F}_{\phi}}{\varepsilon_0 \partial \dot{\phi}}\varepsilon_0 \Delta\dot{\phi} \tag{3.64}$$

From equations (3.63) and (3.64) the fluid-film forces in the radial and tangential directions, respectively can be represented as:

$$\bar{F}_{\varepsilon} = \bar{F}_{\varepsilon}(\varepsilon, \phi_0, \dot{\varepsilon}, \dot{\phi}) \tag{3.65}$$

$$\bar{F}_{\phi} = \bar{F}_{\phi}(\varepsilon, \phi_0, \dot{\varepsilon}, \dot{\phi}) \tag{3.66}$$

From equations (3.63) and (3.64) stiffness coefficients are given by:

$$\bar{K}_{\varepsilon\varepsilon} = \frac{\Delta \bar{F}_{\varepsilon}}{\Delta\varepsilon}; \bar{K}_{\phi\phi} = \frac{\Delta \bar{F}_{\phi}}{\varepsilon_0 \Delta\phi}$$

$$\bar{K}_{\varepsilon\phi} = \frac{\Delta \bar{F}_{\varepsilon}}{\varepsilon_0 \Delta\phi}; \bar{K}_{\phi\varepsilon} = \frac{\Delta \bar{F}_{\phi}}{\Delta\varepsilon}; \tag{3.67}$$

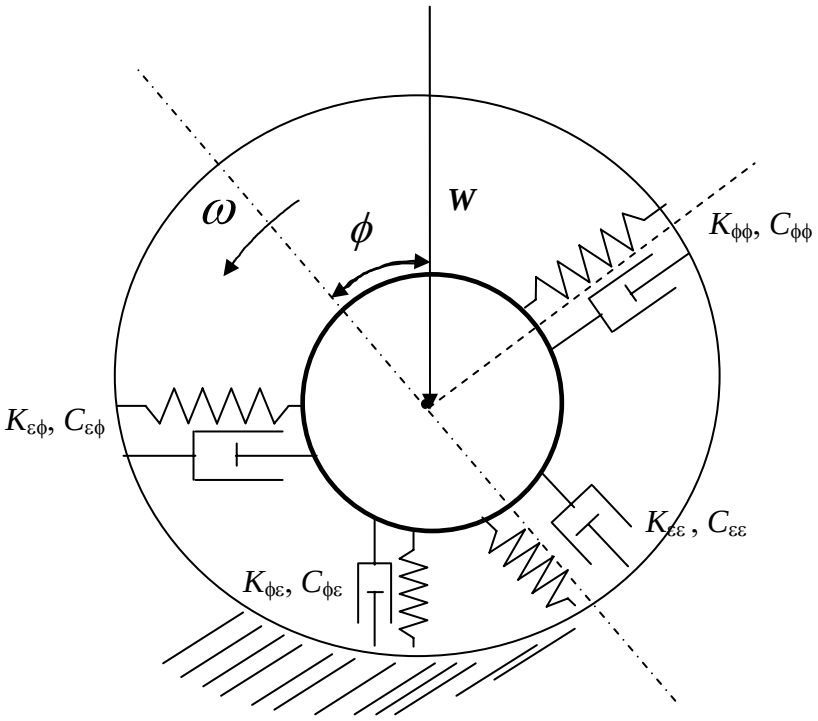

Figure 3.8: Dynamic Coefficients of a Journal Bearing System

and damping coefficients are given by:

$$\bar{C}_{\varepsilon\varepsilon} = \frac{\Delta \bar{F}_{\varepsilon}}{\Delta \dot{\varepsilon}}; \bar{C}_{\phi\phi} = \frac{\Delta \bar{F}_{\phi}}{\varepsilon_0 \Delta \dot{\phi}};$$

$$\bar{C}_{\varepsilon\phi} = \frac{\Delta \bar{F}_{\varepsilon}}{\varepsilon_0 \Delta \dot{\phi}}; \bar{C}_{\phi\varepsilon} = \frac{\Delta \bar{F}_{\phi}}{\Delta \dot{\varepsilon}}; \qquad (3.68)$$

where $\Delta\dot{\varepsilon}$ and $\varepsilon_0 \Delta\dot{\phi}$ are the journal radial and tangential velocities in (ε, ϕ) co-ordinate system. Force coefficients can be transformed into (*X*, *Y*) rectangular co-ordinate system as defined by equations A1 and A2 (see Appendix A).

Rotordynamic coefficients in present the analysis are computed numerically by perturbing steady state oil film thickness $\bar{h}_0$ given by equation (3.69) in the radial and tangential directions.

$$\bar{h}_0 = 1 + \varepsilon_0 \cos\theta \tag{3.69}$$

where $\theta = \theta' - \phi_0$.

First order perturbed oil film thickness, which is perturbed about the steady state position (ε_0, ϕ_0) is given by:

$$\bar{h} = \bar{h}_0 \pm \Delta h = 1 + (\varepsilon_0 \pm \Delta\varepsilon)\cos(\theta \pm \Delta\phi) \tag{3.70}$$

Trigonometric sine and cosine function of $\Delta\phi$ in equation (3.70) may be expanded using Taylor series expansion as shown in equation B1and B2 (see Appendix B).The detailed procedure to calculate the rotordynamic coefficients is presented in section 5.3.

The dimensionless dynamic coefficients with the short bearing assumption in (*X, Y*) fixed co-ordinate system is given by [11].

Stiffness Coefficients are [11]

$$\bar{K}_{xx} = \frac{4\left[2\pi^2 + (16-\pi^2)\varepsilon^2\right]}{\left[\pi^2 + (16-\pi^2)\varepsilon^2\right]^{1.5}}$$

$$\bar{K}_{xy} = \frac{-\pi\left[-\pi^2 + 2\pi^2\varepsilon^2 + (16-\pi^2)\varepsilon^4\right]}{\varepsilon(1-\varepsilon^2)^{1.5}\left[\pi^2 + (16-\pi^2)\varepsilon^2\right]^{1.5}}$$

$$\bar{K}_{yx} = \frac{-\pi\left[\pi^2 + (32+\pi^2)\varepsilon^2 + 2(16-\pi^2)\varepsilon^4\right]}{\varepsilon(1-\varepsilon^2)^{1.5}\left[\pi^2 + (16-\pi^2)\varepsilon^2\right]^{1.5}}$$

$$\bar{K}_{yy} = \frac{4\left[\pi^2 + (32+\pi^2)\varepsilon^2 + 2(16-\pi^2)\varepsilon^4\right]}{(1-\varepsilon^2)\left[\pi^2 + (16-\pi^2)\varepsilon^2\right]^{1.5}} \tag{3.71}$$

Damping Coefficients are [11]

$$\bar{C}_{xx} = \frac{2\pi(1-\varepsilon^2)^{1.5}\left[\pi^2 + 2(\pi^2-8)\varepsilon^2\right]}{\varepsilon\left[\pi^2 + (16-\pi^2)\varepsilon^2\right]^{1.5}}$$

$$\bar{C}_{xy} = \frac{-8\left[\pi^2 + 2(\pi^2-8)\varepsilon^2\right]}{\left[\pi^2 + (16-\pi^2)\varepsilon^2\right]^{1.5}}$$

$$\bar{C}_{yx} = \bar{C}_{xy}$$

$$\bar{C}_{yy} = \frac{2\pi\left[\pi^2 + 2(24-\pi^2)\varepsilon^2 + \pi^2\varepsilon^4\right]}{\varepsilon(1-\varepsilon^2)^{1.5}\left[\pi^2 + (16-\pi^2)\varepsilon^2\right]^{1.5}} \tag{3.72}$$

The whirl threshold for rigid shaft as function of dynamic stiffness and damping coefficients which are functions of eccentricity ratio is given by equation (3.73) [22]:

$$\bar{\omega}_r = \sqrt{\frac{g_2 g_{32} g_4}{g_4^2 - g_2 g_{31} g_4 + g_2^2 g_5}} \tag{3.73}$$

Where

$$g_2 = \bar{C}_{xx} + \bar{C}_{yy}$$

$$g_{31} = \bar{K}_{xx} + \bar{K}_{yy}$$

$$g_{32} = \bar{C}_{xx}\,\bar{C}_{yy} - \bar{C}_{xy}\,\bar{C}_{yx}$$

$$g_4 = \bar{K}_{xx}\,\bar{C}_{yy} + \bar{K}_{yy}\,\bar{C}_{xx} - \bar{K}_{xy}\,\bar{C}_{yx} - \bar{K}_{yx}\,\bar{C}_{xy}$$

$$g_5 = \bar{K}_{xx}\,\bar{K}_{yy} - \bar{K}_{xy}\,\bar{K}_{yx}$$

The stability map for the various Sommerfeld number against threshold speed is shown in Figure 3.9. The region below the threshold line is **stable region**. While region above threshold line is **unstable region**. For a particular rotor bearing system first the

Sommerfeld number for a given operating conditions and bearing geometry is computed followed by the calculation of the non-dimensional operating speed $\bar{\omega}$. If the $\bar{\omega}$ for the corresponding Sommerfeld number lies above the threshold line then the bearing will unstable, otherwise if its below the threshold line then the bearing will be free from oil whirl instability.

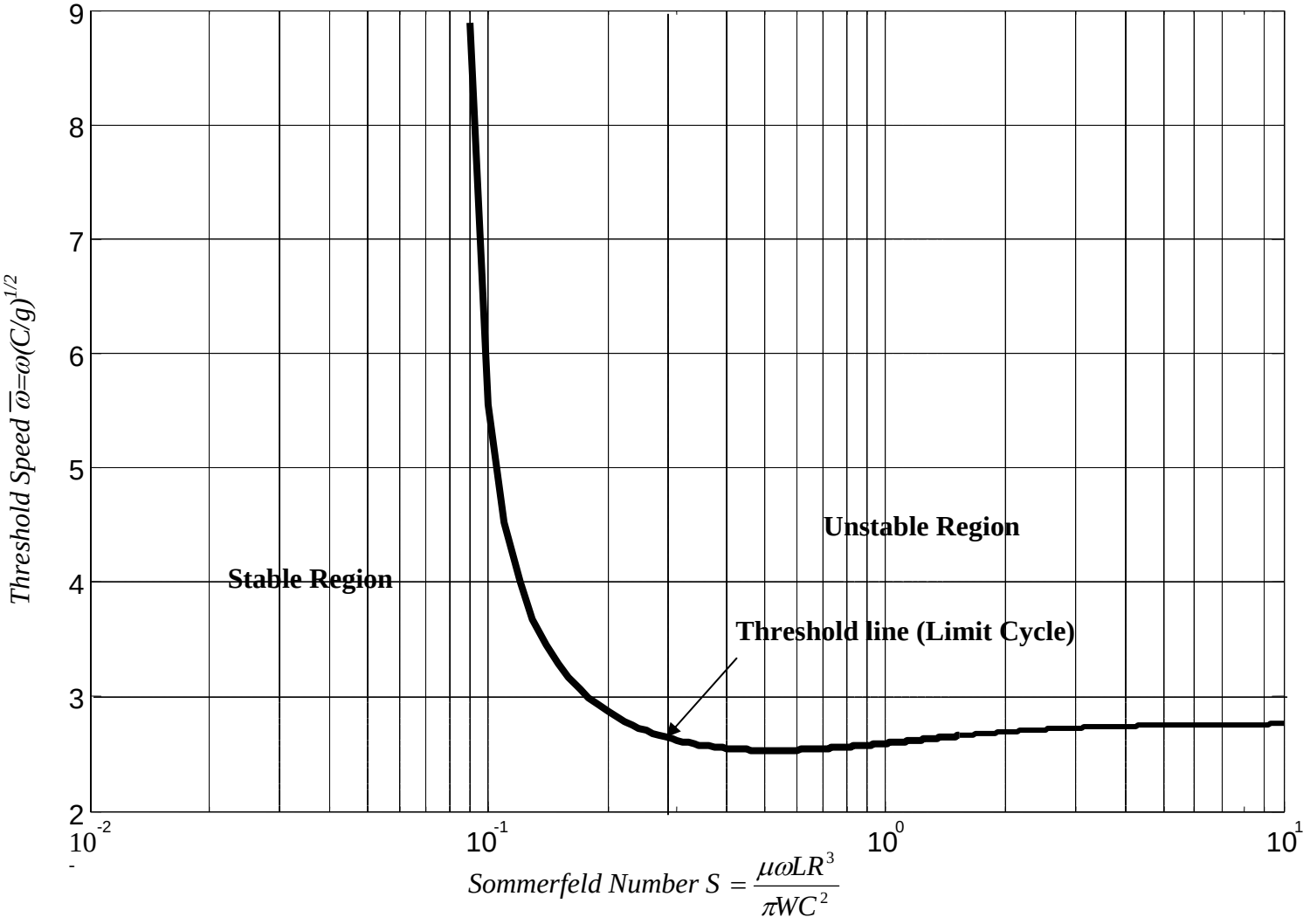

Figure 3.9: Stability of single mass on a 360^0 Journal Bearing

4. Orbit Analysis of Journal Bearing System

The procedure for predicting the onset of oil whirl instability using the linear stability analysis was presented in the previous chapter. The stability map presented is based on the linearized bearing reactions which is only valid for the small amplitude vibration. By performing a **non-linear transient analysis** of a journal bearing system (orbit analysis) one can gain significant insights into the phenomenon of oil whirl. By performing orbit analysis one can also simulate the response of rotor unbalance on the oil film bearing reactions.

The present chapter discusses about the stable, unstable and limit cycles types of whirl orbits encountered in practice. A brief discussion on the effect of unbalance on oil whirl is also presented.

4.1 Equations of Motion

By non-dimensionalising the equations (3.27), (3.28), (3.61) and (3.62):

$$\ddot{\varepsilon} - \dot{\phi}^2 \varepsilon + \bar{F}_{\varepsilon} - \frac{\cos\phi}{\bar{M}} = 0 \tag{4.1}$$

$$\ddot{\phi}\varepsilon + 2\dot{\varepsilon}\dot{\phi} - \bar{F}_{\phi} + \frac{\sin\phi}{\bar{M}} = 0 \tag{4.2}$$

The fluid film forces based on short bearing theory is given by [21]:

$$\bar{F}_{\varepsilon} = -\frac{\mu RL}{mC\omega^2}\left(\frac{L}{C}\right)^2 \left[\frac{(\omega - 2\dot{\phi})\varepsilon^2}{\left(1-\varepsilon^2\right)^2} + \frac{\pi(1+2\varepsilon^2)\dot{\varepsilon}}{2\left(1-\varepsilon^2\right)^{2.5}} \right] \tag{4.3}$$

$$\bar{F}_{\phi} = \frac{\mu RL}{mC\omega^2}\left(\frac{L}{C}\right)^2\left[\frac{\pi(\omega - 2\dot{\phi})\varepsilon}{4\left(1-\varepsilon^2\right)^{1.5}} + \frac{2\varepsilon\dot{\varepsilon}}{\left(1-\varepsilon^2\right)^2}\right] \tag{4.4}$$

where $\bar{F}_{\varepsilon}$, $\bar{F}_{\phi}$ are the non-dimensional fluid-film forces in radial and tangential directions, respectively . $\bar{M}$ is the critical rotor mass and is given by, $\bar{M} = MC\omega^2/W$.

Equations (4.1)-(4.4) form the set of initial value, second order ordinary differential equations (ODE) which are highly non-linear, with no closed-form solution. These equations were solved numerically by applying fourth order Runge-Kutta method. First the two second order ODE's were reduced to four first order ODE's and then simultaneously integrated over time.

These equations are the initial value problem which requires four initial conditions, two for position and two for their time derivative i.e. velocity.

$$\varepsilon(0) = \varepsilon_0$$

$$\phi(0) = \phi_0$$

$$\dot{\varepsilon}(0) = 0$$

$$\dot{\phi}(0) = 0 \tag{4.5}$$

The first two initial conditions represent the position, from where the shaft is released. Other two are initial velocity conditions. Steady state initial attitude angle can be calculated by equation (3.59). In the case of short bearing assumption ϕ_0 for any ε_0 is given by the equation [20]:

$$\phi_0 = \tan^{-1}\left[\frac{\pi(1-\varepsilon_0^2)^{0.5}}{4\varepsilon_0}\right] \tag{4.6}$$

Equation (4.5) shows that the shaft in released from (ε_0, ϕ_0) with zero initial radial and tangential velocities. Once the initial conditions were fed to the computer program; equations (4.1) – (4.4) were solved to generate the locus of the shaft center within the **clearance circle** (Figure 3.2).

4.2 Types of Orbits for Balanced Rotor:

Consider the following bearing design parameters:

Table 4.1 Bearing Geometry Specifications

	SI Units
D	.0508 (m)
L	.0254 (m)
μ	.0254 ($N.s/m^2$)
N	125 (rps)
W	356 (N)
C	1.27×10^{-4} (m)
k_0	0.13 *(W/mK)*
α_0	$0.756 \times 10^{-7} m^2/s$
β_1	$0.0458/K$

Figure 4.1-4.5 shows a series of journal orbit generated by non-linear transient analysis program using the bearing parameters reported in Table 4.1.

To verify the results obtained by the non-linear transient analysis, the eccentricity ratio and the attitude angle were computed by the THD bearing design procedure given by Jang and Khonsari [17]. For the bearing with the bearing geometry given in Table 4.1 and operating with the speed of N=103 rps and under a load of W= 147 *N*, the eccentricity ratio is found to be $\varepsilon_0 = 0.435$ and corresponding attitude angle was found to be $\phi = 58^0$.

Figure 4.1 shows the locus of journal center released from near the center and finally settles down to a steady state equilibrium position at eccentricity ratio of $\varepsilon_0 = 0.45$ and attitude angle of ϕ=56^0 which is also the location of the **minimum film thickness**. It was concluded that the results from THD bearing design method and non-linear transient was in good agreement.

Figure 4.1 shows the case where the rotor-bearing system is **stable** as it reaches the steady state position. Figure 4.2 shows the situation where shaft is released from near the equilibrium position where the initial conditions are $\varepsilon(0) = .44$, ϕ=68^0, $\dot{\varepsilon}(0) = 0$, $\dot{\phi}(0) = 0$, journal settles down to the steady position very quickly. Figure 4.3 shows the situation with same bearing dimension (*D, L* ,μ, *C*) as given in Table 4.1 but with the increased load of 178 N and operating at the speed of 126 rps. As seen from the Figure 4.3, the shaft is released near the center and orbits around in the clearance circle with increasing orbit without settling to an equilibrium point. Under this condition the bearing may eventually fail due to the collapse or loss of lubricating oil film as minimum film thickness is also revolving in orbit. In this case the rotor bearing system is **unstable**. Figure 4.4 shows very interesting case known as **limit cycle** or **threshold speed**

Under this operating condition the rotor orbits in the bearing to form a trajectory, which neither converges nor diverges with time. A small perturbation in the speed can make the system either unstable or stable. This is a type of orbit which represents the threshold state on the stability map, as shown in Figure 3.12. In this situation journal orbits around in “limit cycle” without settling down to equilibrium position. It will neither grow nor is

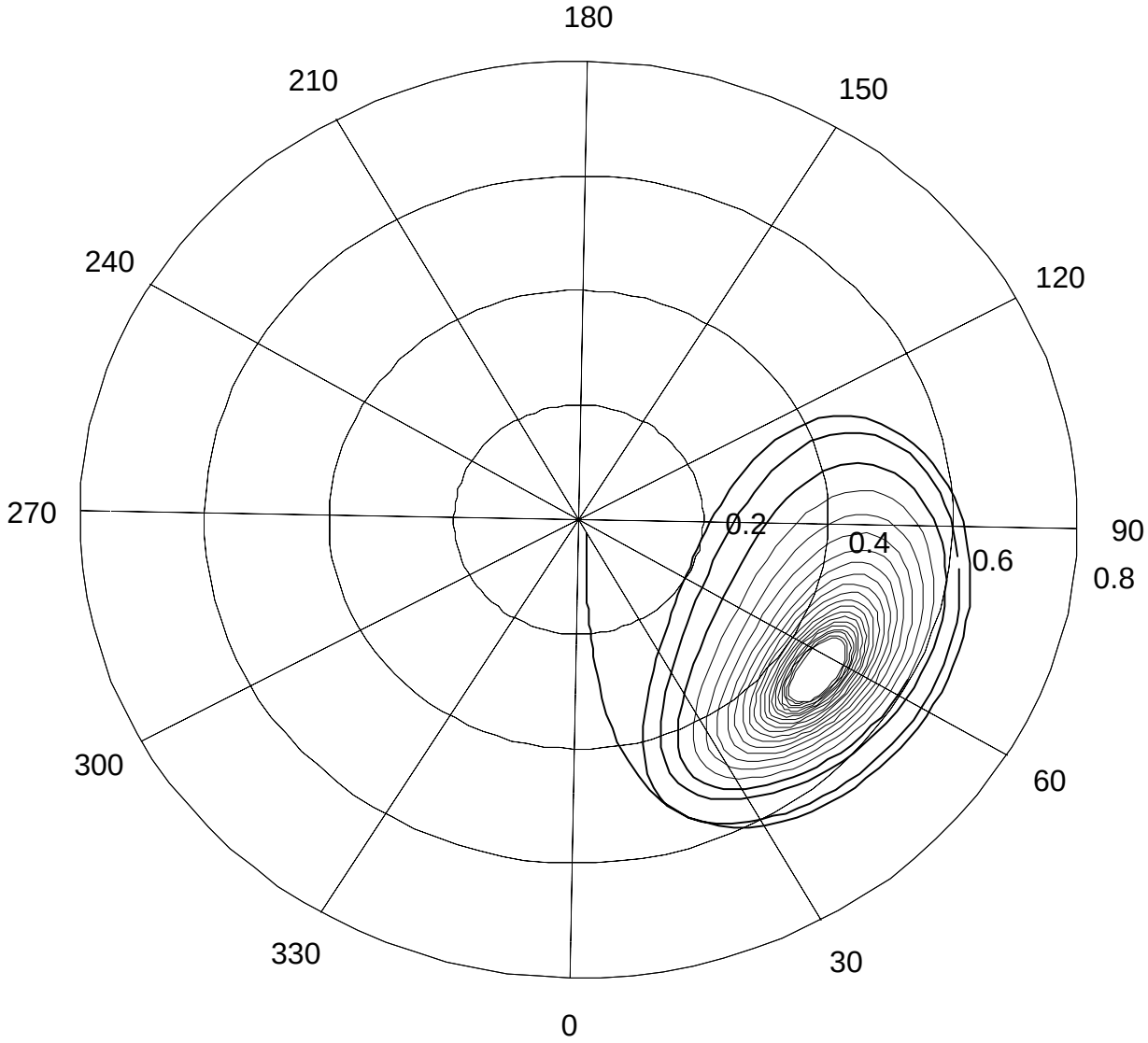

Figure 4.1: Stable Journal Locus ($N = 103$ *rps*, $W = 147$ $N, \varepsilon_0 = 0.45$)

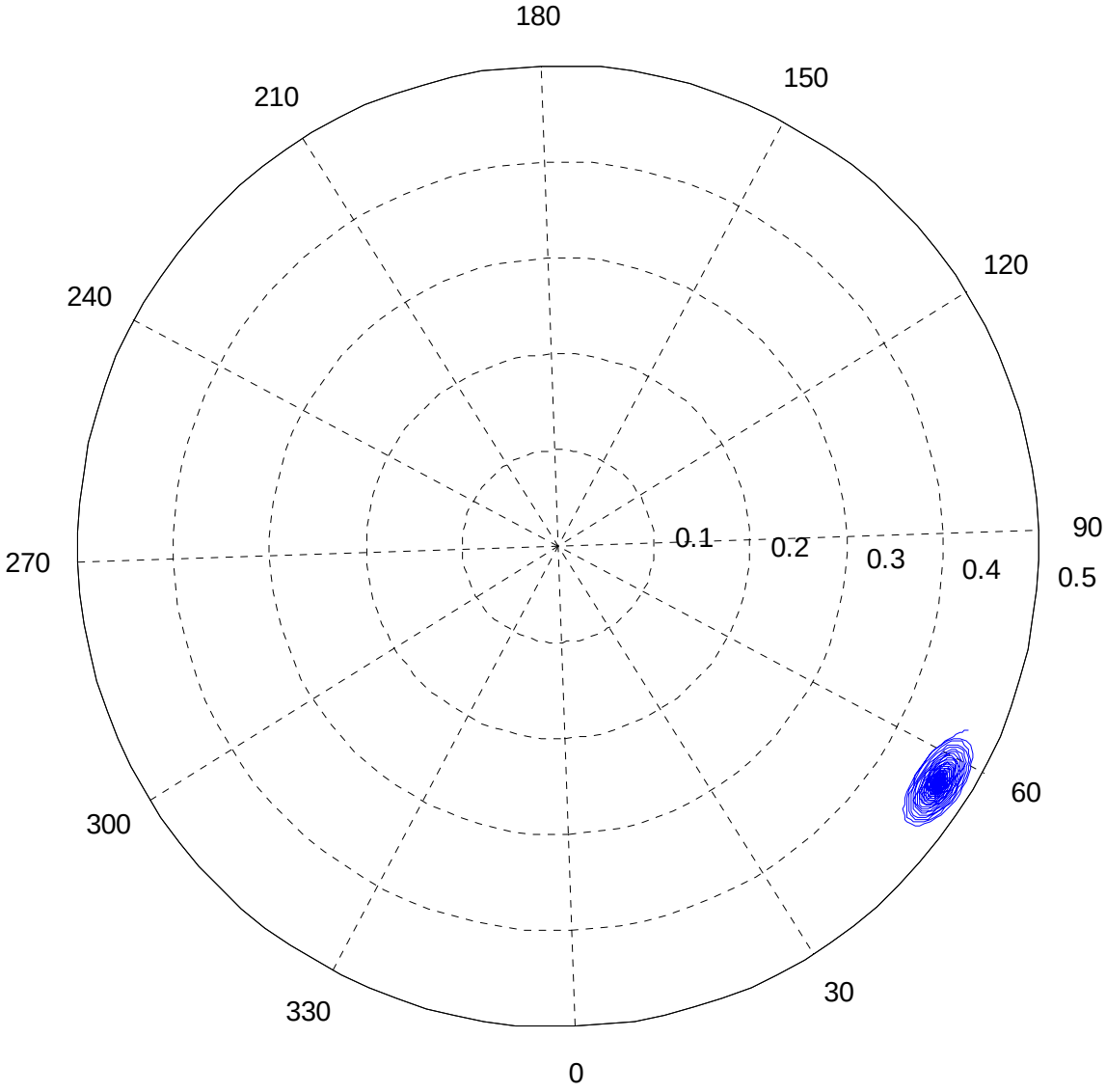

Figure 4.2: Stable Journal Locus ($N = 103$ *rps*, $W = 147$ $N, \varepsilon_0 = 0.45$)

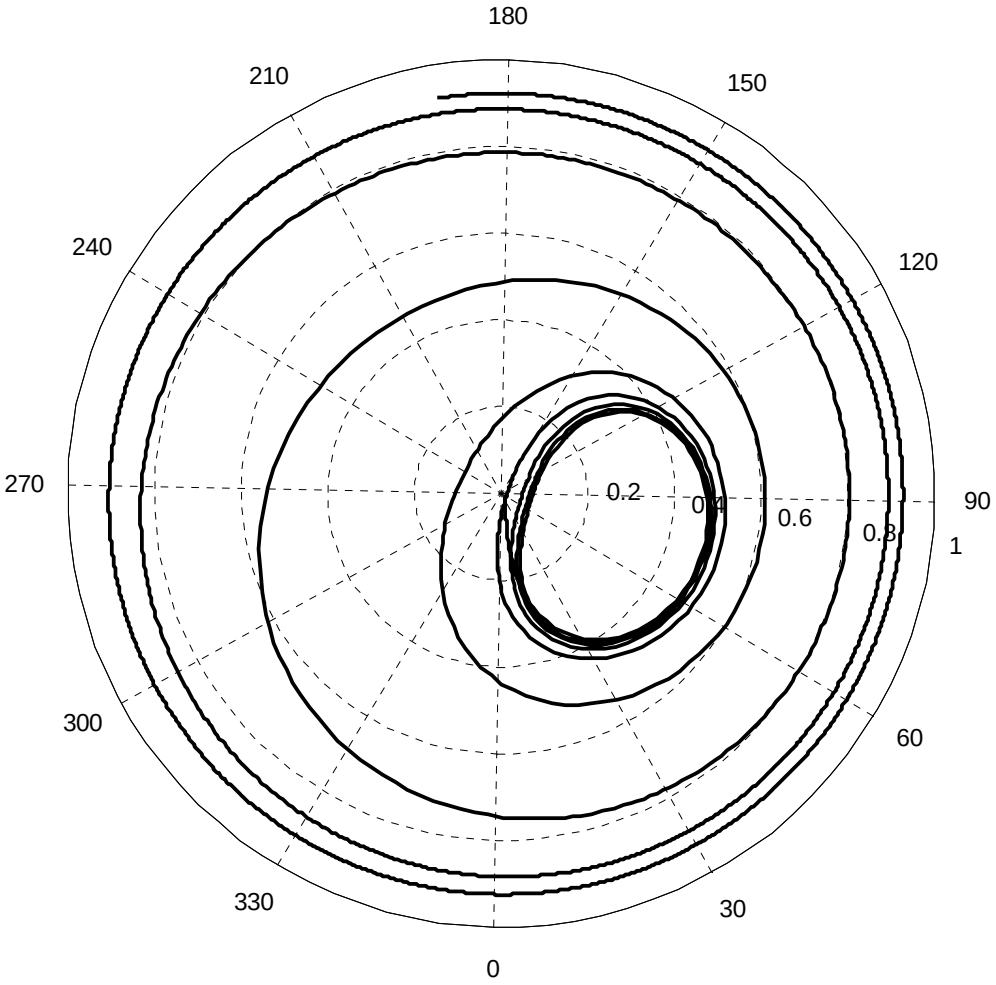

Figure 4.3: Unstable Journal Locus ($N = 126$ *rps*, $W = 178$ $N, \varepsilon_0 = 0.01$)

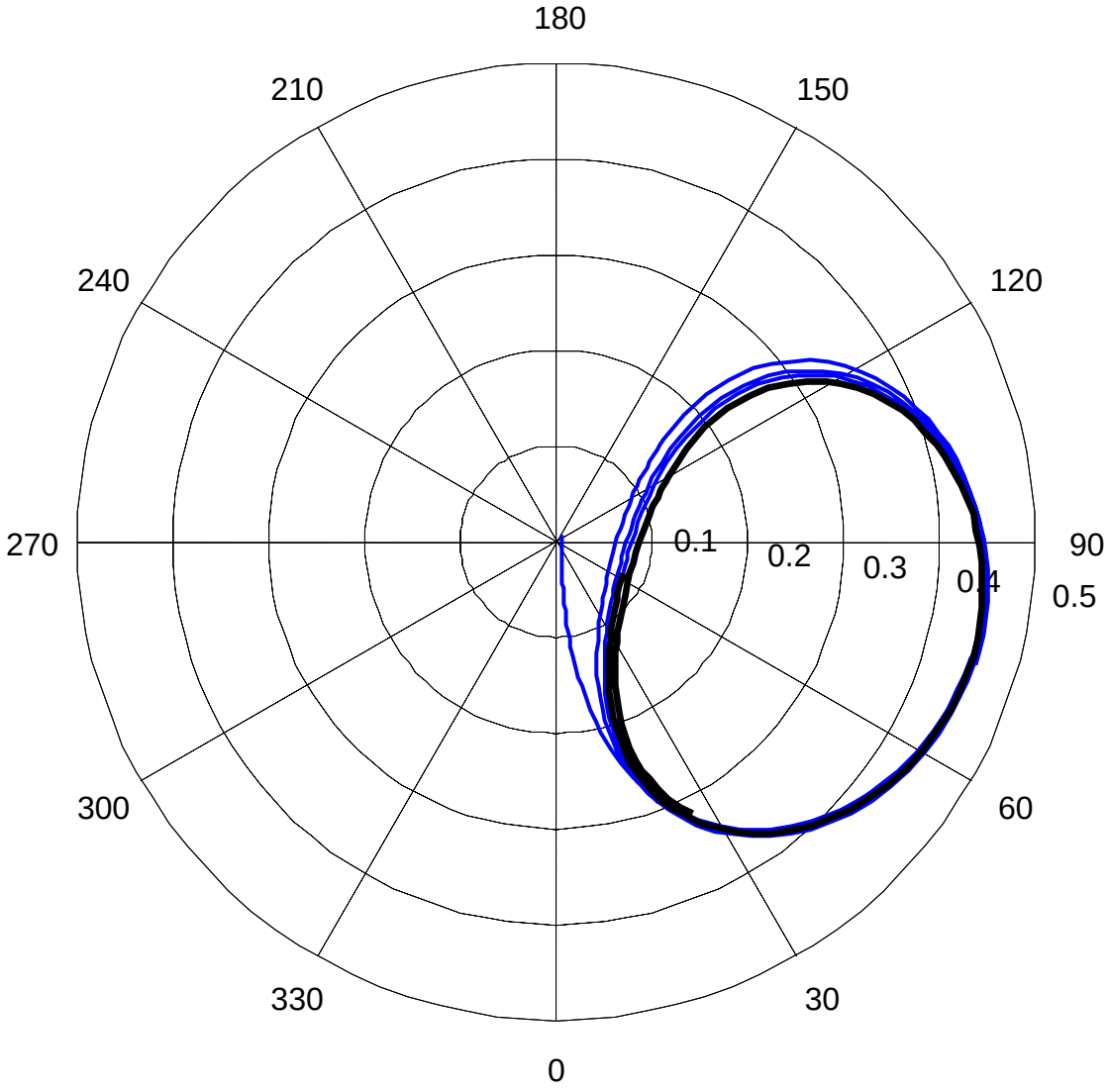

Figure 4.4: Limit Cycle Journal Locus ($N = 125\ rps, W = 160\ N, \varepsilon_0 = 0.01$)

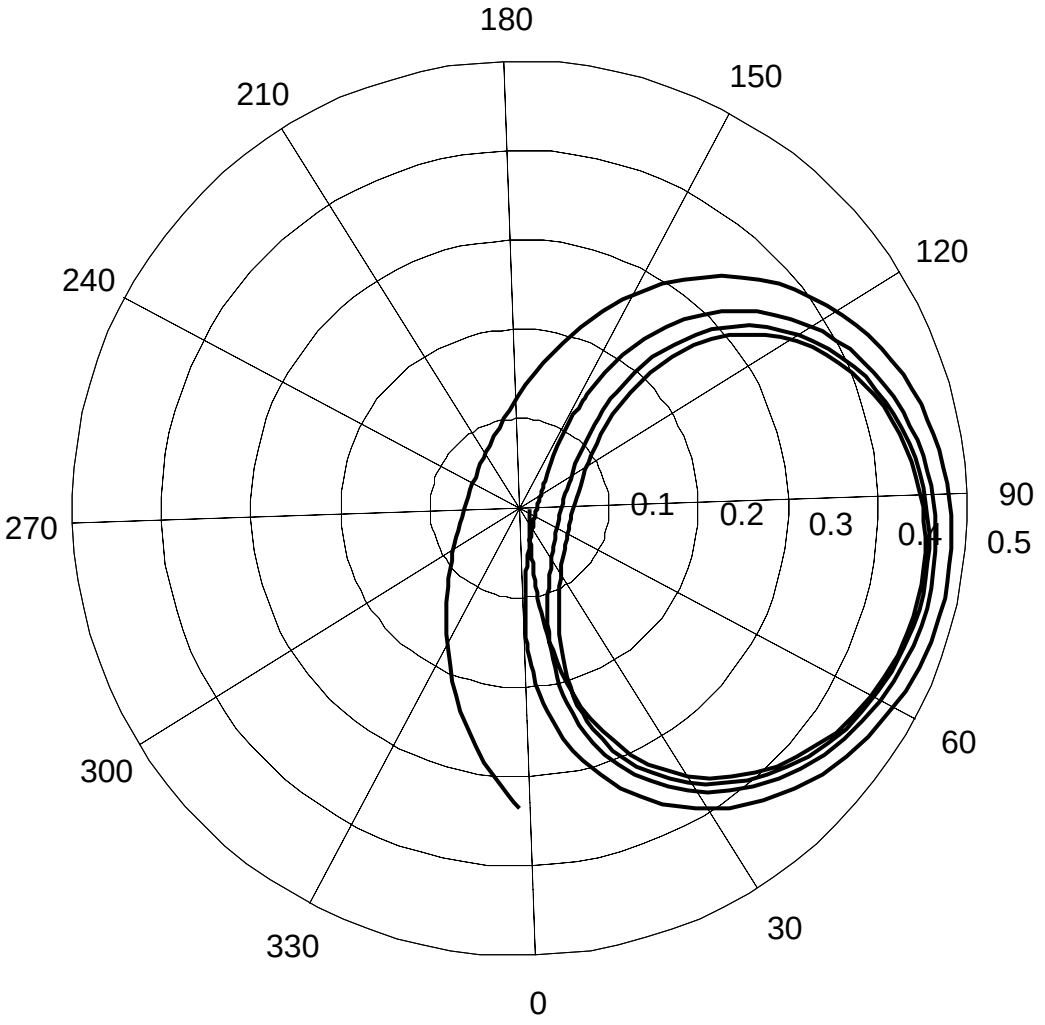

Figure 4.5: Unstable Journal Locus ($N = 126\ rps, W = 160\ N, \varepsilon_0 = 0.01$)

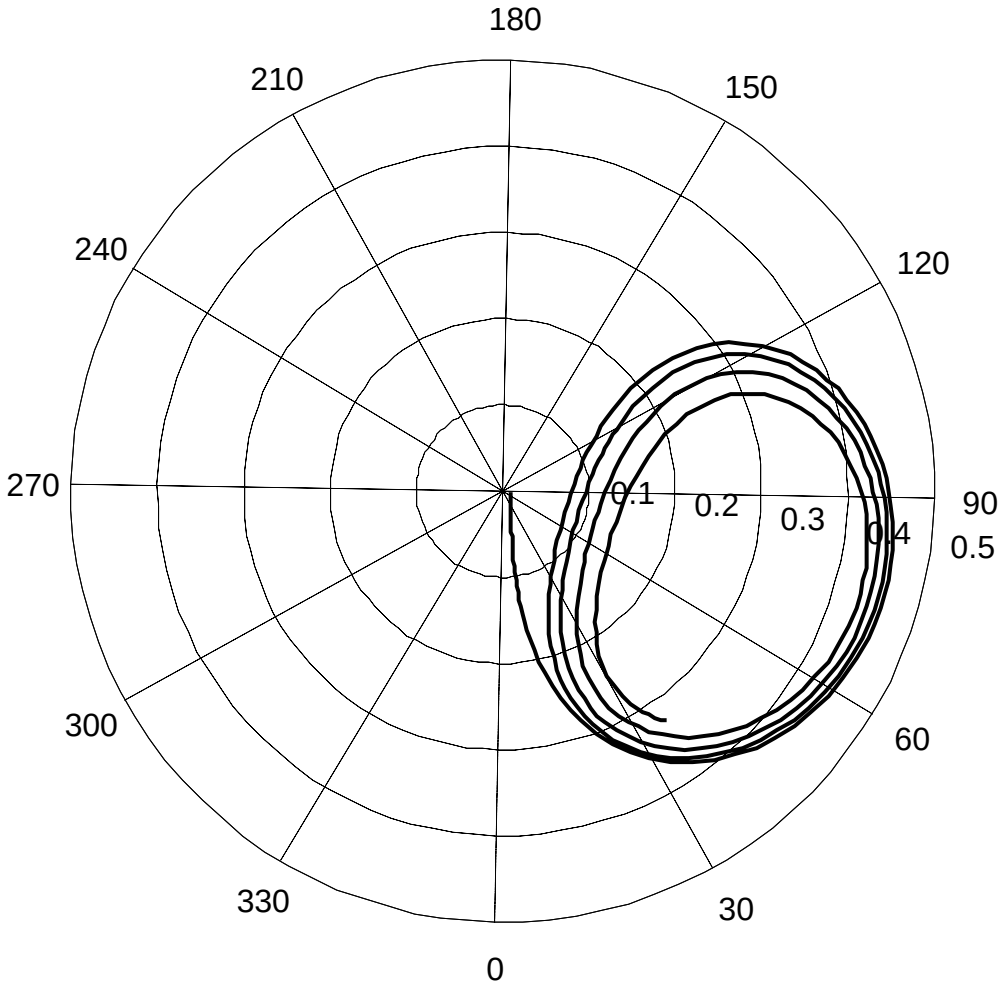

Figure 4.6 Stable Journal Locus ($N = 124\ rps, W = 160\ N, \varepsilon_0 = 0.01$)

it unstable. As seen from Figure 4.5, that a system can be made unstable by increasing the operating speed by 1 rps. Similarly from Figure 4.6 just by decreasing operating speed by 1 rps makes the system stable. Whenever the system forms the limit cycle, it is on the **verge of instability**.

This criterion for determining the state of limit cycle was repeated at various Sommerfeld numbers to obtain the threshold stability map.

4.3 Effect of Out of Balance on the Rotor-Bearing System

We have seen in the previous section the trajectories of shaft centers for the perfectly balanced rotor bearing systems. In practice small amount of unbalance is always present in the system, due to manufacturing run out or from the system assembly at the installation stage.

In order to simulate the effects of unbalance, the unbalanced force term is introduced in the dimensionless equations of motion (4.1) and (4.2). The dimensionless equations of motion including the unbalance are given by:

$$\ddot{\varepsilon} - \dot{\phi}^2 \varepsilon + \bar{F}_\varepsilon - \frac{\cos\phi}{\bar{M}} - \varepsilon_\mu \cos(\omega \bar{t} - \phi) = 0 \tag{4.7}$$

$$\ddot{\phi}\varepsilon + 2\dot{\varepsilon}\dot{\phi} - \bar{F}_\phi + \frac{\sin\phi}{\bar{M}} - \varepsilon_\mu \sin(\omega \bar{t} - \phi) = 0 \tag{4.8}$$

where $\varepsilon_\mu = \xi / C$ is the degree of unbalance or the unbalance factor. To see the effects of unbalance on shaft trajectory, simulations are performed by varying the unbalance factor, ε_μ . ε_μ =0 represents the balanced case at given operating speed and load.

Figures 4.7 – 4.9 shows a series of simulation results obtained by introducing an unbalance into the system. Figure 4.7 shows the locus of journal with very small unbalance where ε_{μ} =0.01, $N = 103\ rps, W = 147$ N. Unlike the balanced case where the journal settles down to a steady state position (as shown in Figure 4.1), in an unbalanced system the journal never settles down to an equilibrium point but orbits around the equilibrium point as shown in exploded view in Figure 4.7. Figure 4.8 represents the case where the out of balance component is increased ten times while keeping the load and speed similar to previous case, as seen from the Figure 4.8 shaft orbits around the equilibrium position with a larger orbit.

Figure 4.9 shows the effect of unbalance on the oil whirl stability. Figure 4.9 shows the locus of a shaft in which bearing is operating at N=126 rps and W=160 N with an unbalance factor ε_{μ} =0.01. It is interesting to note that the perfectly balanced system operating at same speed and load is found to be unstable, as shown in Figure 4.5, while with the introduction of small unbalance system is operating in the stable condition, as shown in Figure 4.9. From this case it appears that the small unbalance may stabilize the system.

In order to further investigate the effect of unbalance on the oil whirl instability threshold following procedure was followed:

1) Non-linear oil whirl threshold speed at different Sommerfeld numbers were computed for the perfectly balanced system by using the limit circle criterion.

2) This threshold speed was raised by one rps, which made the system unstable.

3) A range of degree of unbalance factors were computed, which made the system stable.

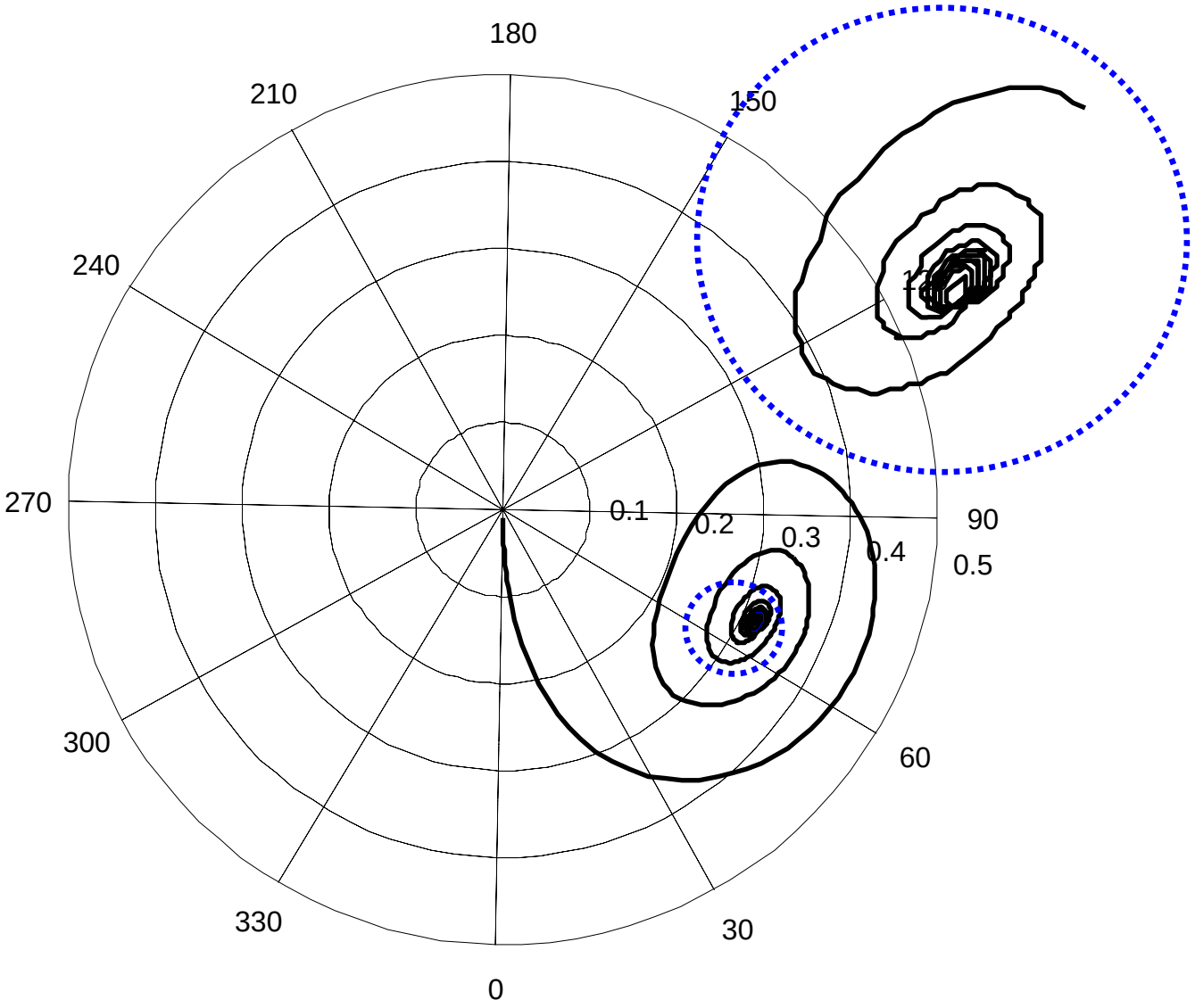

Figure 4.7: Stable Journal Locus ($N = 103\ rps, W = 147\ N, \varepsilon_0 = 0.01, \varepsilon_\mu = 0.01$)

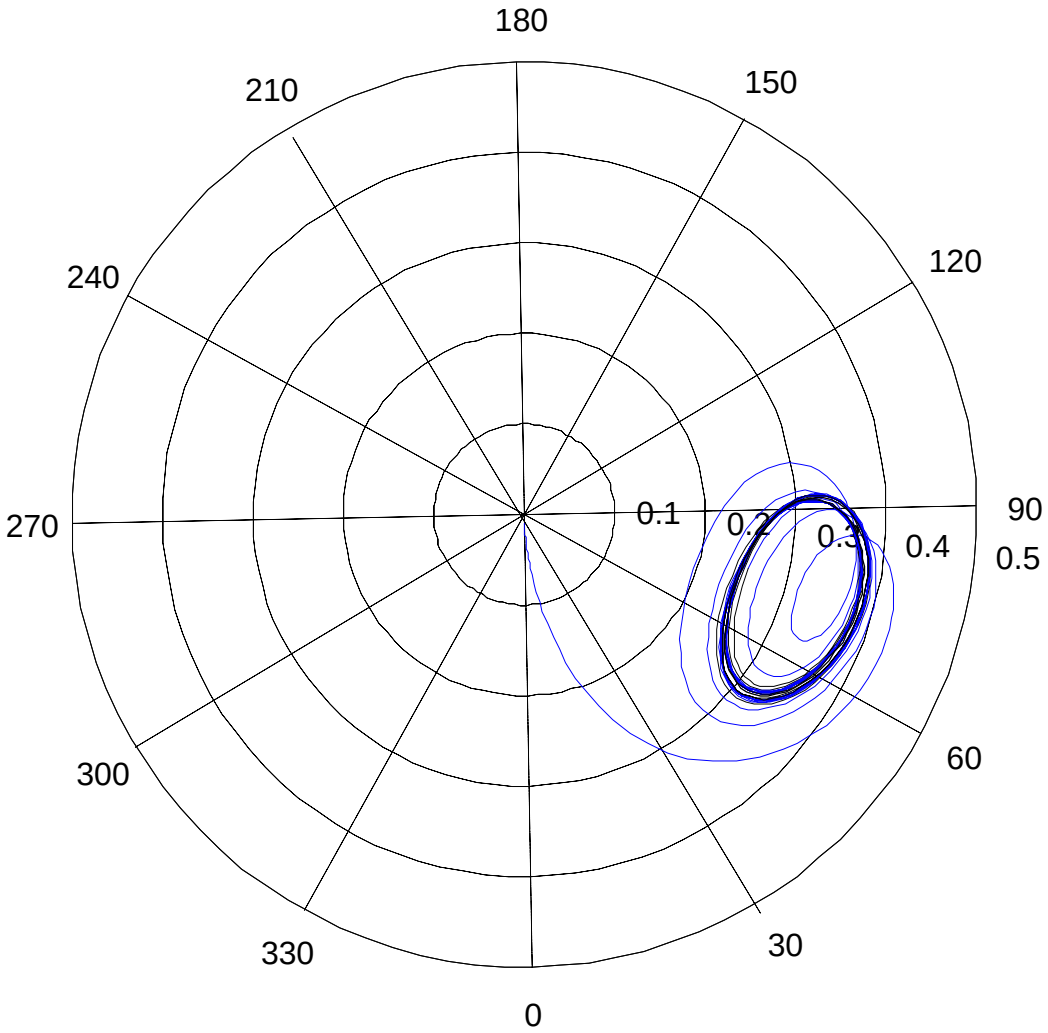

Figure 4.8: Stable Journal Locus ($N = 103\ rps, W = 147\ N, \varepsilon_0 = 0.01, \varepsilon_\mu = 0.1$)

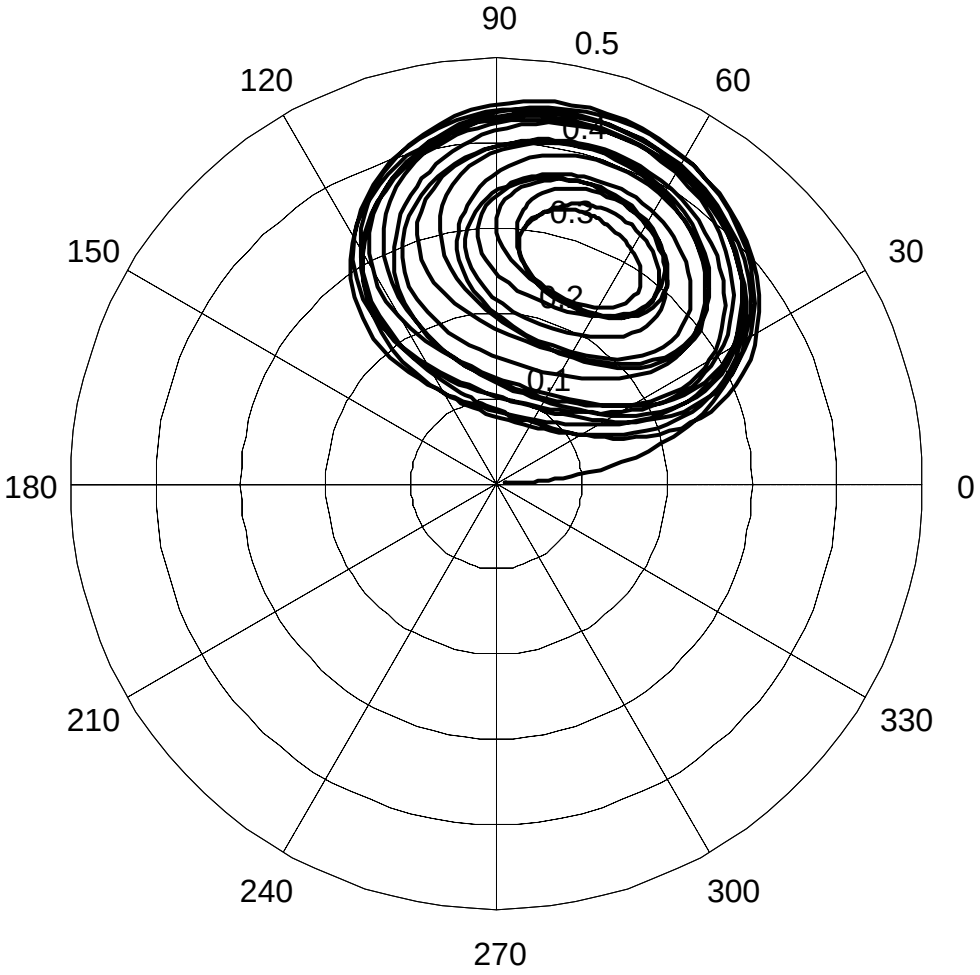

Figure 4.9: Stable Journal Locus ($N = 126\ rps, W = 160\ N, \varepsilon_0 = 0.01, \varepsilon_\mu = 0.01$)

Results from the above analysis are presented in Figure 4.10. Results indicate that, whenever the bearing is operating just above threshold speed, a small amount of unbalance always helps in decreasing the amplitude of vibration within the clearance circle caused by oil whirl. Also there exists a range of unbalance load which can decrease the amplitude of vibration near the threshold speeds. Figure 4.10 shows the range of unbalance which helps in decreasing the amplitude of vibration at various Sommerfeld number when the bearing is operating near the threshold speed.

From the above analysis it can be concluded that, unbalance effects play a major role on the whirl threshold speed. However, in the following sections unbalance has not been considered and system is assumed to be perfectly balanced.

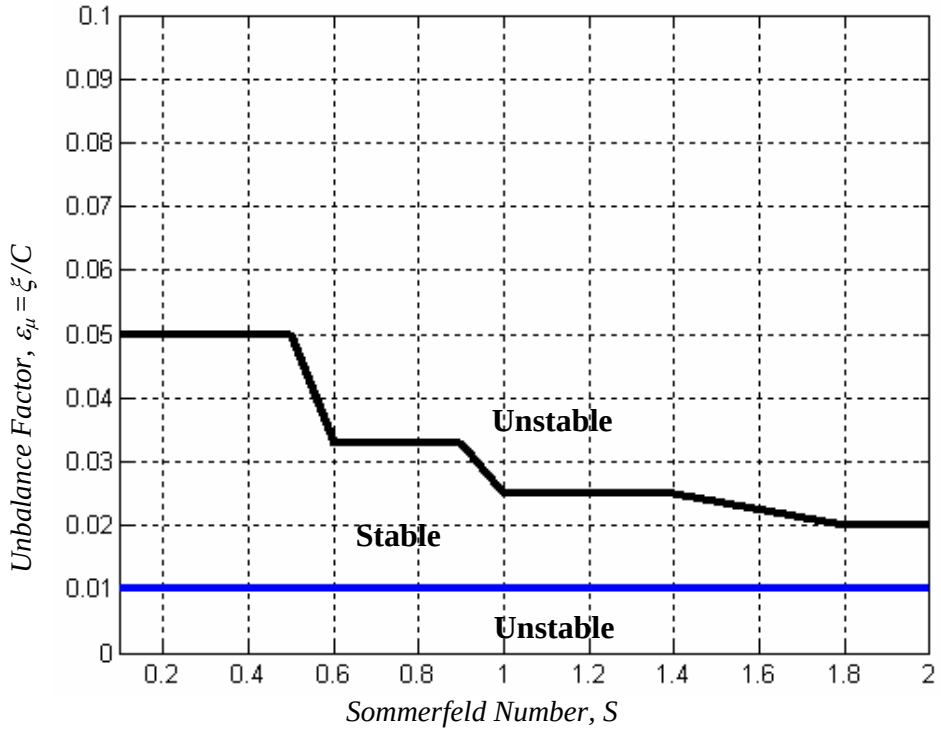

Figure 4.10: Degree of Unbalance vs. Sommerfeld Number

5. Reynolds Equation with Parabolic Distribution

In the previous sections, the Reynolds equation for the pressure generated in the lubricant oil film was solved by neglecting the pressure gradient in circumferential direction (Short Bearing Approximation). This assumption gives reasonable predictions for $L/D < 0.5$. The Short bearing solutions deviates significantly from the finite difference solutions of the full Reynolds equation without neglecting axial pressure gradient for $L/D \geq 0.5$, particularly at higher eccentricity ratios, as shown in Figure 5.1.

In order to obtain reasonable prediction of bearing performance parameters, the pressure gradient in axial direction must be included in the Reynolds equation. That means by considering the pressure gradient in axial direction, ordinary differential equation Reynolds equation becomes Partial differential equation, which has to be solved numerically using finite difference method. This would require an extensive amount of computational time for a transient analysis where Reynolds equation has to be solved for each time step. Furthermore, consideration of thermal effects (energy equation coupled with Reynolds equation) in the transient analysis adds to the requirement of computational time.

In this section we will take a close look at Ocvirk's [23] assumption of parabolic pressure distribution in axial direction. Ettles [5] modifications over Ocvirk's assumption are discussed. Detailed procedure for the calculation of rotordynamic coefficients is presented. Finally the comparison of rotordynamic coefficients obtained from short bearing analytical model and present analysis is presented.

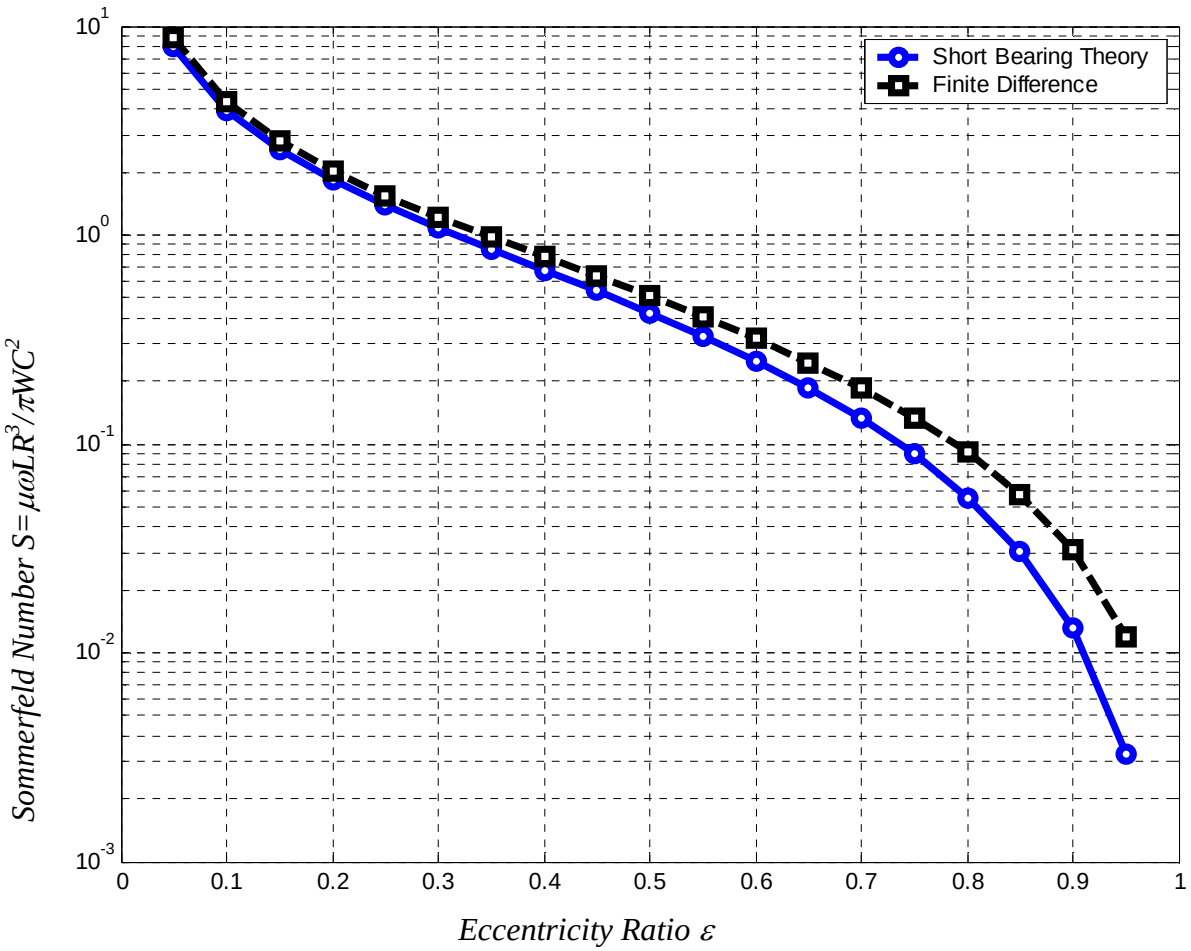

Figure 5.1: Comparison of Sommerfeld Number vs. Eccentricity Ratio for Finite Difference and Short Bearing Theory

$$\left(L/D = 0.5\right)$$

5.1 Parabolic Assumption (Ocvirk's Theory)

Ocvirk [23] assumed that the pressure gradient in the circumferential direction is small compared with the gradient in axial direction. By this assumption, the s*econd degree Partial differential* Reynolds equation reduces to s*econd degree ordinary differential equation* as shown in the equations (5.1)-(5.16). An outcome of the Ocvirk's [23] assumption is that the pressure profile varies parabolically in the axial direction as shown in the equation (5.5).

The pressure distribution in rectangular co-ordinate system for a journal bearing is given by:

$$\frac{\partial}{\partial x}\left(\frac{h^3}{12\mu}\frac{\partial P(x,z)}{\partial x}\right)+\frac{\partial}{\partial z}\left(\frac{h^3}{12\mu}\frac{\partial P(x,z)}{\partial z}\right)=\frac{1}{2}U\frac{\partial h}{\partial x} \tag{5.1}$$

To non-dimensionalize the above equation, we substitute

$$\theta=\frac{x}{R},\ \bar{z}=\frac{z}{L/2},\bar{\mu}=\frac{\mu}{\mu_i},\bar{h}=\frac{h}{C},\bar{P}=\frac{P}{P_{ref}},U=2\pi N_s R$$

Substituting the above parameters in equation (5.1) yields:

$$\frac{C^2P_{ref}}{R^2\mu_i}\frac{\partial}{\partial\theta}\left(\frac{\bar{h}^3}{12\bar{\mu}}\frac{\partial\bar{P}(\theta,z)}{\partial\theta}\right)+\frac{4C^2P_{ref}}{L^2\mu_i}\frac{\partial}{\partial\bar{z}}\left(\frac{\bar{h}^3}{12\bar{\mu}}\frac{\partial\bar{P}(\theta,z)}{\partial\bar{z}}\right)=\frac{1}{2}2\pi N_s\frac{\partial\bar{h}}{\partial\theta} \tag{5.2}$$

Simplifying the results in following equation

$$\frac{\partial}{\partial\theta}\left(\frac{\bar{h}^3}{12\bar{\mu}}\frac{\partial\bar{P}(\theta,z)}{\partial\theta}\right)+\frac{4R^2}{L^2}\frac{\partial}{\partial\bar{z}}\left(\frac{\bar{h}^3}{12\bar{\mu}}\frac{\partial\bar{P}(\theta,z)}{\partial\bar{z}}\right)=\frac{R^2\mu_i N_s}{C^2P_{ref}}\pi\ \frac{\partial\bar{h}}{\partial\theta} \tag{5.3}$$

Let

$$P_{ref}=\frac{R^2\mu_i N_s}{C^2}\qquad \lambda=\frac{L}{D}\ \text{(Aspect ratio)}$$

$$\frac{\partial}{\partial\theta}\left(\bar{h}^3\frac{\partial\bar{P}(\theta,z)}{\partial\theta}\right)+\frac{1}{\lambda^2}\frac{\partial}{\partial\bar{z}}\left(\bar{h}^3\frac{\partial\bar{P}(\theta,z)}{\partial\bar{z}}\right)=12\pi\bar{\mu}\frac{\partial\bar{h}}{\partial\theta} \tag{5.4}$$

Assuming that the pressure distribution in axial direction is parabolic, with maximum pressure at the mid plain and zero at plain $z = \pm L/2$, we can write:

$$\bar{P}(\theta, z) = \bar{P}_\theta \left[1 - \bar{z}^2 \right] \tag{5.5}$$

Differentiating $\bar{P}(\theta, z)$ with respect to θ yields:

$$\frac{\partial \bar{P}(\theta, z)}{\partial \theta} = \frac{\partial \bar{P}_\theta}{\partial \theta} \left[1 - \bar{z}^2 \right] \tag{5.6}$$

again differentiating with respect to θ

$$\frac{\partial^2 \bar{P}(\theta, z)}{\partial \theta^2} = \frac{\partial^2 \bar{P}_\theta}{\partial \theta^2} \left[1 - \bar{z}^2 \right] \tag{5.7}$$

Differentiating $\bar{P}(\theta, z)$ with respect to $\bar{z}$

$$\frac{\partial \bar{P}(\theta, z)}{\partial \bar{z}} = \bar{P}_\theta \left[-2\bar{z} \right] \tag{5.8}$$

again differentiating with respect to $\bar{z}$

$$\frac{\partial^2 \bar{P}(\theta, z)}{\partial \bar{z}^2} = -2\bar{P}_\theta \tag{5.9}$$

Substituting the values from the equations (5.6), (5.7), (5.8) and (5.9) in equation (5.4)

$$3\bar{h}^2 \frac{\partial \bar{h}}{\partial \theta} \frac{\partial \bar{P}_\theta}{\partial \theta} \left[1 - \bar{z}^2 \right] + \bar{h}^3 \frac{\partial^2 \bar{P}_\theta}{\partial \theta^2} \left[1 - \bar{z}^2 \right] - \frac{\bar{h}^3}{\lambda^2} 2\bar{P}_\theta = 12\pi \bar{\mu} \frac{\partial \bar{h}}{\partial \theta} \tag{5.10}$$

simplifying the equation (5.10) results in:

$$\left[1 - \bar{z}^2 \right] \left(3\bar{h}^2 \frac{\partial \bar{h}}{\partial \theta} \frac{\partial \bar{P}_\theta}{\partial \theta} + \bar{h}^3 \frac{\partial^2 \bar{P}_\theta}{\partial \theta^2} \right) - \frac{2\bar{h}^3 \bar{P}_\theta}{\lambda^2} = 12\pi \bar{\mu} \frac{\partial \bar{h}}{\partial \theta} \tag{5.11}$$

The peak pressure at the mid plain where $\bar{z} = 0$ is given by

$$3\bar{h}^{2}\frac{\partial \bar{h}}{\partial \theta}\frac{\partial \bar{P}_{\theta}}{\partial \theta}+\bar{h}^{3}\frac{\partial^{2}\bar{P}_{\theta}}{\partial \theta^{2}}-\frac{2\bar{h}^{3}P_{\theta}}{\lambda^{2}}=12\pi\bar{\mu}\frac{\partial \bar{h}}{\partial \theta} \tag{5.12}$$

Rearranging equation (5.12) gives:

$$\bar{h}^{3}\frac{\partial^{2}\bar{P}_{\theta}}{\partial \theta^{2}}=12\pi\bar{\mu}\frac{\partial \bar{h}}{\partial \theta}-3\bar{h}^{3}\frac{\partial \bar{h}}{\partial \theta}\frac{\partial \bar{P}_{\theta}}{\partial \theta}+\frac{2\bar{h}^{3}P_{\theta}}{\lambda^{2}} \tag{5.13}$$

Dividing RHS and LHS of equation (5.13) by $\bar{h}^{3}$ results in the following equation:

$$\frac{\partial^{2}\bar{P}_{\theta}}{\partial \theta^{2}}=\frac{12\pi\bar{\mu}}{\bar{h}^{3}}\frac{\partial \bar{h}}{\partial \theta}-\frac{3}{\bar{h}}\frac{\partial \bar{h}}{\partial \theta}\frac{\partial \bar{P}_{\theta}}{\partial \theta}+\frac{2P_{\theta}}{\lambda^{2}} \tag{5.14}$$

Simplifying the above equation

$$\frac{\partial^{2}\bar{P}_{\theta}}{\partial \theta^{2}}=3\frac{\partial \bar{h}}{\partial \theta}\left(\frac{4\pi\bar{\mu}}{\bar{h}^{3}}-\frac{1}{\bar{h}}\frac{\partial \bar{P}_{\theta}}{\partial \theta}\right)+\frac{2P_{\theta}}{\lambda^{2}} \tag{5.15}$$

This is an ODE which can be written as

$$\frac{d^{2}\bar{P}_{\theta}}{d\theta^{2}}=3\frac{d\bar{h}}{d\theta}\left(\frac{4\pi\bar{\mu}}{\bar{h}^{3}}-\frac{1}{\bar{h}}\frac{d\bar{P}_{\theta}}{d\theta}\right)+\frac{2P_{\theta}}{\lambda^{2}} \tag{5.16}$$

Equation 5.16 is a second order ordinary differential equation. This equation was solved by a fourth order Runge-Kutta integration scheme. Since this was a second degree differential equation which requires two initial conditions. One initial condition used was that the inlet pressure was equal to the supply pressure condition: $(\bar{P}_{\theta})_{\theta=0}=0$. The second condition requires one to determine the pressure gradient $\left(\frac{d\bar{P}_{\theta}}{d\theta}\right)_{\theta=0}$ at the inlet by trial and error method. The pressure is periodic in nature in cylindrical journal bearing i.e. $(\bar{P}_{\theta})_{\theta=0}=(\bar{P}_{\theta})_{\theta=2\pi}=0$. By using the shooting method, the pressure gradient at the inlet

was estimated to satisfy the periodic boundary conditions: $(\bar{P}_\theta)_{\theta=0} = (\bar{P}_\theta)_{\theta=2\pi} = 0$ for the pressure.

After estimating the inlet pressure gradient in the circumferential direction, the mean circumferential pressure $\bar{P}_\theta$ was computed by solving equation (5.16) using a fourth order Runge-Kutta method with a grid size of 241x101. Two dimensional mean pressure field, $\bar{P}$ was obtained by substituting the circumferential pressure $\bar{P}_\theta$ in equation (5.5) where $\bar{z}$ varies from $-1/2$ to $1/2$. Components of $\bar{P}$ in radial and tangential direction was integrated over bearing area as shown in equations (3.55) and (3.56) to obtain hydrodynamic fluid forces $\bar{F}_\varepsilon$ and $\bar{F}_\phi$, respectively. Once the load components were obtained, other design parameters such as attitude angle and Sommerfeld number were computed using equations (3.59) and (3.60), respectively.

The results of design parameters for L/D = 0.5, obtained by solving the equation (5.16) are presented in Figures 5.2-5.4. As seen from the Figure 5.2 there is a significant deviation in Sommerfeld number obtained by solving short bearing approximations and by finite difference solutions. These differences in values can be accounted from the cavitation boundary conditions. From Figure 5.3 we can observe that peak pressure obtained from both the solution method is in agreement at lower eccentricity ratios but deviates significantly at higher eccentricity ratios.

5.2 Modified Parabolic Assumption (Ettles and Shelly [5])

As seen from the previous analysis, the Ocvirk's parabolic assumption holds good only for lower eccentricity ratios. Ettles and Shelly [5] revised the above theory with the

modified exponent in the parabolic assumption as shown in equation (5.17). They showed that with the use of modified exponent the useful range of Ocvirk's parabolic assumption can be extended to higher eccentricity ratios. To estimate the value of modified exponent χ, they curve-matched the pressure fields obtained from finite difference solutions with a pressure profile of the form given by equation (5.17).

In the present analysis, for the eccentricity ratio, $\varepsilon \leq 0.75$, χ =2 was used while for $\varepsilon > 0.75$, χ =2.12 was used, as recommended by Ettles and Shelly for $L/D = 0.5$ [5].

$$\bar{P}(\theta, z) = \bar{P}_\theta \left(1 - \left(\bar{z}^{\chi}\right)\right) \tag{5.17}$$

Where χ =modified exponent.

Substituting value of $\bar{P}(\theta, z)$ from equation (5) into equation (5.4)

$$\frac{\partial}{\partial \theta}\left(\bar{h}^3 \frac{\partial \bar{P}_\theta}{\partial \theta}\right)\left(1 - \left(\bar{z}^{\chi}\right)\right) + \frac{\bar{h}^3}{\lambda^2}\frac{\partial^2}{\partial \bar{z}^2}\bar{P}_\theta\left(1 - \left(\bar{z}^{\chi}\right)\right) = 12\pi\,\bar{\mu}\frac{\partial \bar{h}}{\partial \theta} \tag{5.18}$$

From Ettles and Shelly [5]:

$$B_1 \frac{d^2 \bar{P}_\theta}{d\theta^2} + 3B_1 \frac{d\bar{h}}{d\theta}\left(\frac{1}{\bar{h}}\frac{d\bar{P}_\theta}{\theta}\right) - \frac{3\bar{P}_\theta}{\lambda^2} = \frac{12B_2\pi\bar{\mu}}{\bar{h}^3}\frac{d\bar{h}}{d\theta} \tag{5.19}$$

where $B_1 = \left(\frac{\chi+4}{\chi+3}\right)$ and $B_2 = \left(\frac{\chi+1}{\chi}\right)$ are the weighting factors given by Ettles and Shelly [5].

Results obtained by solving equation (5.19) are presented in Figures 5.5 - 5.8. As seen from the figures, with the modified exponent the Sommerfeld number and the peak pressure agrees well with finite difference solutions at all eccentricity ratios.

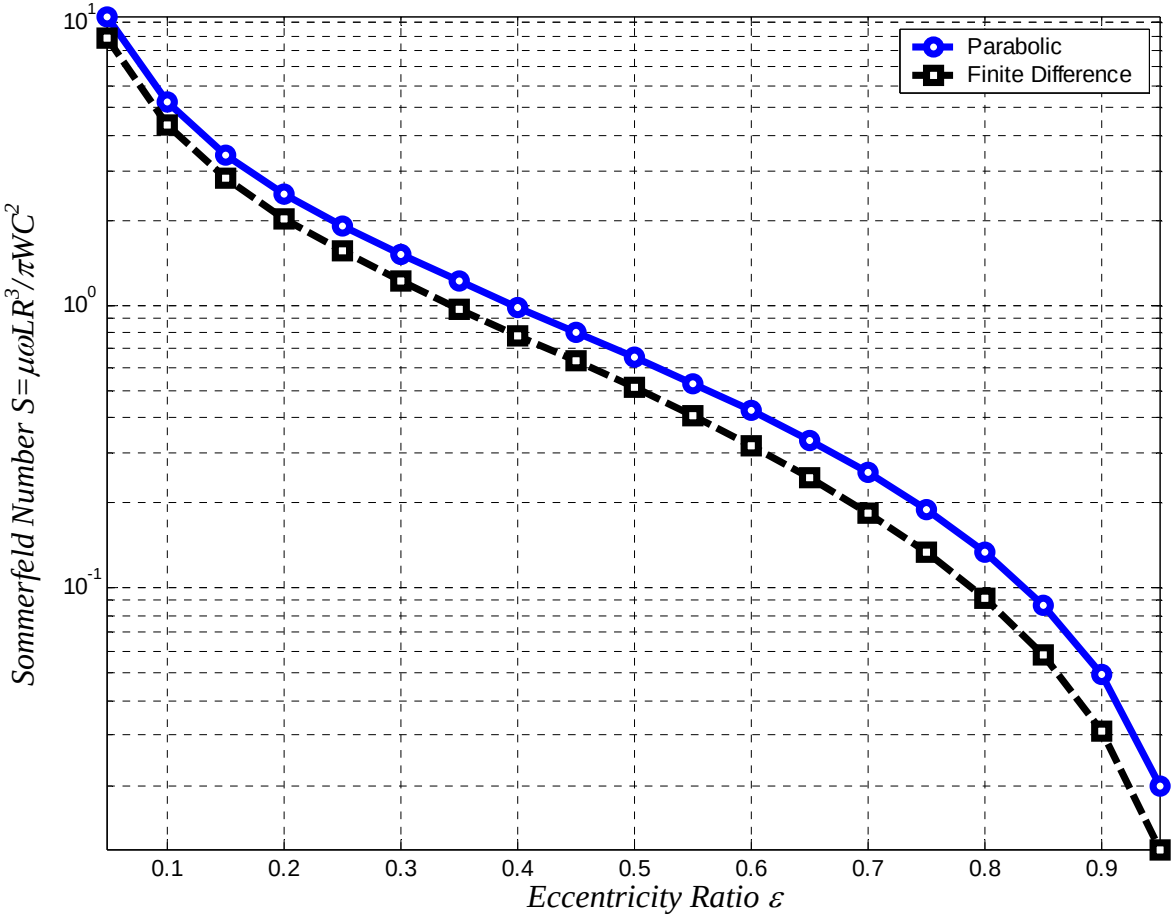

Figure 5.2: Comparison of Sommerfeld Number vs. Eccentricity Ratio for Finite Difference with Parabolic Assumption

($L/D = 0.5$)

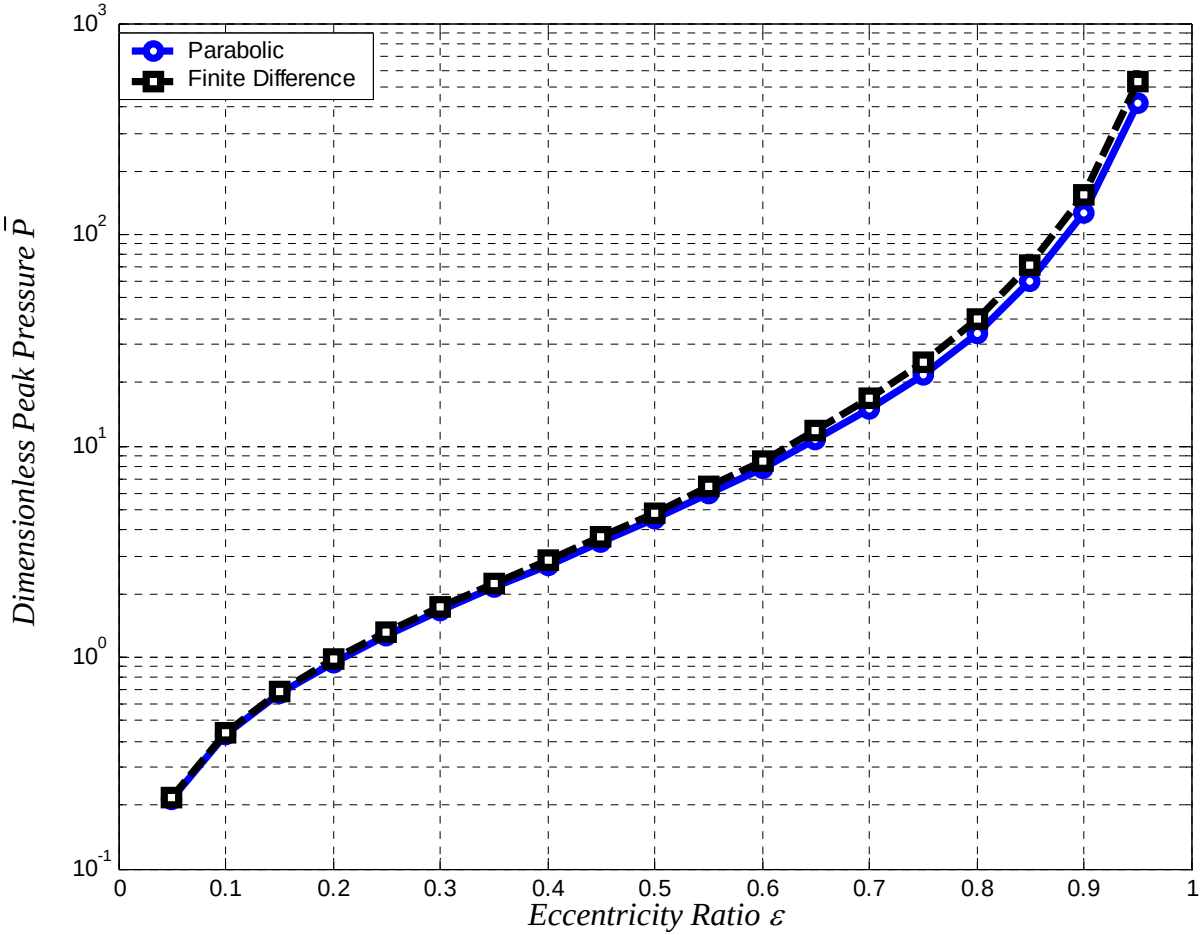

Figure 5.3: Comparison of Peak Pressure vs. Eccentricity Ratio for Finite Difference with Parabolic Assumption ($L / D = 0.5$)

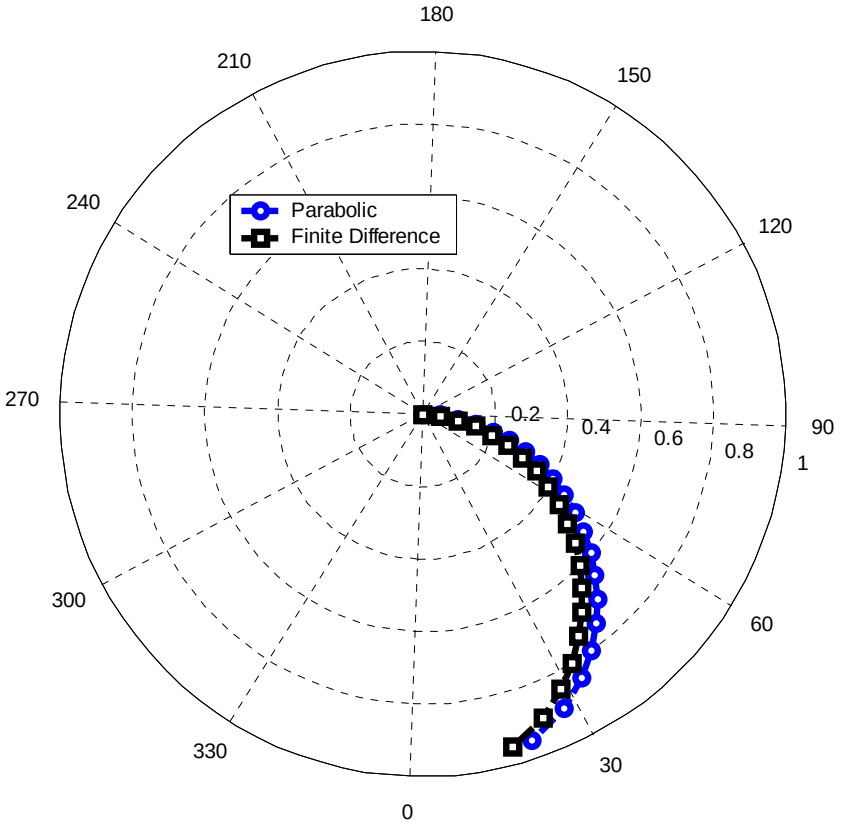

Figure 5.4: Comparison of Attitude Angle vs. Eccentricity Ratio for Finite Difference with Parabolic Assumption ($L / D = 0.5$)

5.3 Rotordynamic Coefficients

In this section the rotordynamic stiffness and damping coefficients for the Reynolds equation with modified exponent equation (5.19) were computed numerically and compared with the analytical values calculated by Lund [24] using the short bearing theory.

Rotordynamic coefficients were computed numerically using a *perturbation analysis.* The procedure is as follows:

1. Reynolds equation (5.19) was solved by applying a fourth order Runge-Kutta scheme using the shooting method. Grid size of 241 x 101 along the circumferential and axial directions, respectively was used keeping the viscosity constant to obtain mean pressure $\bar{P}$ for a given unperturbed film thickness equation (3.69).

2. Once the converged pressure field was obtained for the given steady state oil film thickness equation (3.69). This converged pressure field was integrated over the bearing area to obtain hydrodynamic fluid forces $\bar{F}_{\varepsilon}$ and $\bar{F}_{\phi}$ in the radial and the tangential directions, respectively. The load carrying capacity $\bar{W}$ and attitude angle ϕ_0 were obtained from equations (3.70) and (3.71), respectively.

3. Once the steady state position ε_0 and ϕ_0 were obtained. In order to obtain stiffness coefficients, first the oil film was perturbed in a positive radial direction by $\Delta\varepsilon$, as given by equation (5.20) and steps 1 and 2 were repeated to obtain the hydrodynamic fluid forces $\bar{F}_{\varepsilon}$ and $\bar{F}_{\phi}$ in the radial and the tangential directions, respectively. Then the film was perturbed in the negative radial direction by $\Delta\varepsilon$, as given by equation (5.21)

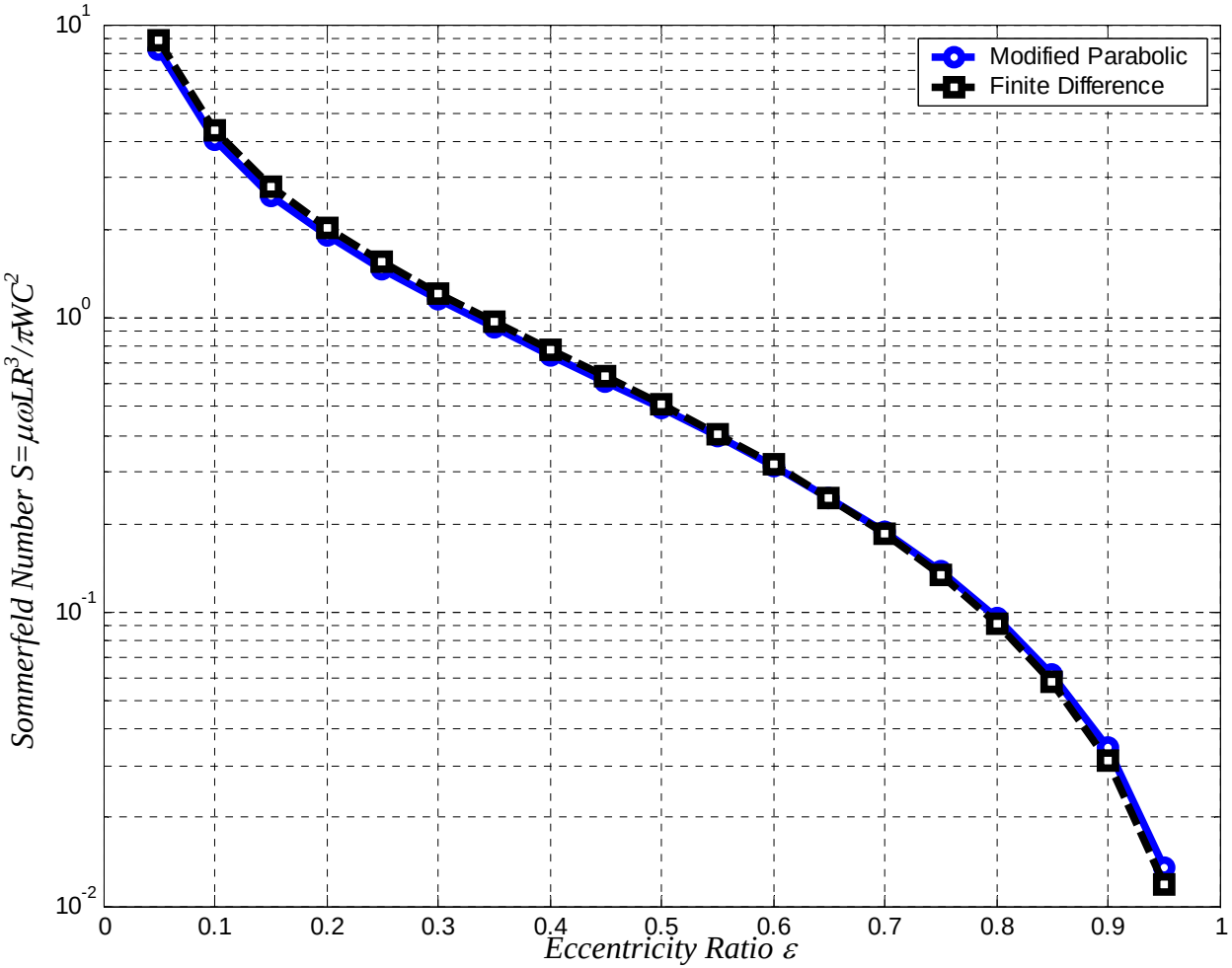

Figure 5.5 Comparison of Sommerfeld Number vs. Eccentricity Ratio for Finite Difference with Modified Parabolic

($L / D = 0.5$)

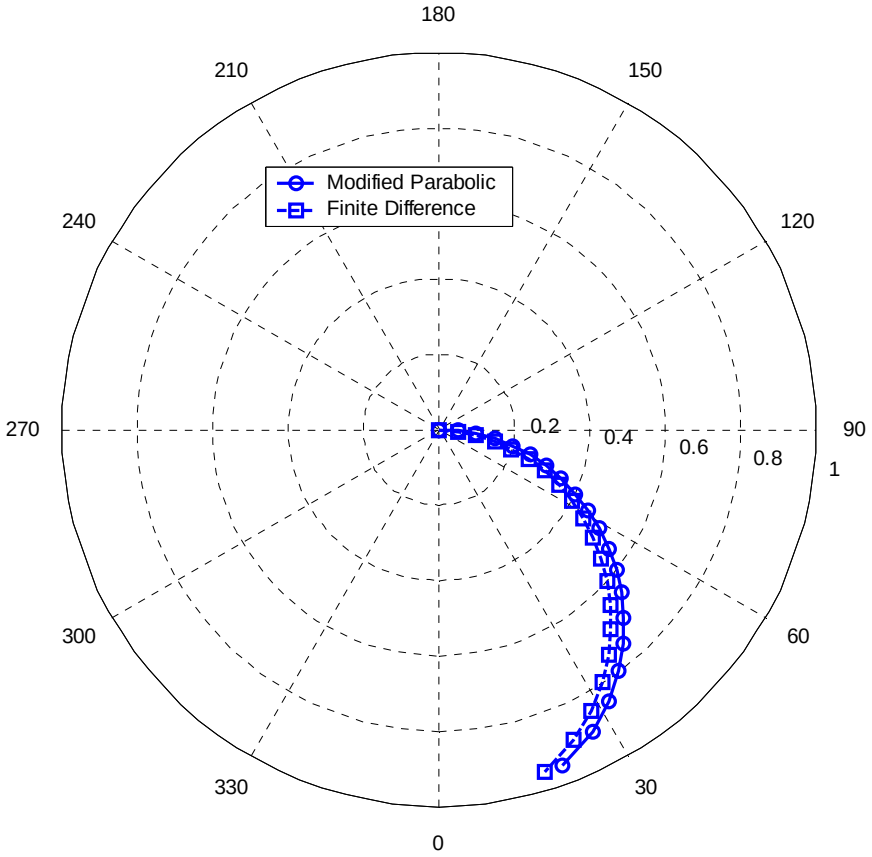

Figure 5.6: Comparison of Attitude Angle vs. Eccentricity Ratio for Finite Difference with Modified Parabolic ($L / D = 0.5$)

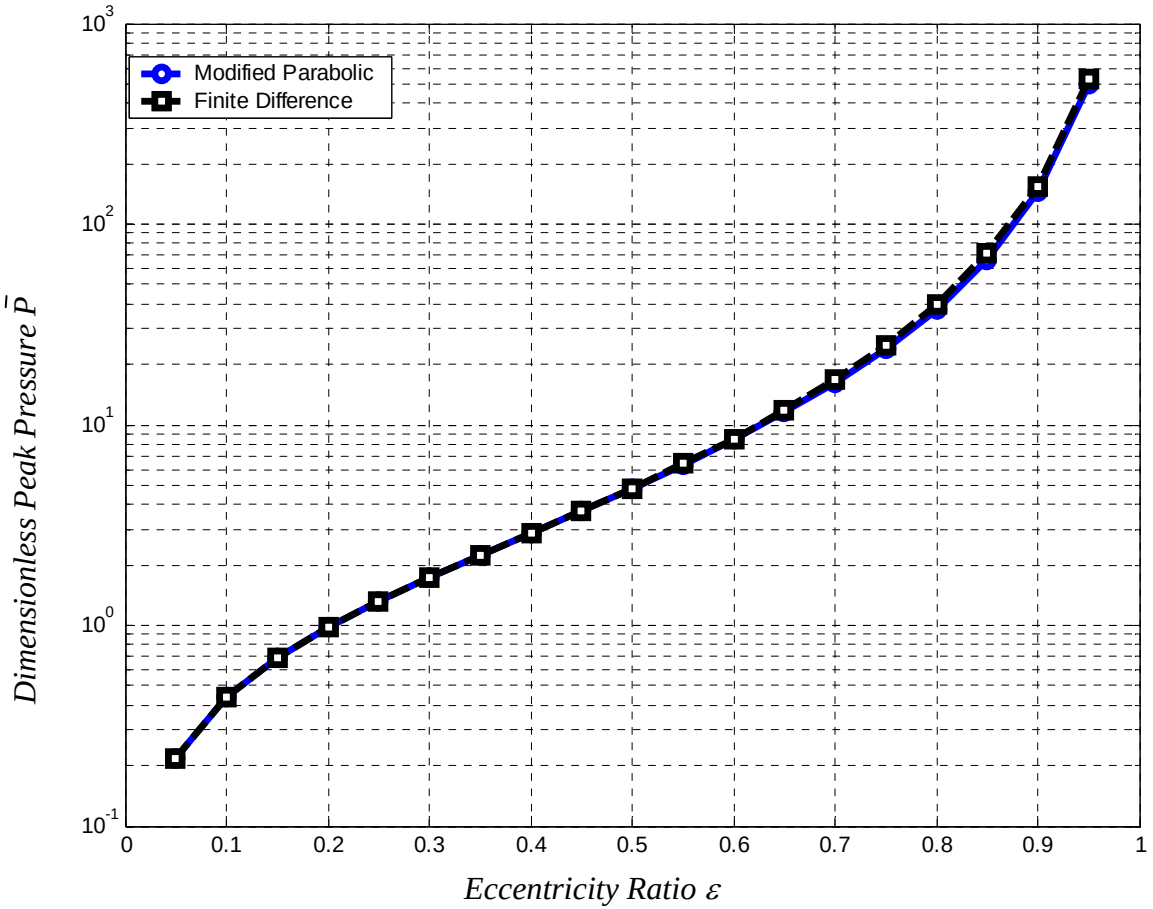

Figure 5.7: Comparison of Peak Pressure vs. Eccentricity Ratio for Finite Difference with Modified Parabolic ($L / D = 0.5$)

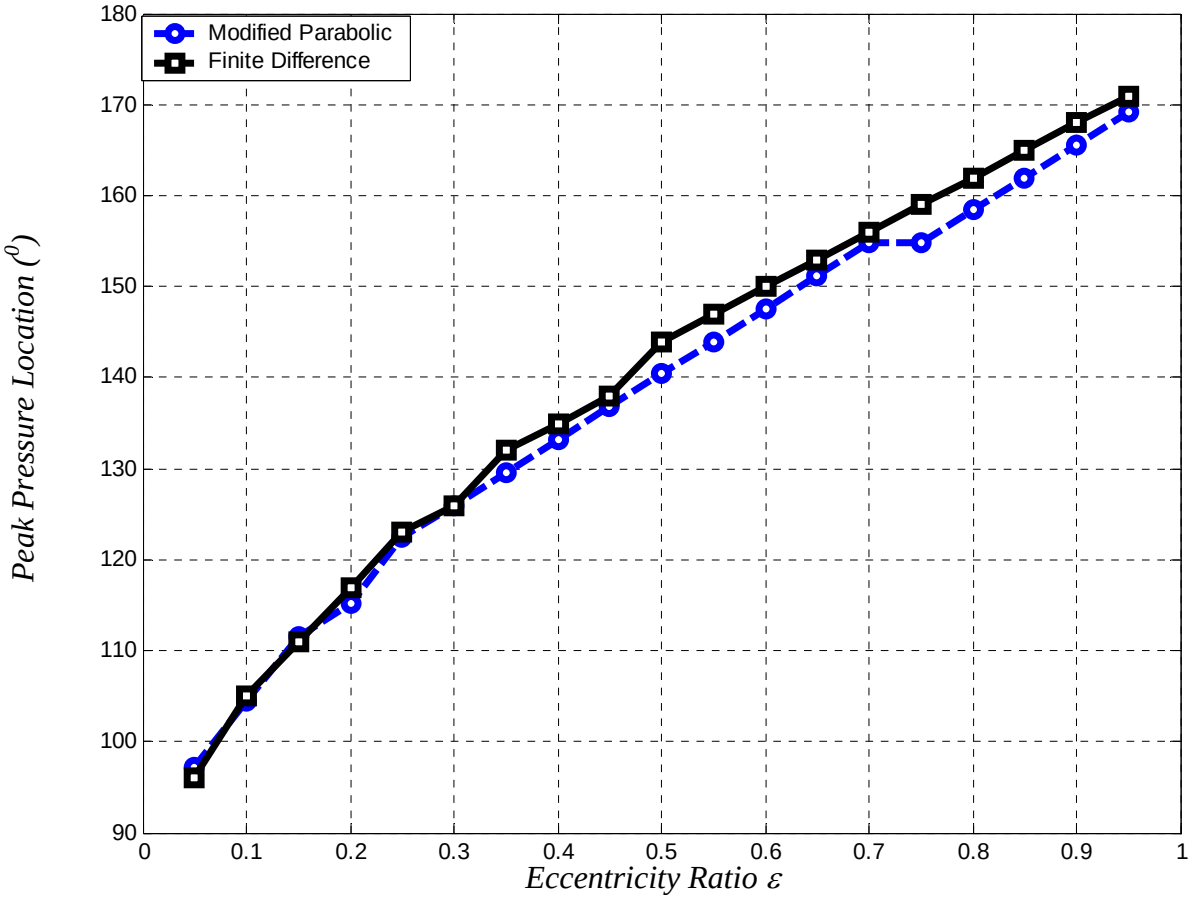

Figure 5.8 Comparison of Peak Pressure Location vs. Eccentricity Ratio for Finite Difference with Modified Parabolic

($L / D = 0.5$)

and steps 1and 2 were repeated to obtain the hydrodynamic fluid forces $\bar{F}_{\varepsilon}$ and $\bar{F}_{\phi}$ in the radial and the tangential directions, respectively. The stiffness coefficients $\bar{K}_{\varepsilon\varepsilon}$ and $\bar{K}_{\phi\varepsilon}$ were calculated as given by equation (5.22). For notations used in equation (5.22) refer to equations (3.65) and (3.66).

$$\bar{h}_{+} = \bar{h}_0 + \Delta h = 1 + (\varepsilon_0 + \Delta\varepsilon)\cos(\theta) \tag{5.20}$$

$$\bar{h}_{-} = \bar{h}_0 - \Delta h = 1 + (\varepsilon_0 - \Delta\varepsilon)\cos(\theta) \tag{5.21}$$

$$\bar{K}_{\varepsilon\varepsilon} = \frac{\Delta \bar{F}_{\varepsilon}(\varepsilon_0 + \Delta\varepsilon, \phi_0, \dot{\varepsilon} = 0, \dot{\phi} = 0) - \Delta \bar{F}_{\varepsilon}(\varepsilon_0 - \Delta\varepsilon, \phi_0, \dot{\varepsilon} = 0, \dot{\phi} = 0)}{2\Delta\varepsilon}$$

$$\bar{K}_{\phi\varepsilon} = \frac{\Delta \bar{F}_{\phi}(\varepsilon_0 + \Delta\varepsilon, \phi_0, \dot{\varepsilon} = 0, \dot{\phi} = 0) - \Delta \bar{F}_{\phi}(\varepsilon_0 - \Delta\varepsilon, \phi_0, \dot{\varepsilon} = 0, \dot{\phi} = 0)}{2\Delta\varepsilon} \tag{5.22}$$

4. In order to obtain the other two stiffness coefficients, first the oil film was perturbed in a positive tangential direction by $\Delta\phi$, as given by the equation (5.23) and steps 1 and 2 were repeated to obtain the hydrodynamic fluid forces $\bar{F}_{\varepsilon}$ and $\bar{F}_{\phi}$ in the radial and the tangential directions, respectively. Then, the film was perturbed in the negative tangential direction by $\Delta\phi$, as given by equation (5.24) and steps 1 and 2 were repeated to obtain the hydrodynamic fluid forces $\bar{F}_{\varepsilon}$ and $\bar{F}_{\phi}$ in the radial and the tangential directions, respectively. The stiffness coefficients $\bar{K}_{\varepsilon\phi}$ and $\bar{K}_{\phi\phi}$ were calculated as given by equation (5.25).

$$\bar{h}_{+} = \bar{h}_0 + \Delta h = 1 + \varepsilon_0 \cos(\theta + \Delta\phi) \tag{5.23}$$

$$\bar{h}_{-} = \bar{h}_0 - \Delta h = 1 + \varepsilon_0 \cos(\theta - \Delta\phi) \tag{5.24}$$

$$\bar{K}_{\varepsilon\phi} = \frac{\Delta \bar{F}_{\varepsilon}(\varepsilon_0, \phi + \Delta\phi, \dot{\varepsilon} = 0, \dot{\phi} = 0) - \Delta \bar{F}_{\varepsilon}(\varepsilon_0, \phi - \Delta\phi, \dot{\varepsilon} = 0, \dot{\phi} = 0)}{2\varepsilon_0 \Delta\phi}$$

$$\bar{K}_{\phi\phi} = \frac{\Delta \bar{F}_{\phi}(\varepsilon_0, \phi + \Delta\phi, \dot{\varepsilon} = 0, \dot{\phi} = 0) - \Delta \bar{F}_{\phi}(\varepsilon_0, \phi - \Delta\phi, \dot{\varepsilon} = 0, \dot{\phi} = 0)}{2\varepsilon_0 \Delta\phi} \tag{5.25}$$

It is very important to mention that the trigonometric sine and cosine functions of $\Delta\phi$ in equations (5.23) and (5.24) were expanded using the Taylor series expansion as given by equations B1 and B2 (see Appendix B).

5. In order to obtain the damping coefficients the squeeze film term was added to the steady state pressure equation (5.19). The detailed derivation of transient Reynolds equation is shown in section 6.1. The squeeze term was the time derivative of film thickness and for equation (5.20) and (5.21) is given by equation (5.26) and (5.27), respectively:

$$\left(\frac{d\,\bar{h}_{+}}{dt} \right) = \Delta\dot{\varepsilon}\cos(\theta) \tag{5.26}$$

$$\left(\frac{d\,\bar{h}_{-}}{dt} \right) = -\Delta\dot{\varepsilon}\cos(\theta) \tag{5.27}$$

To compute $\bar{C}_{\varepsilon\varepsilon}$ and $\bar{C}_{\phi\varepsilon}$, first the film thickness was perturbed with the positive radial velocity of $\Delta\dot{\varepsilon}$ and steps 1 and 2 were repeated to obtain the hydrodynamic fluid forces $\bar{F}_{\varepsilon}$ and $\bar{F}_{\phi}$ in the radial and the tangential directions, respectively. Then the film thickness was perturbed with a negative radial velocity of $\Delta\dot{\varepsilon}$ and steps 1 and

2 were repeated to obtain the hydrodynamic fluid forces $\bar{F}_{\varepsilon}$ and $\bar{F}_{\phi}$ in the radial and the tangential directions, respectively. The damping coefficients were calculated using equation (5.28):

$$\bar{C}_{\varepsilon\varepsilon} = \frac{\Delta \bar{F}_{\varepsilon}(\varepsilon_0, \phi_0, \dot{\varepsilon} = \Delta\dot{\varepsilon}, \dot{\phi} = 0) - \Delta \bar{F}_{\varepsilon}(\varepsilon_0, \phi_0, \dot{\varepsilon} = -\Delta\dot{\varepsilon}, \dot{\phi} = 0)}{2\Delta\dot{\varepsilon}};$$

$$\bar{C}_{\phi\varepsilon} = \frac{\Delta \bar{F}_{\phi}(\varepsilon_0, \phi_0, \dot{\varepsilon} = \Delta\dot{\varepsilon}, \dot{\phi} = 0) - \Delta \bar{F}_{\phi}(\varepsilon_0, \phi_0, \dot{\varepsilon} = -\Delta\dot{\varepsilon}, \dot{\phi} = 0)}{2\Delta\dot{\varepsilon}} \qquad (5.28)$$

6. The time derivative or squeeze term for the film thickness given by equations (5.23) and (5.24) reduces to:

$$\left(\frac{d\bar{h}_{+}}{dt}\right) = -\varepsilon_0 \sin(\theta)\Delta\dot{\phi} \qquad (5.29)$$

$$\left(\frac{d\bar{h}_{-}}{dt}\right) = \varepsilon_0 \sin(\theta)\Delta\dot{\phi} \qquad (5.30)$$

To compute $\bar{C}_{\varepsilon\phi}$ and $\bar{C}_{\phi\phi}$, first the film thickness was perturbed with a positive tangential velocity of $\varepsilon_0\Delta\dot{\phi}$ and steps 1 and 2 were repeated to obtain the hydrodynamic fluid forces $\bar{F}_{\varepsilon}$ and $\bar{F}_{\phi}$ in the radial and the tangential directions, respectively. Then the film thickness was perturbed with a negative radial velocity of $\varepsilon_0\Delta\dot{\phi}$ and steps 1 and 2 were repeated to obtain the hydrodynamic fluid forces $\bar{F}_{\varepsilon}$ and

$\bar{F}_{\phi}$ in the radial and the tangential directions, respectively. The damping coefficients were calculated using equation (5.31):

$$\bar{C}_{\varepsilon\varepsilon} = \frac{\Delta \bar{F}_{\varepsilon}(\varepsilon_0, \phi_0, \dot{\varepsilon} = 0, \dot{\phi} = \Delta\dot{\phi}) - \Delta \bar{F}_{\varepsilon}(\varepsilon_0, \phi_0, \dot{\varepsilon} = 0, \dot{\phi} = -\Delta\dot{\phi})}{2\varepsilon_0 \Delta\dot{\phi}};$$

$$\bar{C}_{\phi\phi} = \frac{\Delta \bar{F}_{\phi}(\varepsilon_0, \phi_0, \dot{\varepsilon} = 0, \dot{\phi} = \Delta\dot{\phi}) - \Delta \bar{F}_{\phi}(\varepsilon_0, \phi_0, \dot{\varepsilon} = 0, \dot{\phi} = -\Delta\dot{\phi})}{2\varepsilon_0 \Delta\dot{\phi}} \qquad (5.31)$$

It is important to mention that for the calculation of damping coefficients only first order terms of Taylor series had been considered, while neglecting the higher order terms, hence $\cos(\Delta\phi) \approx 1$, and $\sin(\Delta\phi) \approx \Delta\phi$ for small amplitude motion.

During the calculation of rotordynamic coefficients, the perturbation sizes Δ ranging from $\pm 1\times10^{-3}$ to $\pm 1\times10^{-6}$ were found to be reasonable for all of eight rotordynamic coefficients.

Results from the above analysis are compared with Lund's [24] analytical solution as presented in Figures 5.9- 5.10.

The dimensionless rotordynamic coefficients in rotating co-ordinate *(ε,ϕ)* were calculated by the Modified Sommerfeld Number [25]:

$$\sigma = \frac{\left(1-\varepsilon^2\right)^2}{\varepsilon\sqrt{16\varepsilon^2 + \pi^2(1-\varepsilon^2)}} \qquad (5.32)$$

$$f_{ro} = \frac{4\sigma\varepsilon^2}{(1-\varepsilon^2)^2} \qquad (5.33)$$

$$f_{to} = \frac{\pi\sigma\varepsilon}{(1-\varepsilon^2)^{3/2}} \qquad (5.34)$$

The dimensionless force coefficients in (ε,ϕ) coordinates system [25]:

$$\bar{K}_{\varepsilon\varepsilon} = f_{ro}\frac{2(1+\varepsilon^2)}{\varepsilon(1-\varepsilon^2)} = -\frac{\partial F_r}{\partial e}$$

$$\bar{K}_{\phi\varepsilon} = -f_{to}\frac{(1+2\varepsilon^2)}{\varepsilon(1-\varepsilon^2)} = -\frac{\partial F_t}{\partial e}$$

$$\bar{K}_{\phi\phi} = f_{ro}\frac{1}{\varepsilon} = -\frac{\partial F_t}{\varepsilon_0 \partial \phi}$$

$$\bar{K}_{\varepsilon\phi} = f_{to}\frac{1}{\varepsilon} = -\frac{\partial F_r}{\varepsilon_0 \partial \phi}$$

$$\bar{C}_{\varepsilon\varepsilon} = f_{to}\frac{2(1+2\varepsilon^2)}{\varepsilon(1-\varepsilon^2)} = -\frac{\partial F_r}{\partial \dot{e}}$$

$$\bar{C}_{\varepsilon\phi} = \bar{C}_{\phi\varepsilon} = -f_{ro}\frac{2}{\varepsilon} = -\frac{\partial F_t}{\partial \dot{e}} = -\frac{\partial F_r}{\varepsilon_0 \partial \dot{\phi}}$$

$$\bar{C}_{\phi\phi} = f_{to}\frac{2}{\varepsilon} = -\frac{\partial F_t}{\varepsilon_0 \partial \dot{\phi}} \qquad (5.35)$$

Figures 5.8 and 5.9 shows that the damping and stiffness coefficients obtained from present analysis is in agreement with analytical solutions.

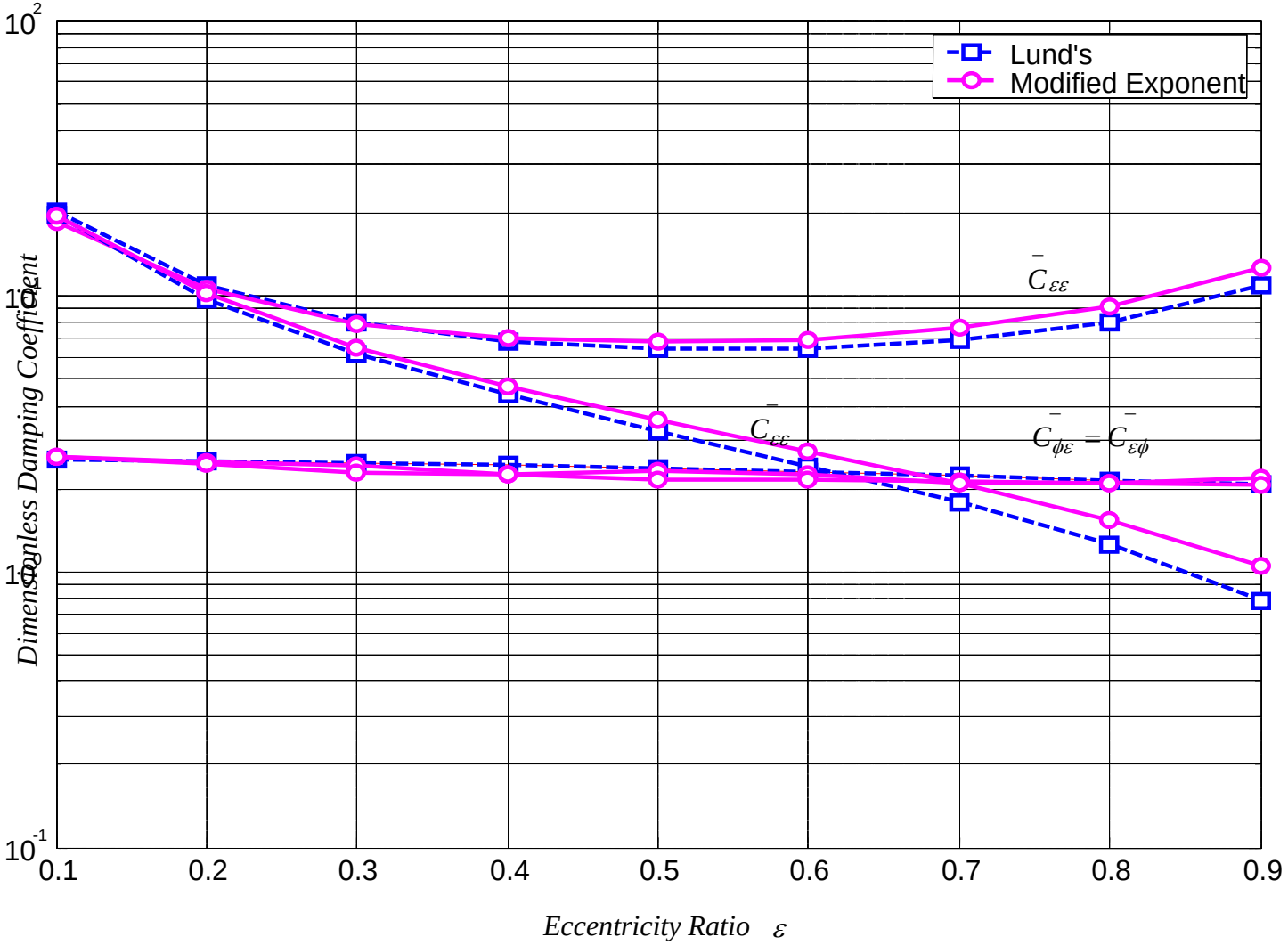

Figure 5.9: Comparison of Damping Coefficients for Lund's with Modified Parabolic ($L/D = .5$).

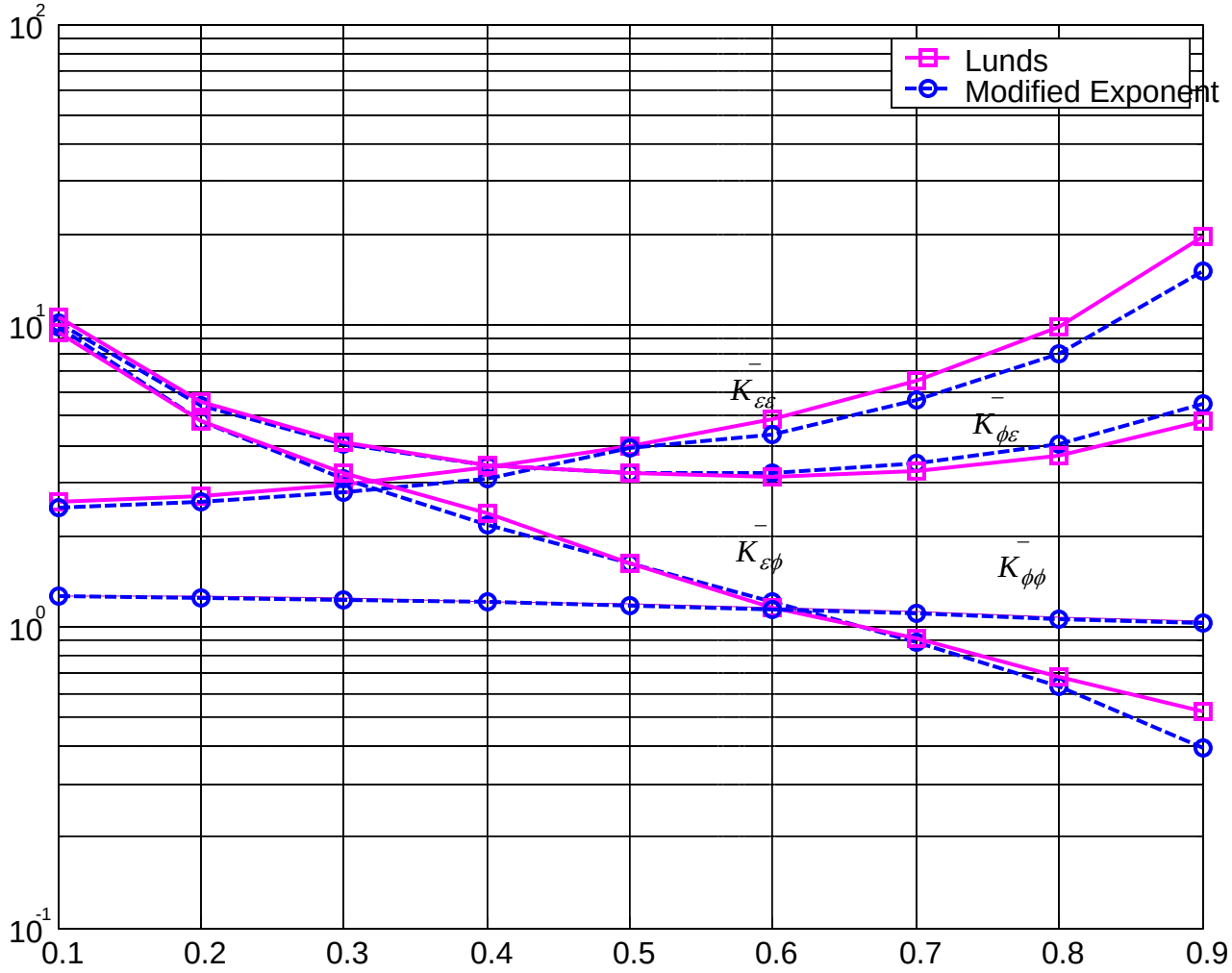

Figure 5.10: Comparison of Stiffness Coefficients for Lund's with Modified Parabolic ($L / D = .5$).

6. Non-Linear Transient Analysis

In the previous chapter rotordynamic stiffness and damping coefficients were calculated using the modified parabolic approximation and results were compared with those of Short bearing approximation. In this chapter just like chapter 4 transient analysis using modified parabolic approximation to obtain fluid forces is performed to obtain whirl threshold stability map. Equation (5.1) was modified by adding *squeeze film* ($\partial h/\partial t$) term which makes the Reynolds equation **transient** (time dependent).

6.1 Steady State Reynolds Equation with Squeeze Film Term

The pressure distribution in journal bearing is given by

$$\frac{\partial}{\partial x}\left(\frac{h^3}{12\mu}\frac{\partial P(x,z)}{\partial x}\right)+\frac{\partial}{\partial z}\left(\frac{h^3}{12\mu}\frac{\partial P(x,z)}{\partial z}\right)=\frac{1}{2}U\frac{\partial h}{\partial x}+\frac{\partial h}{\partial t} \tag{6.1}$$

To non dimensionalize the above equation substitute

$$\theta=\frac{x}{R},\ \bar{z}=\frac{z}{L/2},\bar{\mu}=\frac{\mu}{\mu_i},\bar{h}=\frac{h}{C},\bar{P}=\frac{P}{P_{ref}},U=R\omega,\bar{t}=\omega t$$

Substituting above parameters in equation (1)

$$\frac{C^2P_{ref}}{R^2\mu_i}\frac{\partial}{\partial\theta}\left(\frac{\bar{h}^3}{12\bar{\mu}}\frac{\partial\bar{P}(\theta,z)}{\partial\theta}\right)+\frac{4C^2P_{ref}}{L^2\mu_i}\frac{\partial}{\partial\bar{z}}\left(\frac{\bar{h}^3}{12\bar{\mu}}\frac{\partial\bar{P}(\theta,z)}{\partial\bar{z}}\right)=\frac{\omega}{2}\frac{\partial\bar{h}}{\partial\theta}+\omega\frac{\partial\bar{h}}{\partial\bar{t}} \tag{6.2}$$

Simplifying

$$\frac{\partial}{\partial\theta}\left(\frac{\bar{h}^3}{12\bar{\mu}}\frac{\partial\bar{P}(\theta,z)}{\partial\theta}\right)+\frac{4R^2}{L^2}\frac{\partial}{\partial\bar{z}}\left(\frac{\bar{h}^3}{12\bar{\mu}}\frac{\partial\bar{P}(\theta,z)}{\partial\bar{z}}\right)=\frac{R^2\mu_i\omega}{C^2P_{ref}}\left(\frac{1}{2}\frac{\partial\bar{h}}{\partial\theta}+\frac{\partial\bar{h}}{\partial\bar{t}}\right) \tag{6.3}$$

Let

$$P_{ref}=\frac{R^2\mu_i\omega}{C^2}\qquad\lambda=\frac{L}{D}\ \text{(aspect ratio)}$$

$$\frac{\partial}{\partial\theta}\left(\bar{h}^3\frac{\partial\bar{P}(\theta,z)}{\partial\theta}\right)+\frac{1}{\lambda^2}\frac{\partial}{\partial\bar{z}}\left(\bar{h}^3\frac{\partial\bar{P}(\theta,z)}{\partial\bar{z}}\right)=6\bar{\mu}\frac{\partial\bar{h}}{\partial\theta}+12\bar{\mu}\frac{\partial\bar{h}}{\partial\bar{t}} \tag{6.4}$$

We assume the pressure distribution in axial direction to be parabolic in nature with maximum pressure at the mid plain and zero at plain $z = \pm L/2$.

$$\bar{P}(\theta,z)=\bar{P}_\theta\left(1-\left(\bar{z}^{\chi}\right)\right) \tag{6.5}$$

Substituting value of $\bar{P}(\theta,z)$ from equation (6.5)

$$\frac{\partial}{\partial\theta}\left(\bar{h}^3\frac{\partial\bar{P}_\theta}{\partial\theta}\right)\left(1-\left(\bar{z}^{\chi}\right)\right)+\frac{\bar{h}^3}{\lambda^2}\frac{\partial^2}{\partial\bar{z}^2}\bar{P}_\theta\left(1-\left(\bar{z}^{\chi}\right)\right)=6\bar{\mu}\frac{\partial\bar{h}}{\partial\theta}+12\bar{\mu}\frac{\partial\bar{h}}{\partial\bar{t}} \tag{6.6}$$

From Ettles et al [5]

$$B_1\frac{d^2\bar{P}_\theta}{d\theta^2}+3B_1\frac{d\bar{h}}{d\theta}\left(\frac{1}{\bar{h}}\frac{d\bar{P}_\theta}{\theta}\right)-\frac{3P_\theta}{\lambda^2}=\frac{6B_2\bar{\mu}}{\bar{h}^3}\left(\frac{\partial\bar{h}}{\partial\theta}+2\frac{\partial\bar{h}}{\partial\bar{t}}\right) \tag{6.7}$$

where $B_1=\left(\frac{\chi+4}{\chi+3}\right)$ $\quad B_2=\left(\frac{\chi+1}{\chi}\right)$

6.2 Solution Procedure

A non-linear analysis of a journal bearing system requires the solution of equations of motion (4.1) and (4.2) coupled with Reynolds equation (6.1) as a function of time. A non-linear transient analysis was performed by using a Runge- Kutta solver with variable step size for non-dimensional time, $\bar{t}$ so that the relative error tolerance was within $1x10^{-5}$ and the absolute tolerance was within $1x10^{-8}$. The journal center trajectories were calculated as follows.

1. To solve the equations of motion value of $\bar{M}$ was assumed and the shaft was assumed to be initially, at rest making the initial velocity derivatives $\dot{\varepsilon}(0) = 0$ and $\dot{\phi}(0) = 0$ at t = 0. The shaft was assumed to be released from near the center of bushing using following initial conditions of the position, $\varepsilon(0) = 0.01$ and $\phi(0) = \phi_0$ for t = 0, where ϕ_0 was calculated for corresponding ε_0 =0.01 from the equation (4.6).

2. The Reynolds equation (6.1) including the squeeze term was solved for a given $\varepsilon, \phi, \dot{\varepsilon}, \dot{\phi}$ to obtain a non-dimensional pressure $\bar{P}_\theta$ in the circumferential direction. This non dimensional circumferential pressure $\bar{P}_\theta$ was substituted in equation (6.5) to obtain a two dimensional mean pressure $\bar{P}$ where $\bar{z}$ varies from $-L/2$ to $L/2$. Components of $\bar{P}$ in radial and tangential directions were integrated over bearing area as given by equations (3.55) and (3.56) to obtain the hydrodynamic fluid forces $\bar{F}_\varepsilon$ and $\bar{F}_\phi$, respectively.

3. Hydrodynamic fluid forces obtained in the previous step was introduced in the equations of motion (4.1) and (4.2) to calculate $\varepsilon, \phi, \dot{\varepsilon}, \dot{\phi}$ for the next time step.

4. Subsequently new values of $\varepsilon, \phi, \dot{\varepsilon}, \dot{\phi}$ were introduced in Reynolds equation (6.1) and the new mean hydrodynamic forces $\bar{F}_\varepsilon$ and $\bar{F}_\phi$ were determined. Equations of motion were again solved as explained in step 3 to obtain new values of $\varepsilon, \phi, \dot{\varepsilon}, \dot{\phi}$. During the

entire computational procedure $\bar{M}$ was assumed to be constant. Hydrodynamic forces $\bar{F}_{\varepsilon}$ and $\bar{F}_{\phi}$ were kept constant for given a time step.

5. Steps 3 and 4 were repeated until sufficient data points for ε and ϕ were obtained to plot trajectory of the journal center inside the clearance circle.

To obtain the threshold stability curve, the above procedure was repeated by trial and error method for different $\bar{M}$ values keeping Sommerfeld number *S*, constant. The dimensionless threshold speed $\bar{\omega}$ was obtained at which the system reaches critical state or the "*limit cycle"* below which it is stable and above which it is unstable. Different values of $\bar{\omega}$ were plotted against Sommerfeld number, *S* to obtain the non-linear whirl threshold stability map. Transient analysis by solving full Reynolds equation took approximately ten times more computational time than similar analysis with the analytical solutions of film forces. At higher eccentricities i.e. lower Sommerfeld number computational time further increases. As seen from Figure 6.1 non linear analysis is in agreement with linear analysis at higher Sommerfeld number i.e. lower eccentricity but there is some deviation at lower Sommerfeld number. This may be due to difference in the fluid film forces obtained by solving full Reynolds equation and analytical solution.

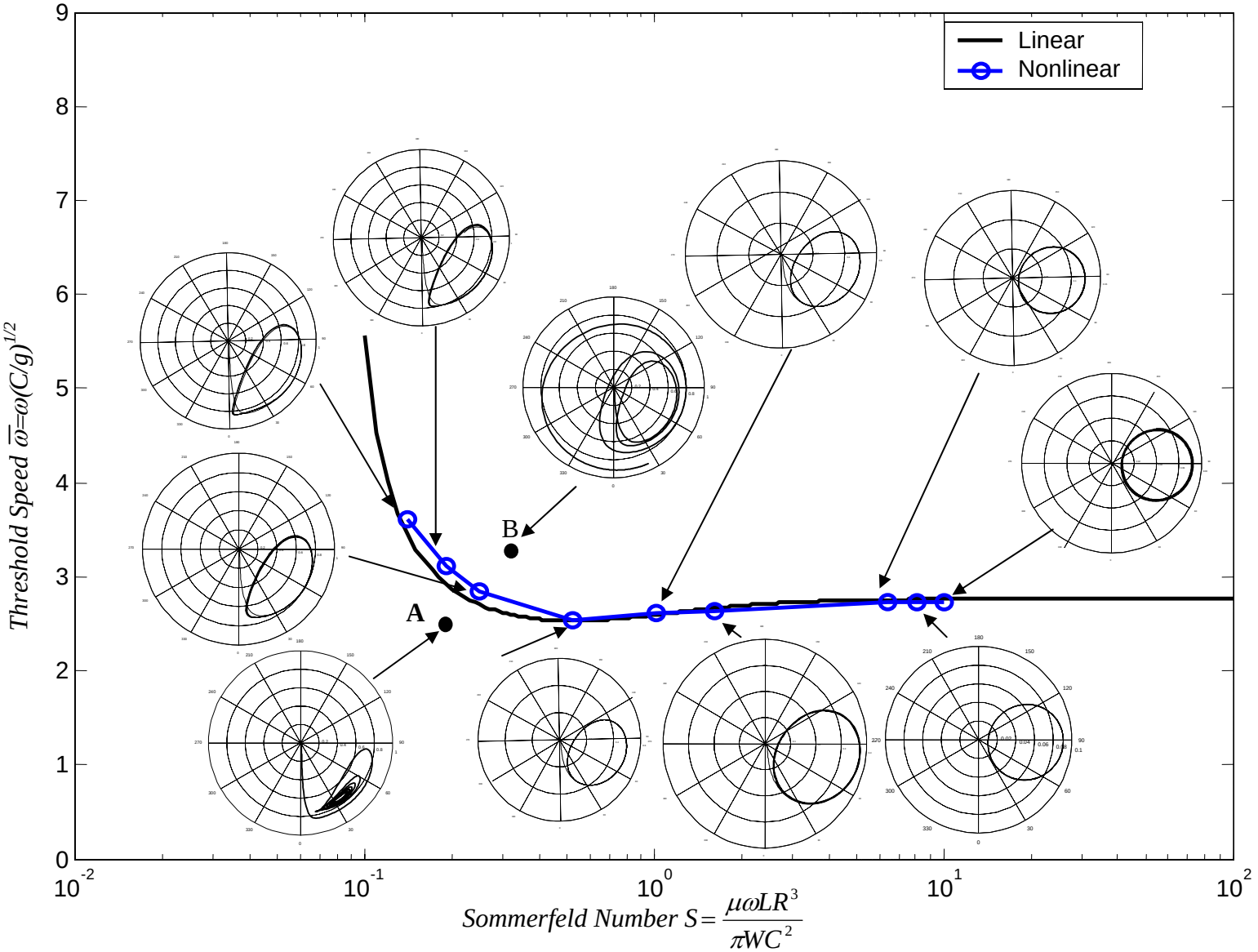

Figure 6.1 Non Linear Whirl Threshold Stability Map

7. Simplified Thermohydrodynamic (THD) Analysis

Viscosity of oil significantly affects the load carrying capacity of the bearings. Viscosity of oil decreases exponentially with an increase in temperature as a result, the load carrying capacity decreases as viscosity decreases. The relation between the temperature and the viscosity is given by Vogel's equation.

In the previous chapters all the calculations were made assuming the uniform viscosity along the circumferential direction and the pressure distributions were obtained by eliminating the viscosity term in Reynolds equation as constant. However, in practice, there exists a significant thermal gradient along the circumferential direction hence there exists a viscosity field around the bearing.

Thermohydrodynamic analysis (THD) of a bearing refers to a realistic solution of Reynolds equation in which viscosity field is predicted based on the computation of temperature field obtained from energy equation. Predictions of the bearing performance parameters based on THD analysis requires simultaneous solution of the Reynolds equation (pressure field) coupled with the energy equations (temperature field) through the Vogel's viscosity equation (viscosity field).

In this chapter modified parabolic Reynolds equation including the viscosity variation is derived. The temperature and pressure fields are compared with the published experimental results. THD design charts for the rapid evaluation of dynamic coefficients and the threshold speed are developed to investigate the effects of temperature on oil whirl instability.

7.1 Reynolds Equation with Variable Viscosity

Reynolds equation with variable viscosity is derived in a similar fashion as shown in section 6.1. The dimensionless Reynolds equation with variable viscosity is :

$$\frac{d^2\bar{P}_\theta}{d\theta^2} = 3\frac{d\bar{h}}{d\theta}\left(\frac{2B_2 e^{\beta\bar{T}}}{B_1\bar{h}^3} - \frac{1}{\bar{h}}\frac{d\bar{P}_\theta}{d\theta}\right) + \beta\frac{d\bar{T}}{d\theta}\frac{d\bar{P}_\theta}{d\theta} + \frac{2\bar{P}_\theta}{B_1\lambda^2} + 12\left(\frac{B_2 e^{\beta\bar{T}}}{B_1\bar{h}^3}\left(\frac{d\bar{h}}{dt}\right)\right) \quad (7.1)$$

7.2 Energy Equation

The following assumptions are made in deriving energy equation:

1) Heat conduction within the fluid film is entirely neglected.

2) Axial gradients are ignored.

3) All the heat generated by viscous shearing is convected out of bearing by oil.

Above assumptions leads to very simplified energy equation as given by Knight and Barrett [15]. Energy equation at the mid plane is given by:

$$\frac{dT}{d\theta} = \frac{\frac{h^3}{12\mu R}\left(\frac{dP}{d\theta}\right)^2 + \frac{\mu R^3\omega^2}{Ch}}{\rho c_v\left(\frac{R\omega h}{2} - \frac{h^3}{12\ \mu R}\left(\frac{dP}{d\theta}\right)\right)} \quad (7.2)$$

For non-dimensionalising the above equation we substitute:

$$\bar{h} = \frac{h}{C},\ \bar{P} = \frac{P}{P_{ref}}, \bar{T} = \frac{T - T_i}{T_{ref}}, \beta = \beta_1 T_{ref}, \bar{\mu} = \frac{\mu}{\mu_i} = e^{\beta_1(T-T_i)}, P_{ref} = \frac{R^2\mu_i\omega}{C^2}$$

Substituting the above parameters in equation (7.2)

$$T_{ref}\frac{d\bar{T}}{d\theta}=\frac{\dfrac{h^3\bar{C}^3P_{ref}^2}{12\bar{\mu}\mu_1R}\left(\dfrac{d\bar{P}}{d\theta}\right)^2+\dfrac{\bar{\mu}\mu_1R^3\omega^2}{C\bar{h}}}{\rho c_v\left(\dfrac{R\omega C\bar{h}}{2}-\dfrac{C^3h^3\bar{P}_{ref}}{12\bar{\mu}\mu_1R}\left(\dfrac{d\bar{P}}{d\theta}\right)\right)} \tag{7.3}$$

Multiplying and dividing equation (7.3) by $RC\omega$ gives:

$$T_{ref}\frac{d\bar{T}}{d\theta}=\frac{\dfrac{h^3\bar{C}^2P_{ref}^2}{12\bar{\mu}\mu_iR^2\omega}\left(\dfrac{d\bar{P}}{d\theta}\right)^2+\dfrac{\bar{\mu}\mu_1R^2\omega}{C^2\bar{h}}}{\rho c_v\left(\dfrac{\bar{h}}{2}-\dfrac{C^2h^3\bar{P}_{ref}}{12\bar{\mu}\mu_1R^2\omega}\left(\dfrac{d\bar{P}}{d\theta}\right)\right)} \tag{7.4}$$

Replacing $\dfrac{R^2\mu_i\omega}{C^2}=P_{ref}$

$$T_{ref}\frac{d\bar{T}}{d\theta}=\frac{\dfrac{P_{ref}\bar{h}^3}{12\bar{\mu}}\left(\dfrac{d\bar{P}}{d\theta}\right)^2+\dfrac{P_{ref}\bar{\mu}}{\bar{h}}}{\rho c_v\left(\dfrac{\bar{h}}{2}-\dfrac{\bar{h}^3}{12\bar{\mu}}\left(\dfrac{d\bar{P}}{d\theta}\right)\right)} \tag{7.5}$$

$$\frac{d\bar{T}}{d\theta}=\frac{\dfrac{\bar{h}^3}{12\bar{\mu}}\left(\dfrac{d\bar{P}}{d\theta}\right)^2+\dfrac{\bar{\mu}}{\bar{h}}}{\left(\dfrac{\bar{h}}{2}-\dfrac{\bar{h}^3}{12\bar{\mu}}\left(\dfrac{d\bar{P}}{d\theta}\right)\right)} \tag{7.6}$$

$$T_{ref}=\frac{P_{ref}}{\rho c_v}=\frac{R^2\mu_i\omega}{\rho c_vC^2} \tag{7.7}$$

The viscosity of the lubricant is considered to be uniform across the film but variable around the circumference. The relationship between the viscosity and the temperature is

given by Vogel's law where the viscosity decreases exponentially with the increasing temperature.

$$\bar{\mu} = \frac{\mu}{\mu_i} = e^{\beta_1 (T - T_i)} \tag{7.8}$$

$$\bar{T} = \frac{T - T_i}{T_{ref}} \tag{7.9}$$

$$\bar{\mu} = e^{\beta_1 \bar{T} T_{ref}} \tag{7.10}$$

$$\bar{\mu} = e^{-\kappa_1 \bar{T}} \tag{7.11}$$

where $\kappa_1 = \dfrac{\beta_1 R^2 \mu_i \omega}{\rho c_v C^2}$ is called the **temperature rise parameter** [16]**.** κ_1 is a non-dimensional parameter which is the function of oil properties, bearing geometry and the shaft linear velocity. This temperature rise parameter is known to play a significant role on the bearing temperature field and the pressure field. As seen from the equation (7.11), κ_1 uniquely describes the viscosity field for a specified temperature distribution. Change in viscosity field affects the pressure field which in turn effects the temperature distribution in the bearing. Khonsari et al. [16] gave a detailed derivation of this parameter and presented a systematic analysis on the effect of κ_1 on the temperature and the pressure field.

To confirm the validity of the above equations and the computer code, the results from the above analysis was compared with experimental values of Dowson's [12], Mitsui's [26] and Ferron's [27] bearing. These are illustrated in example 1, 2 and 3.

Example 1 Consider the Dowson's bearing [12].The bearing specifications are:

$L/D = 0.75$; $R/C = 800$; L=0.0762 m;

$\alpha_0 = 0.756 \times 10^{-7}\, m^2/s$; $k_0 = 0.13 W/mK$;

$\beta_1 = 0.0414/K;\ W = 11000N;\ \omega = 157.08\ rad/s;$

$T_i = 36.8^0 C;\ \mu_i = 0.03\ Pa.s;\ P_s = 280\,KPa\ .$

Table 7.1 shows the results of Dowson's experimental data along with isothermal and present analysis. Figure 7.1 shows the temperature profile across the bearing circumferentially. The maximum bearing temperature measured experimentally is 51.5 ^{0}C and present analysis shows the maximum temperature to be 56 ^{0}C. This difference is arise due to the assumption made that all the heat is convected out by oil and there is no heat flux going into either bushing or shaft. This leads to the higher prediction of maximum temperature.

Table 7.1: Dowson's Bearing (*N*=1500 *rpm*, *W*=11000 *N*)

Parameters[units]	**Experimental Data**	**Isoviscous Solution @ 50.81^{0}C**	**Present Analysis**
ε		0.586	0.59
Load ,W [N]	11000	11000	11000
T_{max}[^{0}C]	51.5	-	56
Attitude Angle ϕ[^{0}]	57	51.31	57.17
h_{min} [mm]		0.02629	0.026035
Sommerfeld #,S		0.193	0.2238

Example 2. Consider Mitsui's bearing [26].The bearing specifications are:

$L/D = 0.7\ ;\ R/C = 636.94\ ;\ L$=0.07 $m;$

$\alpha_0 = 0.779\times10^{-7}\,m^2/s;\ k_0 = 0.131W/mK;$

$\beta_1 = 0.029/K;\ W = 3920N;\ \omega = 158.08\ rad/s;$

$T_i = 40^0 C;\ \mu_i = 0.0192\,Pa.s;\ P_s = 98\,KPa\ .$

Table 7.2 shows the results of Mitsui's experimental data along with isothermal and present analysis.

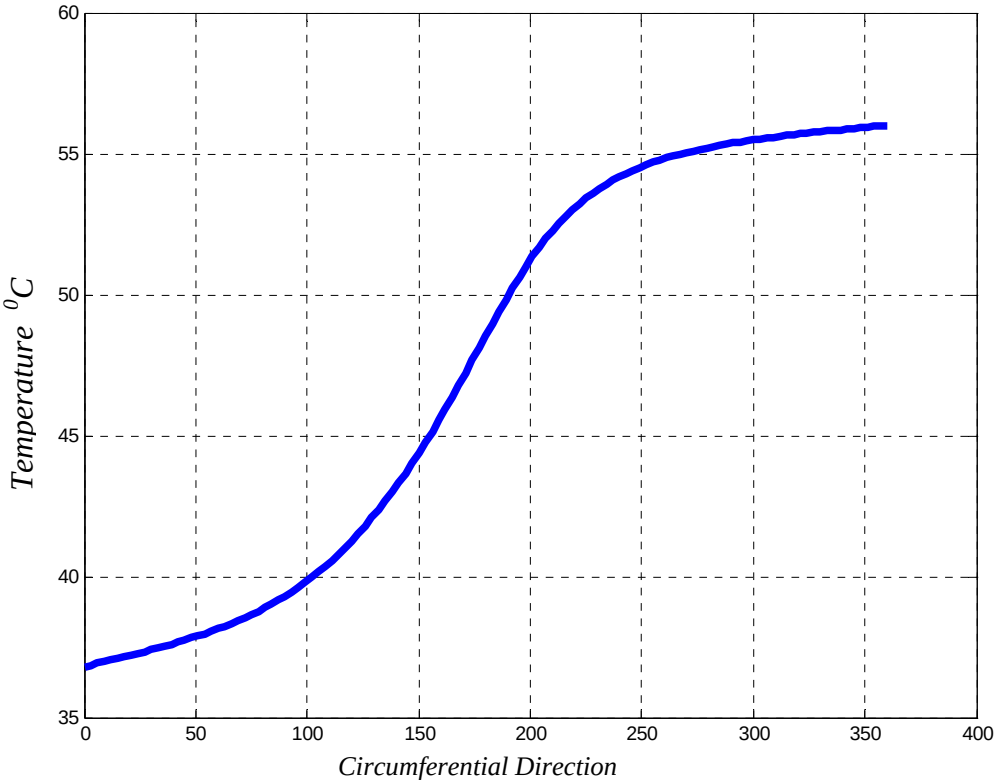

Figure 7.1: Dowson's Bearing (*N*=1500 *rpm*, *W*=11000 *N*)

Table 7.2: Mitsui's Bearing (*N*=2250 *rpm*, *W*=3920 *N*)

Parameters[units]	**Experimental Data**	**Isoviscous Solution @ 51.38^{0}C**	**Present Analysis**
ε		0.446	0.5
Load ,W [N]	3920	3920	3920
T_{max}[^{0}C]	56	-	56.52
Attitude Angle ϕ[^{0}]		60.22	61.928
h_{min} [mm]		0.04349	0.03925
Sommerfeld #,S		0.375	0.328

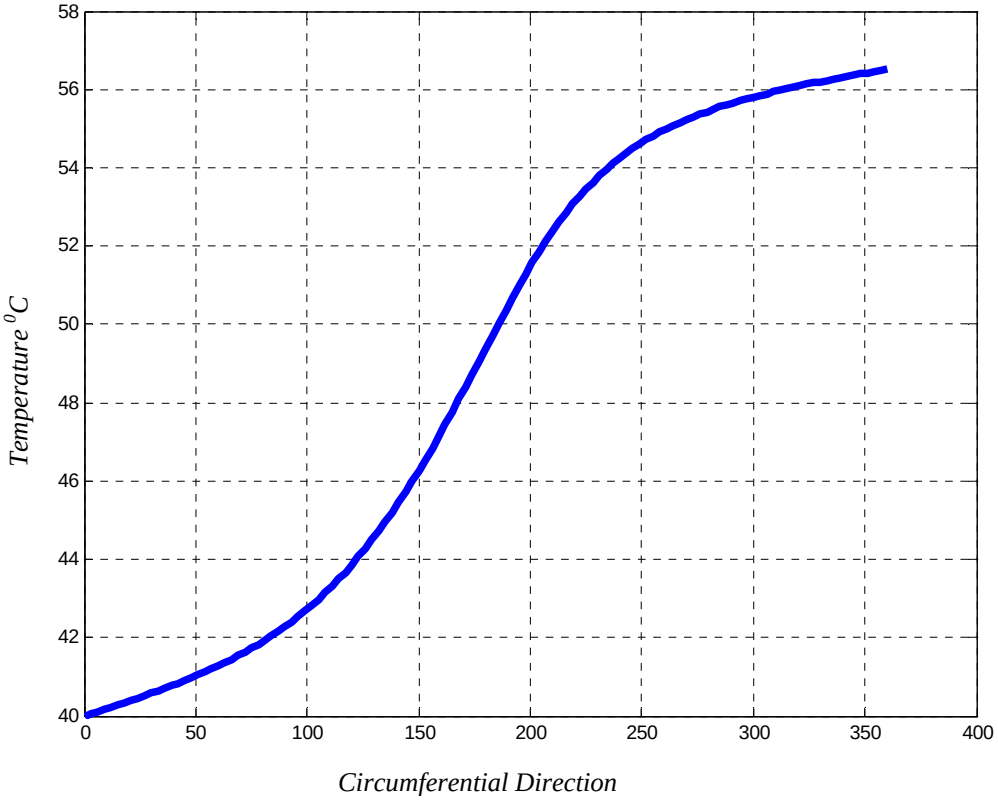

Figure 7.2: Mitsui's Bearing (*N*=2250 *rpm*, *W*=3920 *N*)

Example 3. Consider Ferron's bearing [27]. The bearing specifications are:

$$L/D = 0.8\ ;\ R/C = 344.83\ ;\ L{=}0.08\ m;\ \alpha_0 = 0.756\times10^{-7}\ m^2/s;\ \ k_0 = 0.13\ W/mK;$$

$$\beta_1 = 0.034/K;\ \ T_i = 40^0C;\ W = 4000\ N;\ \ \omega = 209.4\ \ rad/s;$$

$$\mu_i = 0.0277\ Pa.s;\ \ P_s = 70\ KPa\ \ .$$

Table 7.3 shows the results of Ferron's experimental data along with isothermal and present analysis.

As seen from table 7.1, 7.2 and 7.3 that the results from the present analysis for the maximum temperature prediction is in agreement with experimental values for all the three bearings.

Table 7.3: Ferron's Bearing (*N*=2000 *rpm*, *W*=4000 *N*)

Parameters[units]	**Experimental Data**	**Isoviscous Solution @ 51.38^{0}C**	**Present Analysis**
ε		0.575	0.59
Load ,W [N]	4000	4000	4000
T_{max}[^{0}C]	49	-	48.8
Attitude Angle ϕ[^{0}]		52.43	56.532
h_{min} [mm]		0.06163	0.05945
Sommerfeld #,S		0.183	0.181

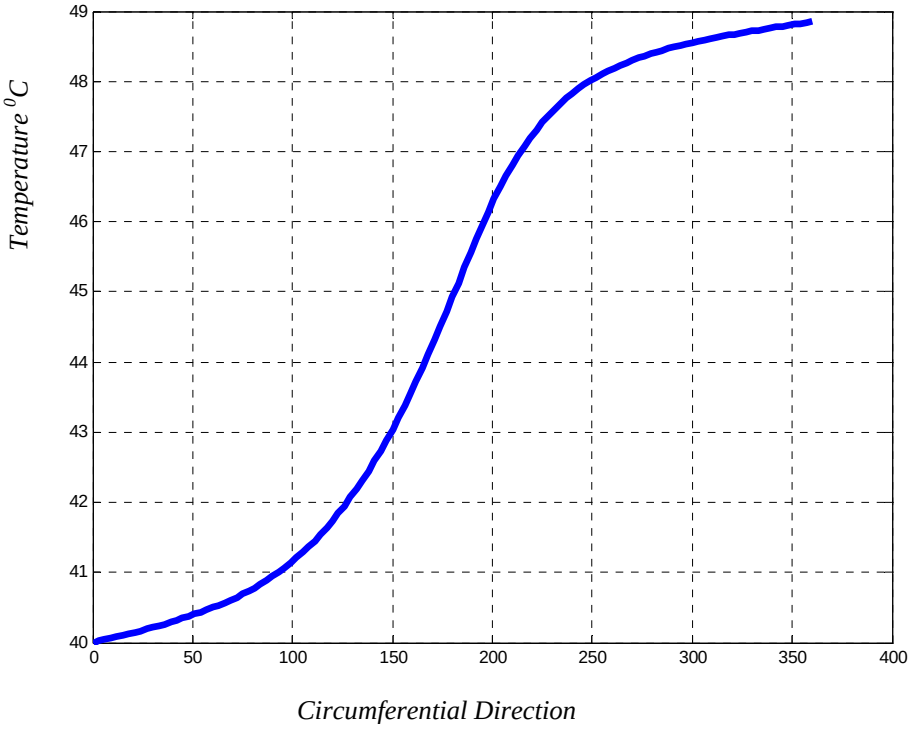

Figure 7.3: Ferron's Bearing (*N*=2000 *rpm*, *W*=4000 *N*)

7.3 Stiffness and Damping Coefficients

Stiffness and damping coefficients including the effects of inlet temperature were calculated as follows.

1. Reynolds equation (7.1) was solved by applying a fourth order Runge-Kutta scheme using the shooting method. Grid size of 241 x 101 was used keeping the viscosity constant to obtain mean pressure $\bar{P}$ for a given temperature rise parameter κ_1 and unperturbed film thickness (3.67).
2. From the pressure and pressure gradient obtained from step 1 the temperature field was obtained by solving equation (7.6) using a fourth order Runge-Kutta method. This initial temperature field was used to calculate viscosity field from equation (7.11).
3. From the viscosity field obtained from step 2 new pressure field was obtained by solving Reynolds equation (7.6) including viscosity effects.
4. Subsequent temperature and viscosity fields were obtained by repeating step 2 and 3.
5. Steps 2 - 4 are repeated until converged pressure and temperature fields are obtained for the given steady state oil film thickness. This converged pressure field was integrated over the bearing area to obtain hydrodynamic fluid forces $\bar{F}_{\varepsilon}$ and $\bar{F}_{\phi}$ in the radial and the tangential direction respectively. The load carrying capacity $\bar{W}$ and attitude angle ϕ_0 was obtained from equation (3.58) and (3.59), respectively.
6. Once the steady state position ε_0 and ϕ_0 were obtained, the oil film was perturbed in radial and tangential direction and steps 1 to 5 were repeated. The direct and cross coupled stiffness and damping coefficients were then calculated from the equations (3.65) and (3.66), respectively. The detailed procedure for the calculation of rotordynamic was presented in section 5.3.

The above procedure was repeated for the range of temperature rise parameter κ_1 values at various eccentricity ratios.

7.4 Results and Discussions

The stiffness and the damping coefficients at the various eccentricity ratios are calculated by varying the non-dimensional temperature rise parameter κ_1. The results are shown in Figures 7.4-7.8 for a range of non-dimensional temperature rise parameter κ_1 varying from 0.05 to 0.25. The non-dimensional temperature rise parameter κ_1 which incorporates all of the oil properties (ρ, c_v, β_1), bearing geometry (*R, C*), shaft velocity (ω) and the inlet viscosity (μ_i) is associated with the viscous dissipation terms in energy equation. In the present analysis, different κ_1 values correspond to the variation of inlet viscosity, while the other parameters are kept constant. This however does not limit the use of the charts only for temperature effects. One may use these charts to predict and/or compare the stability of the bearing with different geometrical dimensions and/or with different oils.

Figures 7.4-7.8 shows the effect of viscosity on the direct and cross coupled stiffness and damping coefficients. As seen from the Figure 7.4a, $\bar{K}_{\varepsilon\varepsilon}$ decreases with the increase in κ_1. At ε=0.2, $\bar{K}_{\varepsilon\varepsilon}$ is reduced by 33.3 % for κ_1= 0.25 as compared to isoviscous solution, while at ε = 0.8 it reduces by 38.4%, suggesting that the change is almost constant over the eccentricity ratios. As seen from the Figures 7.5a and 7.6b, the inlet temperature has negligible effect on $\bar{K}_{\varepsilon\phi}$ and $\bar{C}_{\phi\phi}$. From the Figure 7.7 it is observed that as κ_1 increases which may represent increase in inlet viscosity, both of the cross-coupling coefficients $\bar{C}_{\varepsilon\phi}$ and $\bar{C}_{\phi\varepsilon}$ decrease. At ε = 0.2, $\bar{C}_{\varepsilon\phi}$ and $\bar{C}_{\phi\varepsilon}$ are reduced by 58 % for κ_1=0.25, as compared to isoviscous, while at ε=0.8 they reduce by 29%, suggesting that at

the lower eccentricity ratios inlet viscosity have significant effects on the cross-coupled damping coefficients.

More clear insight onto the effects of inlet viscosity can be gained by examining the THD threshold speed curve, as shown in Figure 7.8, which is the combination of all the eight rotordynamic coefficients. It can be seen from the Figure 7.8 that the threshold speed at all eccentricity ratios decreases with increasing κ_1. At ε = 0.2, the threshold speed is dropped by 6 % for κ_1=0.25 as compared to isoviscous solution; at ε=0.8 it reduces by 25%, suggesting that at the higher eccentricity ratios the inlet viscosity have significant effects on the threshold speed.

7.5 THD Design Procedure

A design procedure to compute the threshold speed including the thermal effects using the results presented in this section is as follows:

Step 1. Compute the Sommerfeld number, *S* with the viscosity evaluated at the supply temperature.

Step 2. Compute the eccentricity ratio, ε from the expression as shown in equation (7.12) given by Jang and Khonsari [17] as function of Sommerfeld number computed in step 1.

$$\varepsilon = -0.36667 + \frac{0.49737}{\sqrt{\lambda}} - 0.20986 ln(S) \qquad (7.12)$$

Step 3. Compute the temperature rise parameter κ_1 using the bearing specifications.

Step 4. Compute the threshold speed from figure 7.8 corresponding to the temperature rise parameter computed in step 3 and the eccentricity ratio computed in step 2.

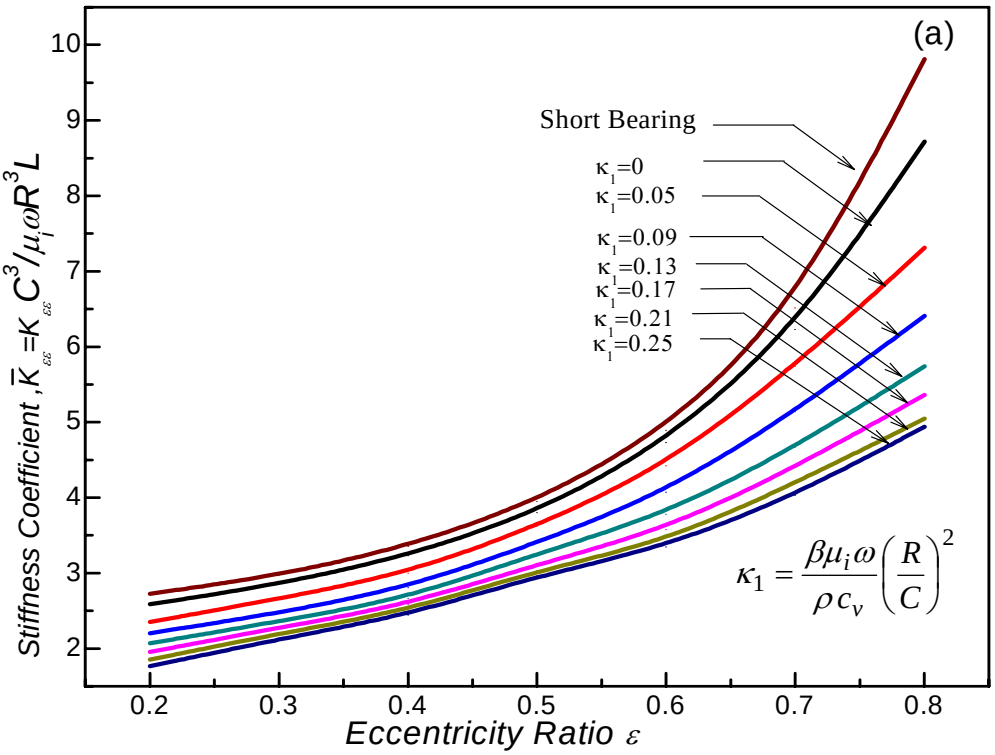

Figure 7.4a: Dimensionless Direct Stiffness Coefficient $\bar{K}_{\varepsilon\varepsilon}$

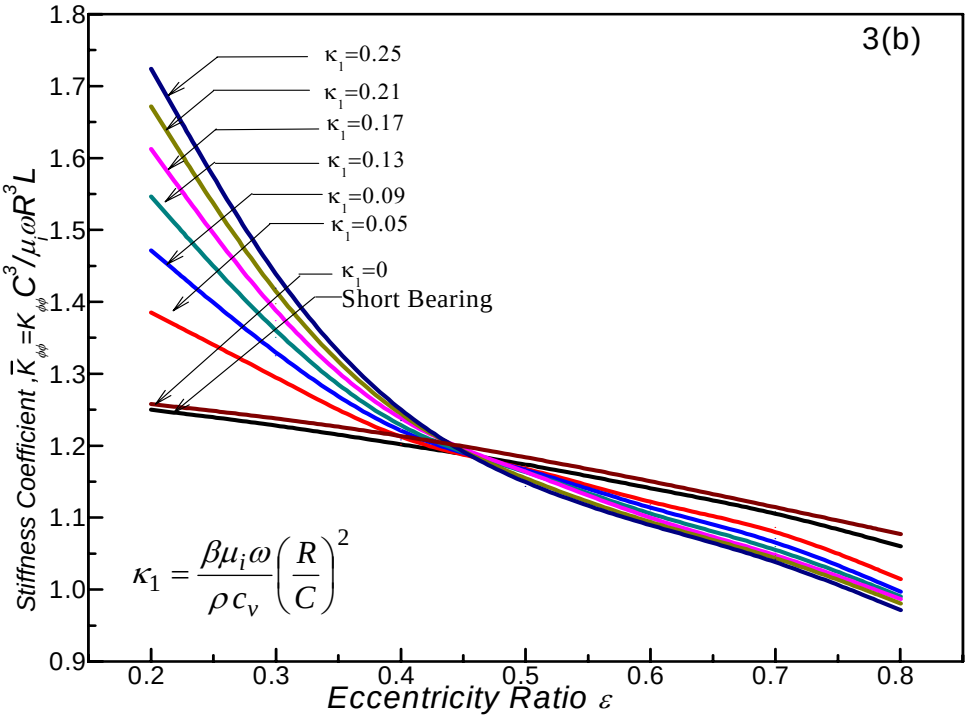

Figure 7.4b: Dimensionless Direct Stiffness Coefficient $\bar{K}_{\phi\phi}$

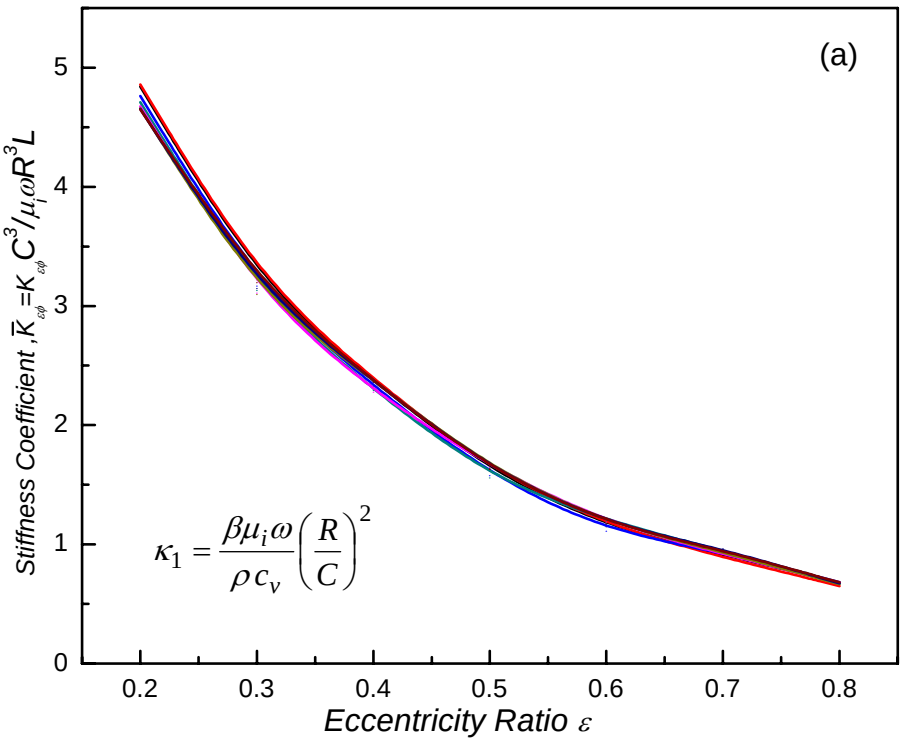

Figure 7.5a: Dimensionless Cross Coupled Stiffness Coefficient $\bar{K}_{\varepsilon\phi}$

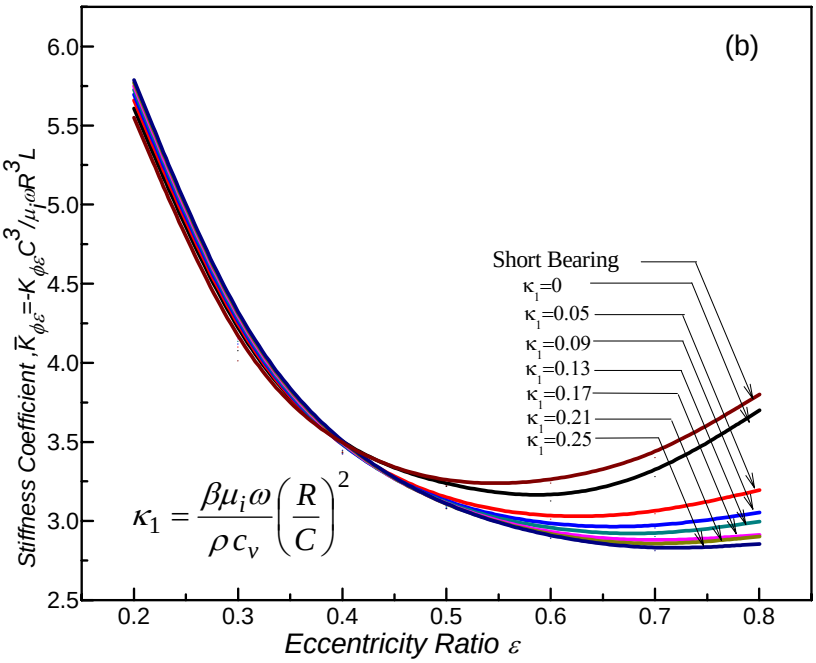

Figure 7.5b: Dimensionless Cross Coupled Stiffness Coefficients $\bar{K}_{\phi\varepsilon}$

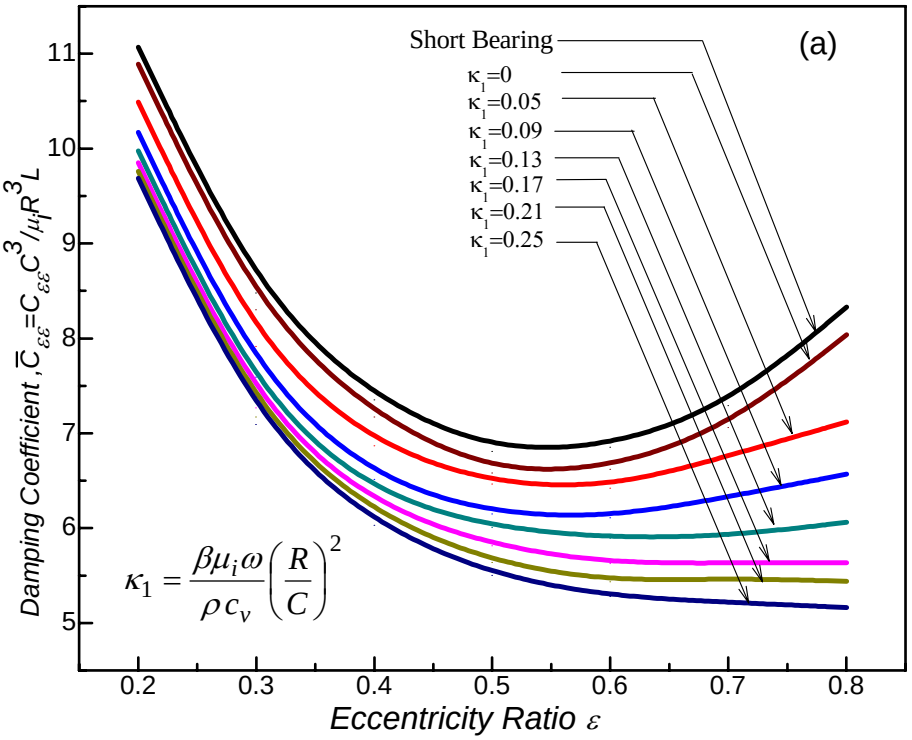

Figure 7.6a: Dimensionless Direct Damping Ccoefficient $\bar{C}_{\varepsilon\varepsilon}$

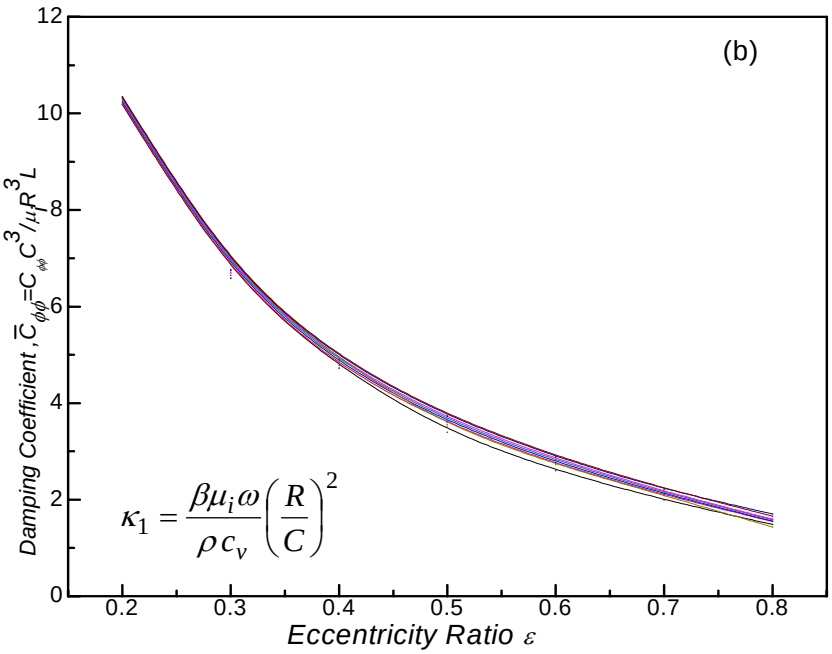

Figure 7.6b: Dimensionless Direct Damping Coefficient $\bar{C}_{\phi\phi}$

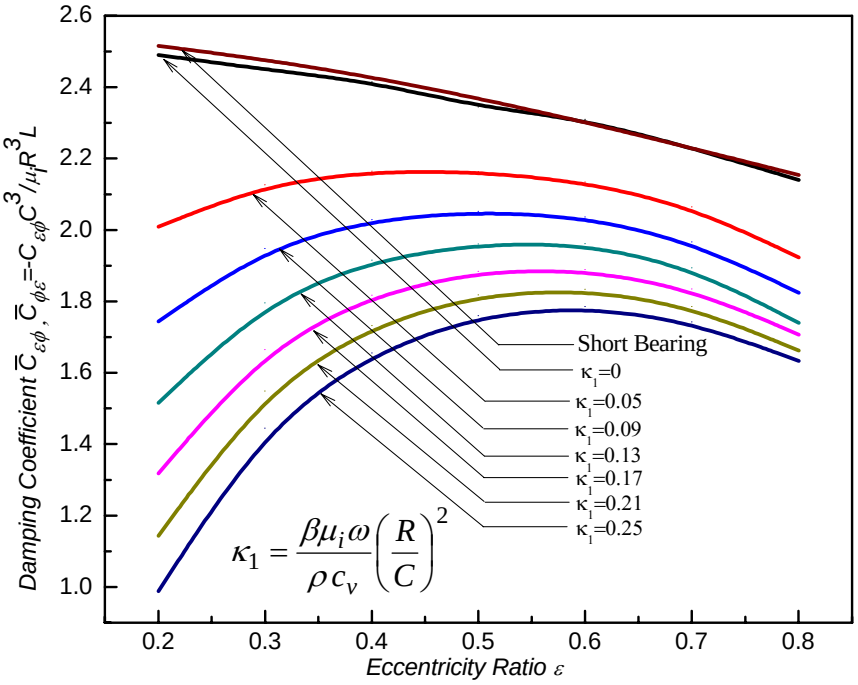

Figure 7.7: Dimensionless Cross Coupled Damping Coefficients $\bar{C}_{\phi\varepsilon}$, $\bar{C}_{\varepsilon\phi}$

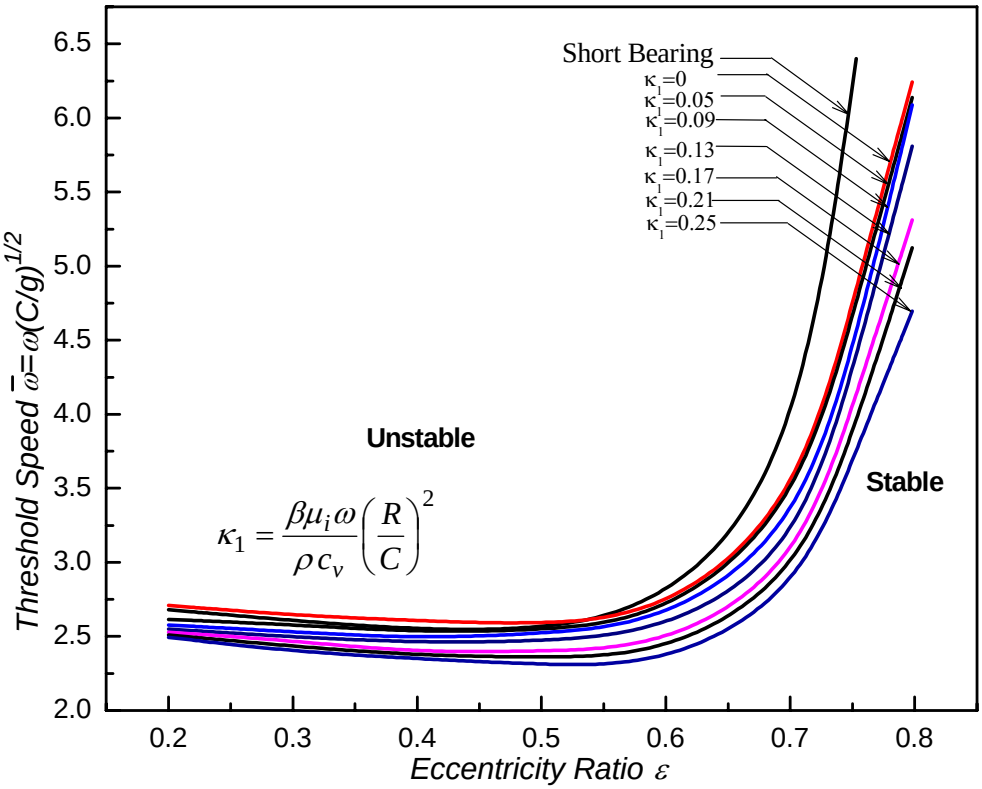

Figure 7.8: Thermohydrodynamic (THD) threshold stability map

To illustrate the above design procedure and the use of THD threshold map following example is presented.

Example 4 Consider the following bearing specification:

$$\lambda = 0.5\ ; {R}/{C} = 800\,; L = 0.0762m\ \ \alpha_0 = 0.756\times10^{-7}\, m^2/s;\ k_0 = 0.13W/mK;$$

$$\beta_1 = 0.0414/K;\ W = 11000\,N;\ \ \mu_i = 0.03\ Pa.s;$$

$$\omega = 157.07\ \ rad/s;\ T_i = 36.8\ ^0C;\ \ P_s = 280\,KPa\ .$$

Using the design procedure given by Jang and Khonsari [17] the eccentricity ratio ε and the temperature rise parameter κ_1 for the above bearing specifications is computed to be $\varepsilon = 0.61$ and $\kappa_1 = 0.0726$, respectively. The bearing coefficients and whirl threshold speed can be evaluated from the THD design charts, figures 7.4-7.8, for the corresponding ε and κ_1, Table 7.4 shows the bearing coefficient and threshold speed for the above bearing specification. As seen from the table 1 the operating speed, $\omega = 157$ *rad/s* lies below the whirl threshold speed, $\Omega = 922$ *rad/s*, hence the rotor will be free from oil whirl instability.

We can observe from the THD threshold chart Figure 7.8, that a bearing can be stabilized at the "same operating speed" by either increasing or decreasing the inlet temperature.
To illustrate the procedure, for stabilizing the unstable bearing by changing the temperature of oil, following example is presented.

Example 5 Consider the following bearing specification [4]:

$$\lambda = 0.5\ ; C = 1.02\times10^{-4}\,m\,; L = 0.0254m\ \ \alpha_0 = 0.756\times10^{-7}\, m^2/s;\ k_0 = 0.13W/mK;$$
$$\beta_1 = 0.0107/K;\ W = 427\,N\,;\ \mu_i = 0.036\,Pa.s\,;\ \omega = 827\,rad/s\,;T_i = 5\ ^0C$$

Table 7.4: Bearing coefficients and threshold speed for example 4

Eccentricity Ratio, ε -	0.611
Load, W (N)-	11000
Sommerfeld Number, S-	0.2704
Direct stiffness coefficients $K_{\varepsilon\varepsilon}, K_{\phi\phi}$ (MN/m)-	774,207
Cross-coupled stiffness coefficients $K_{\phi\varepsilon}, K_{\varepsilon\phi}$ (MN/m)-	-550,200
Direct damping coefficients $C_{\varepsilon\varepsilon}, C_{\phi\phi}$ (MNs/m)-	7.47,3.345
Cross-coupled damping coefficients $C_{\phi\varepsilon}, C_{\varepsilon\phi}$ (MNs/m)-	-2.46
Whirl Threshold speed , Ω (rad/s)-	922

Using the design procedure given by Jang and Khonsari [17] the eccentricity ratio, and the ε temperature rise parameter κ_1 for the above bearing specifications is computed to be ε = 0.42 and κ_1=0.015, respectively. The dimensional whirl threshold speed at the given eccentricity ratio, ε = 0.42 with the inlet temperature of $T_i = 5\,^0C$ corresponding to κ_1 = 0.015, is computed to be Ω = 803 *rad/s*. As the operating speed, $\omega = 827\ rad/s$ falls above the whirl threshold speed for κ_1 = 0.015, represented as operating condition A in Figure 7.9, the rotor will undergo whirling. By increasing the inlet oil temperature to $T_i = 71\,^0C$ inlet viscosity changes to $\mu_i = 0.0157\ Pa.s$ and temperature rise parameter changes to κ_1=0.005. If the operating speed, $\omega = 827\ rad/s$ and load, $W = 427\ N$ is

unchanged then for inlet temperature, $T_i = 71\ ^0C$ the bearing operating condition will move to B as shown in Figure 7.9, where the eccentricity ratio is computed to be ε=0.59 and dimensional whirl threshold speed, Ω= 840 *rad/s* . As the operating speed, $\omega = 827\ rad/s$ is below the whirl threshold speed, Ω= 840 *rad/s*, as shown in Figure 9 the rotor will be free from oil whirl instability.

Example 5 suggests that the whirl can be suppressed thermally by changing the temperature of the inlet oil. To further verify this understanding, non-linear transient including the thermal effects, corresponding to operating conditions A and B, as shown in Figure 7.9 is presented. During the non-linear transient analysis steady state energy equation (7.6) was considered. As seen from Figure 7.9 operating condition A has unstable orbit while B has stable orbit. Results presented in example 2 are in agreement with the experimental findings reported by Newkirk and Lewis [4].

Example 6 Consider the following bearing specification:

$$\lambda = 0.5\ ;\ R/C = 200\ ;\ L = 0.0254m\ ;\ C = 1.27\text{x}10^{-4}m$$

$$\alpha_0 = 0.756\times10^{-7}\ m^2/s;\ k_0 = 0.13W/mK;\ \beta_1 = 0.0458/K;$$
$$W = 401N\ ;\ \mu_i = 0.066\ Pa.s\ ;\ \omega = 733\ rad/s\ ;\ T_i = 25\ ^0C\ .$$

Using the design procedure given by Jang and Khonsari [17] the eccentricity ratio ε, and the temperature rise parameter κ_1 for the above bearing specifications is computed to be ε = 0.34 and κ_1=0.052, respectively. The dimensional whirl threshold speed at the given eccentricity ratio, ε = 0.34 with the inlet temperature of $T_i = 25\ ^0C$ corresponding to κ_1 = 0.052, is computed to be Ω = 710 *rad/s*. As the operating speed, $\omega = 733\ rad/s$ falls above the whirl threshold speed for κ_1 = 0.052, represented as operating condition A in Figure

7.10, the rotor will undergo whirling. By increasing the inlet oil temperature to $T_i = 60\,^0C$ inlet viscosity changes to $\mu_i = 0.014\ Pa.s$ and temperature rise parameter changes to κ_1=0.01. If the operating speed, $\omega = 733\ rad/s$ and load, $W = 401N$ is unchanged then for inlet temperature, $T_i = 60\,^0C$ the bearing operating condition will move to B as shown in Figure 7.10, where the eccentricity ratio is computed to be ε=0.68 and dimensional whirl threshold speed, Ω = 755 *rad/s* . As the operating speed, $\omega = 733\ rad/s$ is below the whirl threshold speed, Ω = 755 *rad/s*, as shown in Figure 7.10 the rotor will be free from oil whirl instability.

.

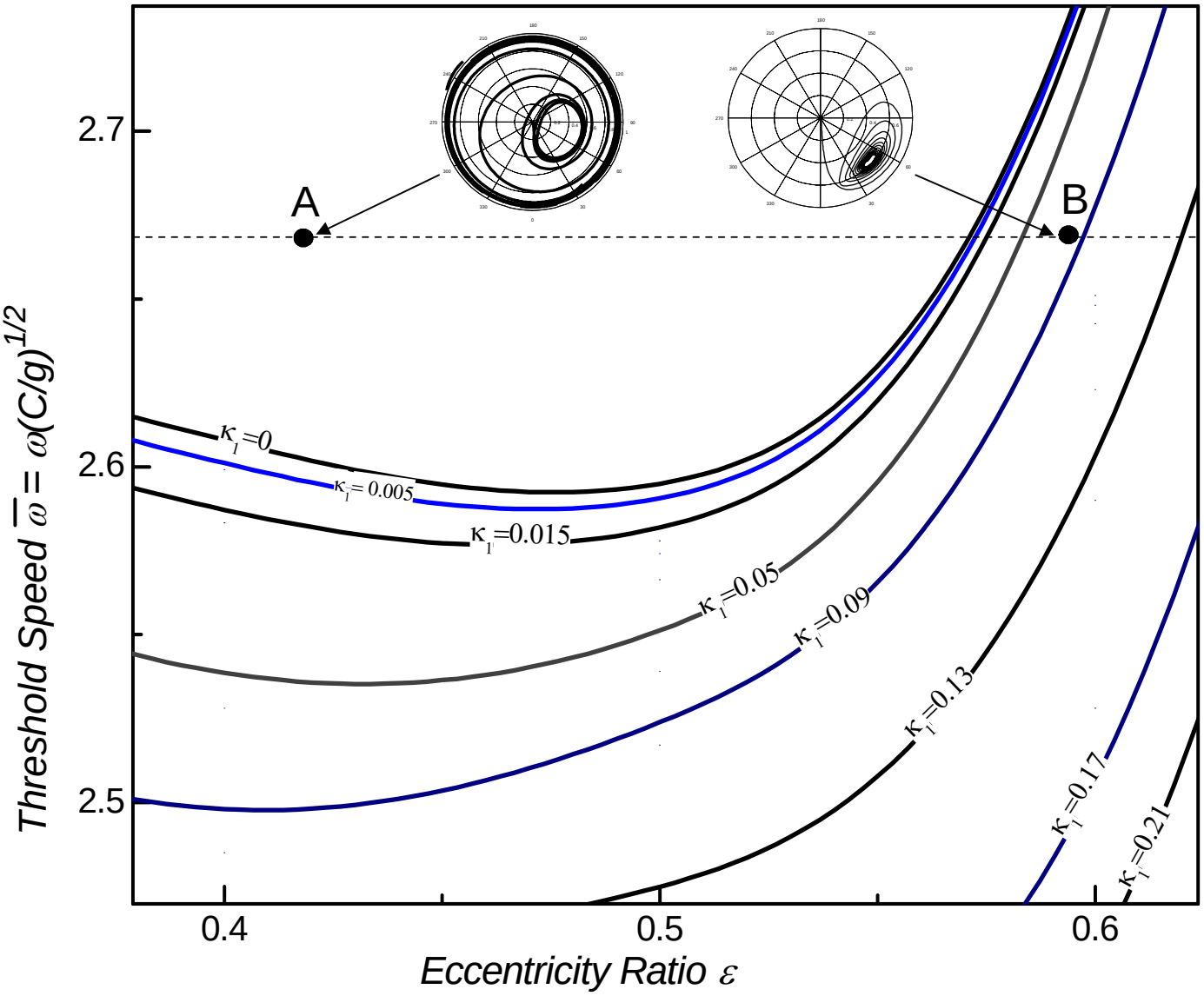

Figure 7.9: Thermohydrodynamic (THD) threshold stability map

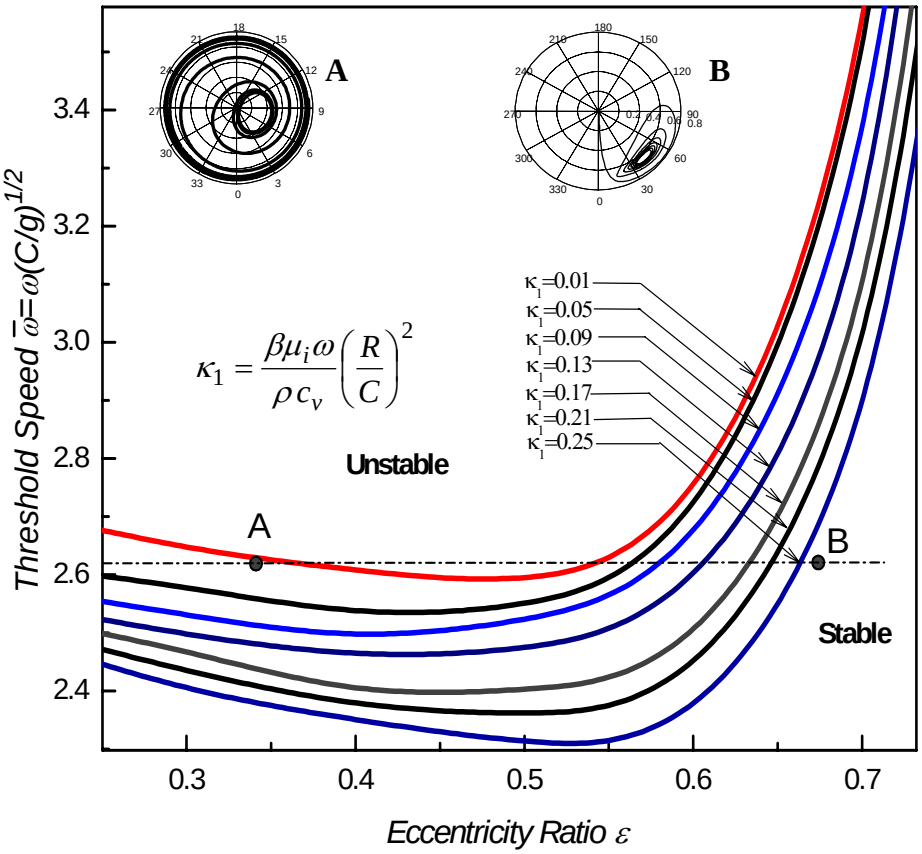

Figure 7.10: Thermohydrodynamic (THD) threshold stability map

8. Conclusions

Since the discovery of oil whirl phenomenon by Newkirk [1] in 1925, many experimental and theoretical investigations have been conducted to understand and predict the onset of this non-synchronous whirling. Experimental investigations by Pinkus [3] and Newkirk et al. [4] showed that the inlet viscosity significantly affects the stability of the rotor bearing system. Later on Ezzat and Maki [18] also concluded that the inlet temperature of lubricant plays a significant role in the dynamics of high-speed bearings. Although the experimental results were repeatable and predictable, no quantitative explanations were given in the papers for this phenomenon. The primary purpose of this thesis was to investigate the effects of inlet viscosity on the stability of rotor bearing system and put this phenomenon on firm foundation.

In this thesis the effect of the inlet viscosity on the stiffness coefficients, damping coefficients and whirl instability threshold for the finite journal bearings had been investigated. Simplified THD study shows that the inlet viscosity significantly affects the cross-coupling damping coefficients. The inlet temperature also influences the whirl threshold speed. The effect of the inlet viscosity on the whirl threshold was found to be more pronounced at higher eccentricity ratios. This study revealed that it is possible to stabilize journal bearing system either by heating the oil or by cooling the oil depending upon the operating region. The stability charts developed in this thesis may be used to predict the change in oil temperature that is required to stabilize the journal bearing system.

In this thesis the effects of out of balance force on the whirl threshold was also investigated. Simulations results indicated that whenever the bearing operates just above threshold speed, a small amount of unbalance tends to help in decreasing the amplitude of

vibration within the clearance circle caused by oil whirl. Also there exists a range of unbalance loads which could decrease the amplitude of vibration near the threshold speeds. These results were obtained based on isothermal calculations. Extension of this portion of the work to include thermal effects is a subject of a future research.

References

1. Newkirk, B. L., and Lewis, J. F.,"Shaft Whipping due to Oil Action in Journal Bearings," *General Electric Review*, (August 1925): 559-568.

2. Khonsari, M. M. "A Review of Thermal Effects in Hydrodynamic Bearings, Part II: Journal Bearings", *ASLE Trans*., Vol. 30, (1987):26-33.

3. Pinkus, O., "Experimental Investigation of Resonant Whip." *Trans. ASME* (1957): 975-983.

4. Newkirk, B. L., and Lewis, J. F., 1956,"Oil Film Whirl-An investigation of Disturbances Due to Oil Films in Journal Bearing ,"*Trans ASME*, 21-27.

5. P. Shelly and C. Ettles," A Tractable Solution for Medium-Length Journal Bearings", *Wear*, 16 (1970) 221-228.

6. Hagg, A. C. "Oil Whip." Westinghouse Research Laboratories.

7. Holmes, R.,"The Vibration of a Rigid Shaft on Short Sleeve Bearings." *Journal of Mechanical Engineering Science* (1960): 337-341.

8. Holmes, R., "Nonlinear Performance of Turbine Bearings." *Journal of Mechanical Engineering Science*, Vol. 12, (1970): 377.

9. Kirk,G. and Gunter, E.J ," Transient Journal Bearing Analysis", NASA CR-1549,Washington,DC, June 1970.

10. Akers, A., Michaelson, S. and Cameron, A., "Stability Contours for a Finite Whirling Journal Bearing," *ASME Journal of Lubrication Technology* ,Vol. 93 ,p.177 (1971).

11. Khonsari, M. and Chang, Y. "Stability Boundary of Non-Linear Orbits within Clearance Circle of Journal Bearings," *ASME Journal of Vibration and Acoustics*, V. 115, (1993): 303-307.

12. Dowson, D., Hudson, J., Hunter, B., and March, C. "An Experimental Investigation of the Thermal Equilibrium of Steadily Loaded Journal Bearings." *Proc. Inst. Mech. Engr*., Vol 101, 3B, (1966-67).

13. Tonnesen, J. and Hansen, P. K.," Some Experiments on the Steady-State Characteristics of a Cylindrical Fluid-Film Bearing Considering Thermal Effects," *J. Lubrication Technology*, October, pp 578-587 (1970).

14. Ma, M. and Taylor, C. M., "An Experimental Investigation of Thermal Effects in Circular and Elliptical Plain Journal Bearings." *Tribology International*, Vol. 29, No. 1, (1996): 19-26.

15. Knight, J.D. and Barrett, L.E.," An Approximate Solution Technique for Multilobe Journal Bearings Including Thermal Effects, with Comparison to Experiments," ASLE Trans, 26(4) 1983, 501-508.

16. Khonsari, M.M. Jang, J. Y., and Fillon, M., "On the Generalization of Thermodynamic Analyses for Journal Bearings." *Journal of Tribology Vol. 118* (1996): 571-579.

17. Jang J Y, Khonsari M. M.,2004,"Design of bearings on the basis of Thermohydrodynamic analysis", *Proc. Inst. Mech. Engrs.*, Part J, **218**.

18. Maki, E. R., and Ezzat, H. A., "Thermally Induced Whirl of a Rigid Rotor on Hydrodynamic Journal Bearings," *Trans ASME*, 102(1) 1980, 8-14.

19. Tondl, A., *Some Problems of Rotor Dynamics*, Chapmann and Hall, 1965.

20. Khonsari, M. M. and Booser, E. R., *Applied Tribology Bearing Design and Lubrication*, John Wiley and Sons, 2001.

21. Vance, John, *Rotordynamics of Turbomachinery*. John Wiley Sons, 1988.

22. Chang, Y. J. *The Effect of Supply Temperature and Shaft Flexibility on the Shaft of Journal Bearings*. Master's thesis, University of Pittsburgh, 1990.

23. Ocvirk, F .W and Dubois, G.B ," Analytical derivation and experimental evaluation of short bearing approximation of full journal bearings", *N.A.C.A. Tech Rept . 1157* , 1953.

24. Lund J. W., 1966," Self excited Stationary Whirl Orbits of a Journal in a Sleeve Bearings", *Ph.D. thesis*, Rensselaer Polytechnic Institute, Troy, N.Y.

25. San Andre`s, "http:// metrib.tamu.edu/me626/notes",*Class Notes*.

26. Mitsui, J., "A Study of Thermohydrodynamic Lubrication in a Circular Journal Bearings," Tribology International, Vol 20, No 6 pp. 331-341.

27. Ferron, J., Frene,J., and Boncompain. R.," A Study of the Thermohydrodynamic Performance of a Plain Journal Bearing Comparison Between Theory and Experiments," *ASME Journal Lubrication Technology*, *Vol 105* (1983) pp.422-428.

28. Hamrock B.J 1994, *Fundamentals of Fluid Film Lubrication*, McGraw-Hill.

29. Den Hartog, J. P., *Mechanical Vibrations.* McGraw-Hill, New York, 1956.

Appendix A: Co-ordinate Transformation

Relationship between rotating (ε, ϕ) and stationary (x, y) co-ordinate system is given by

$$\begin{bmatrix} K_{xx} & K_{xy} \\ K_{yx} & K_{yy} \end{bmatrix} = \begin{bmatrix} \cos\phi_0 & -\sin\phi_0 \\ \sin\phi_0 & \cos\phi_0 \end{bmatrix} \begin{bmatrix} K_{\varepsilon\varepsilon} & K_{\varepsilon\phi} \\ K_{\phi\varepsilon} & K_{\phi\phi} \end{bmatrix} \begin{bmatrix} \cos\phi_0 & \sin\phi_0 \\ -\sin\phi_0 & \cos\phi_0 \end{bmatrix} \tag{A1}$$

$$\begin{bmatrix} C_{xx} & C_{xy} \\ C_{yx} & C_{yy} \end{bmatrix} = \begin{bmatrix} \cos\phi_0 & -\sin\phi_0 \\ \sin\phi_0 & \cos\phi_0 \end{bmatrix} \begin{bmatrix} C_{\varepsilon\varepsilon} & C_{\varepsilon\phi} \\ C_{\phi\varepsilon} & C_{\phi\phi} \end{bmatrix} \begin{bmatrix} \cos\phi_0 & \sin\phi_0 \\ -\sin\phi_0 & \cos\phi_0 \end{bmatrix} \tag{A2}$$

The threshold speed is given by [28]

$$\bar{M} = \left(\bar{\omega}_r \right)^2 = \frac{C_{xx}K_{yy} + K_{xx}C_{yy} - C_{yx}K_{xy} - K_{yx}C_{xy}}{C_{xx} + C_{yy}} \tag{A3}$$

Appendix B: Taylor Series Expansion

Taylor series expansion for sine and cosine functions:

$$\sin\Delta\phi = \Delta\phi - \frac{(\Delta\phi)^3}{3!} + \frac{(\Delta\phi)^5}{5!} - \frac{(\Delta\phi)^7}{7!} + \ldots\ldots\ldots\ldots \quad \text{(B1)}$$

$$\cos\Delta\phi = 1 - \frac{(\Delta\phi)^2}{2!} + \frac{(\Delta\phi)^4}{4!} - \frac{(\Delta\phi)^6}{6!} + \ldots\ldots\ldots\ldots \quad \text{(B2)}$$

Appendix C: THD Program Flow Chart

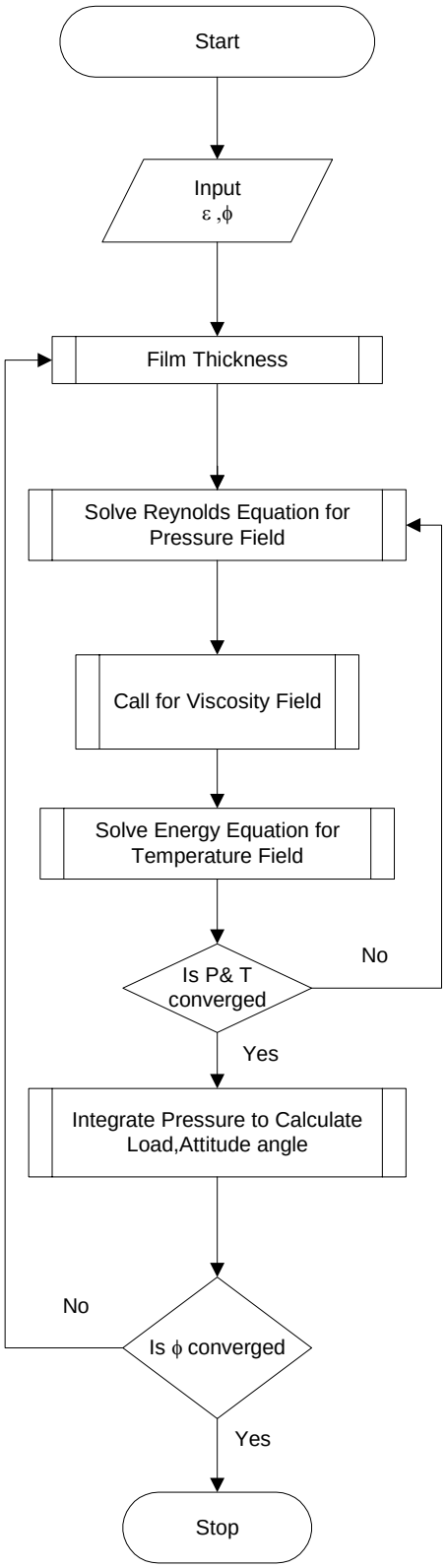

Appendix D: Non-Linear Transient Analysis Flow chart

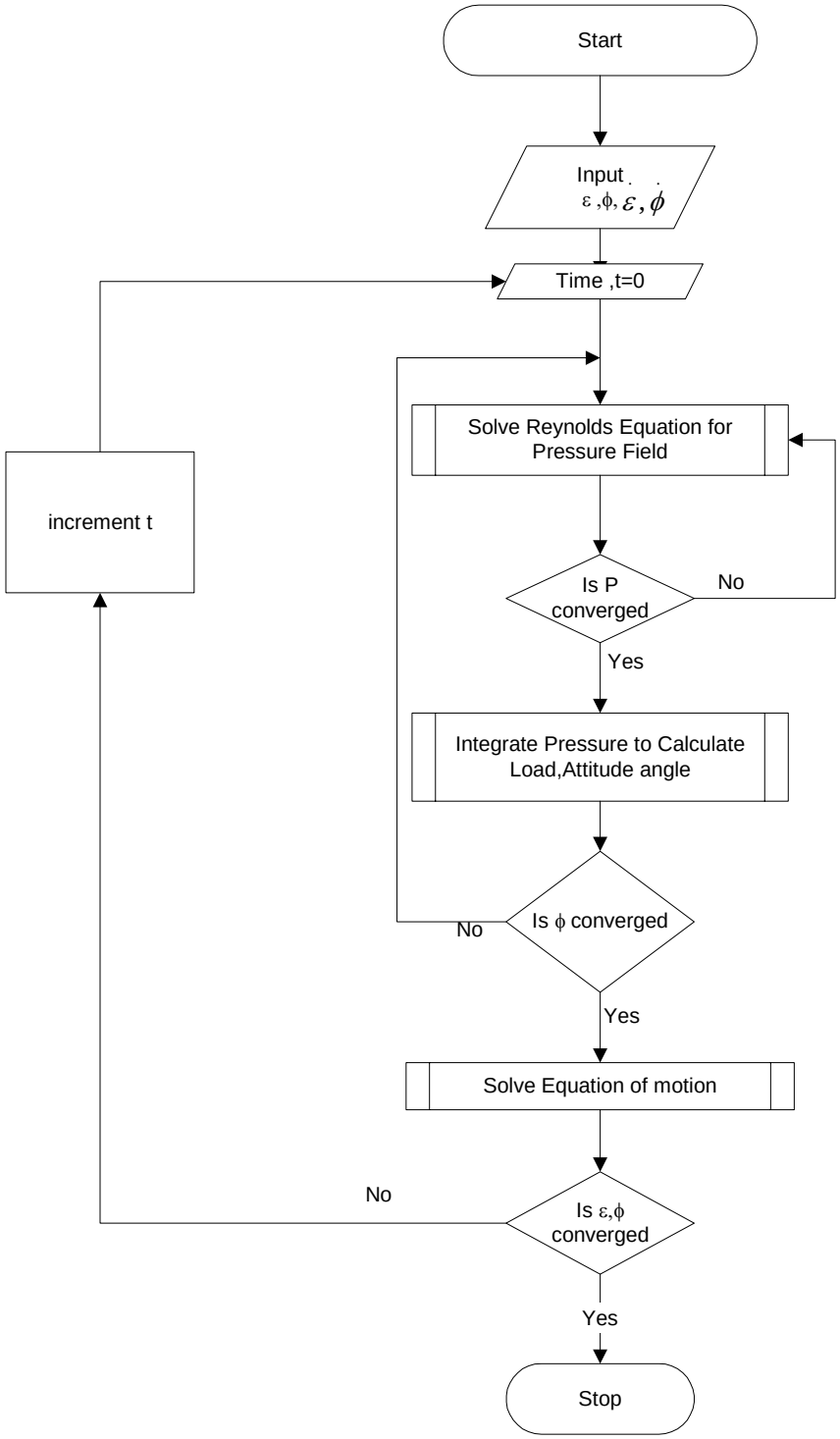

Vita

Mr. Sumit Singhal was born on August 20, 1978, in the steel city Bhilai, India. He earned his bachelor's degree in mechanical engineering from Bhilai Institute of Technology, Bhilai, India. He joined Louisiana State University in January 2001 to pursue a master's degree in mechanical engineering. His areas of interest are tribology, machine design, fluid dynamics, and vibrations. He successfully defended his thesis on May 12, 2004 and will receive the degree of Master of Science in Mechanical Engineering in August 2004.